Evaluation of Canine Fracture Fixation Bone Plates

by

Edward Kalust Tacvorian

A Thesis

Submitted to the Faculty

of the

WORCESTER POLYTECHNIC INSTITUTE

In partial fulfillment of the requirements for the

Degree of Master of Science

In

Biomedical Engineering

November 6, 2012

APPROVED:

_____

Glenn Gaudette, Ph.D., Advisor, Biomedical Engineering

_____

Kristen Billiar, Ph.D., Biomedical Engineering

_____

Michael Kowaleski, DVM, DACVS, Cummings School of Veterinary Medicine

Acknowledgements

Many thanks to my committee members Professor Kristen Billiar and Michael Kowaleski, DVM, DACVS, for their direction, support, and continued guidance throughout my graduate education.

I would like to thank Jeremy Skorinko and Harry Hovagimian for their help throughout the testing process.

I would also like to thank Julien Cabassu, DVM, Cara Blake, DVM, Randy Boudrieau, DVM, DACVS, and (again) Michael Kowaleski, DVM, DACVS, from the Cummings School of Veterinary Medicine at Tufts University for their clinical expertise and assistance which have allowed for the completion of this research.

Without the continued support and encouragement from my mother, father, brother, family, and friends, I would have accomplished nothing.

Finally, I would like to extend my extreme gratitude to Professor Glenn Gaudette for his invaluable guidance and countless hours of support throughout my graduate education and research.

Abstract

The understanding of bone healing and principles of fracture fixation have improved greatly over the past fifty years. Plating systems are ideal for use in fracture fixation as they facilitate direct and indirect bone healing due to the stability they provide at the fracture site. Their main failure mode, however, is through fatigue from the consistent loading and unloading of the plated bone when healing. The goal of this study was to evaluate the mechanical properties of the most prominent veterinary plating systems representing a comminuted fracture when mated to a bone model. These assemblies were loaded to acute failure in four-point bending and cycled in torsion to mimic fatigue loading. Based on the analyzed test data we are able to make a number of conclusions. After performing four-point bending tests, the String Of Pearls (SOP) system sustained the highest bending mechanical properties with a bending stiffness of 80.4±12.5 N/mm, bending structural stiffness of 8.7±1.4 N-m^2, and bending strength of 11.6±1.7 N-mm. The Advanced Locking Plate System #10 (ALPS10) sustained the lowest bending mechanical properties with a bending stiffness of 40.0±1.9 N/mm, bending structural stiffness of 4.3 ± 0.2 N-m^2, and bending strength of 5.1±1.2 N-mm. Analysis of the cyclic fatigue data allow us to conclude that the Dynamic Compression Plate (DCP) system is able to maintain the highest absolute torque value across 15,000 torsion cycles and Fixin the lowest. This translates to 5.4±0.7 N-m and 3.5±0.4 N-m, respectively, when analyzed with Dixon-Mood equations and 5.4±2.5 N-m and 3.5±1.3 N-m, respectively, when analyzed with probability plots. In addition, the ALPS10 system is able to maintain the highest percentage of its failure torque and SOP the lowest. This translates to 76.4±16.3% and 43.6±5.3%, respectively, when analyzed with Dixon-Mood equations, and 72.9±28.6% and 44.2±22.1% when analyzed with probability plots. To aid in proper fracture healing, plating systems offering reduced or no contact with bone when applied in addition to screw holes across the entire plate length are preferred. The results of this evaluation are a start to better understanding plating system mechanics, which to develop further, will require further fatigue life testing in both loading conditions.

Table of Contents

Table of Figures

Table of Figures

1. Introduction

The understanding of bone healing and principles of fracture fixation has greatly developed over the past half century. Depending on the method of fixation, bone may heal in unstable or stable modes. An unstable fracture begins healing spontaneously, forming a protruding callus at the fracture site in the process. If a fracture is left to heal in this mode, it may take between six and nine years to fully complete the healing process. Fracture healing under stable fixation methods occurs without formation of callus, and reduces fracture healing times to about eighteen months. As controlling the movement and exercise of a canine with a fractured leg is difficult, stable fixation is preferred.

Medical devices for human use must meet numerous requirements and regulations set by the Food and Drug Administration (FDA) to ensure their safety and effectiveness. While the FDA recommends that manufacturers of veterinary devices conduct tests to ensure their safety and effectiveness, there are no regulations governing their approval for use. Consequently, very few studies have been conducted calculating different mechanical properties of fracture fixation systems and assessing their similarities and differences. Studies researched varied in their testing methods as analyzed fixation devices were limited in addition to a restricted number of studies utilizing *in vivo* loading considerations. This limitation prevents the surgeon from determining the preferred fixation mode.[1-3]

Forces must be applied to bone to facilitate healing. When fixators are used to stabilize bone fracture fragments, it is important for the stiffness of those fixators to be similar to that of bone. As stated by Wolff's law, bone undergoes many adaptations throughout its life to adapt to its mechanical environment. As such, if fixators absorb a majority of the load placed on the bone, stress shielding will effectively cause the fragment ends to resorb. This can lead to delayed union, nonunion, or lack of bone growth.

Fixation plates are used for the stabilization of fractures in animals and humans. Using the canine femur as a model, there exist numerous principal plate systems, of which the most prominent were evaluated. Each of these systems contains a plate to span the fracture gap and corresponding screws to affix the plate to the bone. These systems vary in their plate dimensions and geometry, screw type, screw hole quantity, healing mode of plate application – ultimately affecting the effectiveness, stiffness, and longevity of the system when placed under acute and cyclic loads. Using a synthetic bone model and set fracture gap, the plating systems were subjected to experiments to determine their bending strength under acute four-point bending loads and their fatigue strength under cyclic torsion loads, as excess loading in these modes are typically responsible for bone fracture.

2. Background

Bones are comprised of numerous tissues, vessels, and chemical structures and serve as a rigid frame for the body's tissues while also protecting internal organs from impact forces.[4] More importantly, fracture or other damage should not occur from strain caused by repetitive everyday activities. However, depending on an activity's intensity level, duration, and repeated loading, microscopic damage may be seen.[5] While osteoclasts and osteoblasts work together to repair and maintain the structural integrity of bone, any damage occurring faster than the rate of repair will experience fracture. Bone fracture may heal through different methods depending on the damage level or fixation stability. Spontaneous healing occurs in fractures that are not fixated in a stable manner, while primary healing occurs in rigidly fixed fractures.[5] As this study focuses on femoral fracture fixator evaluation, the main fracture types associated with the diaphysis of the femur are transverse, oblique, and comminuted. Numerous fixation methods including intramedullary nails, pins, lag screws, and plating systems can be used to fixate these fractures, in addition to allowing them to heal spontaneously without fracture stabilization.

2.1 Bone

The structure of bone can be broken down into multiple levels. While osseous tissue dominates the makeup of bone, numerous structures exist on microscopic and chemical levels. Epiphysis refers to the proximal and distal ends of bone while diaphysis refers to the main shaft. A majority of the epiphysis is comprised of cancellous bone while the majority of the diaphysis is comprised of cortical bone.

2.1.1 Bone Anatomy

Mammalian bone, including that of humans and canines, is a composite material consisting of an organic matrix and inorganic hydroxyapatite. The wet weight of bone is derived 10-20% from water, 45-60% from hydroxyapatite (HA), and 30-35% from organic substances. The organic composition can be further broken down to 90-95% collagen, 1% glycosaminoglycans, and 5% other proteins.[6]

There are four levels associated with the structure of bone. Fundamentally, HA crystals are ingrained between the ends of adjacent collagen fibrils. When separate, HA and collagen do not possess high mechanical properties, but their combined form yields a composite with excellent mechanical properties[6]. Generally, bone is more ductile than HA and is able absorb more energy before failure and bear higher loads as it is more rigid than collagen. On the second level, lamellae form from the combined collagen-HA fibrils and have specific orientations which define the strength limits in their primary loading direction. This arrangement of lamellae is seen on the third level. A tubular Haversian osteon is one functional unit of bone, produced from the circular and concentric lamellae structure and possesses its maximum strength along the long axis.[5] This is seen in Figure 1.

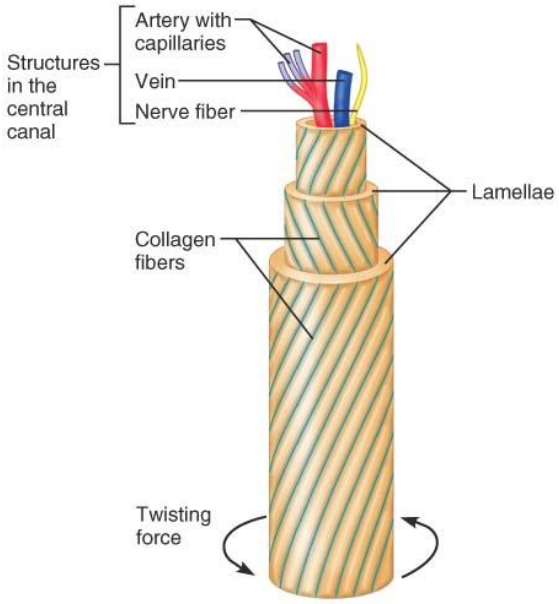

Figure 1: Structure of an Osteon[5]

The macroscopic structure of bone is observed on the fourth level of bone organization. At this level, the main factors determining bone's strength are its density and trabecular orientation. There are two main bone structure types: cortical and cancellous. Cortical, or compact, bone is found mainly in the diaphysis of long bones and the exterior shell of other bone types. Compact bone consists of Haversian osteon systems and interstitial bone regions. Osteons are typically oriented in the longitudinal direction of long bones and are typically 200μm in diameter and 10-20mm long. They are further composed of concentric lamellae 3-9 μm thick.[6] Haversian canals run through the center of osteons and allow blood vessels to deliver nutrients to osteocytes (bone cells). Biomechanically, cortical bone can be characterized as being semi-brittle, viscoelastic, and its strength is orientation dependent. Figure 2 shows the microscopic anatomy of compact bone.

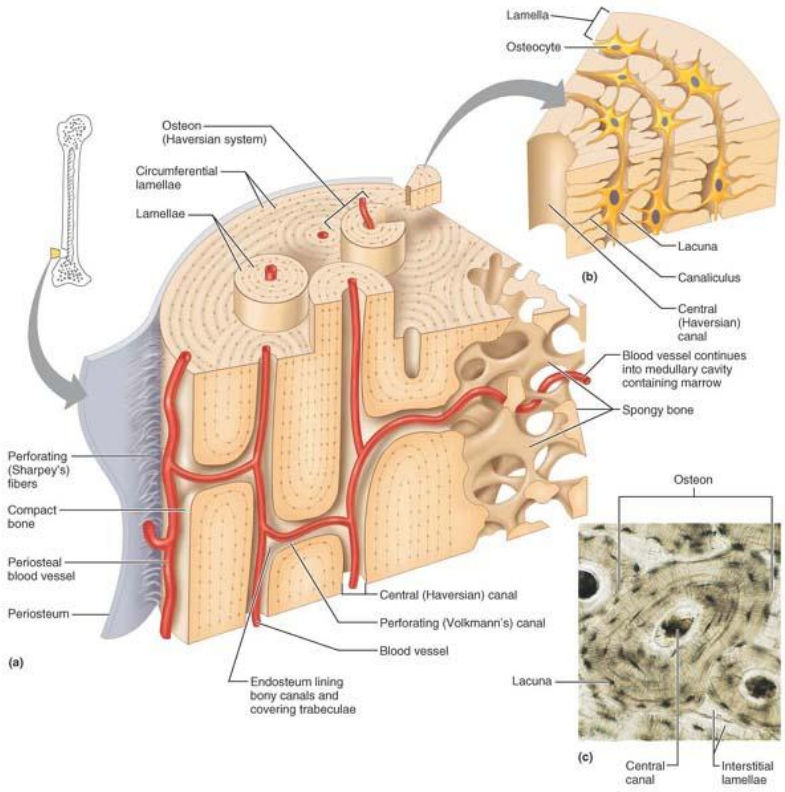

Figure 2: Microscopic Anatomy of Compact Bone.[5]

Cancellous, or trabecular, bone contains a highly porous structure and is located on the epiphysis of the bone. Pores are interconnected and filled with bone marrow, making up 75-95% of the bone volume. Cancellous bone is made up of a matrix of small struts and plates called trabeculae that are between 100-300µm thick and are spaced 300-1500µm apart.[6] This porous structure of cancellous bone has distinctly different mechanical properties from cortical bone. The structural and apparent densities, strength, and moduli of cortical bone are all considerably greater than cancellous bone. Stiffness and strength are the two core mechanical properties of bone. Stiffness is expressed by the elastic modulus and is calculated by the stress required to elastically deform bone. Deformation, or change in shape, occurs in structural materials as they are loaded. If this change in shape reverses with the removal of the load, the material is said to have undergone elastic deformation. If this change in shape is permanent, plastic deformation has occurred. Bone strength is defined as the stress required to cause plastic deformation or fracture.[7] Various mechanical tests can be performed to determine the stiffness and strength of bone. These measurements can be recorded and calculated using a load-displacement curve. Table 1: quantifies the mechanical properties of greyhound and pit-bull long bones as previously examined by Kemp et al.[8] Figure 3 displays the gross structure of a long bone.

Table 1: Greyhound and Pit-bull Long Bone Mechanical Properties.[8]

	Greyhound (28.52±1.98 kg)	Pit-bull (23.61±3.73 kg)
Elastic Modulus (GPa)		
Humerus	7.70±0.65	3.22±0.34
Radius	15.07±0.47	8.64±0.68
Femur	11.22±1.18	6.77±0.62
Tibia	14.05±0.85	9.29±0.44
Yield Stress (MPa)		
Humerus	121.03±21.10	103.63±28.75
Radius	202.36±8.12	168.39±10.86
Femur	166.50±11.26	119.56±10.14
Tibia	177.94±3.22	163.31±2.90

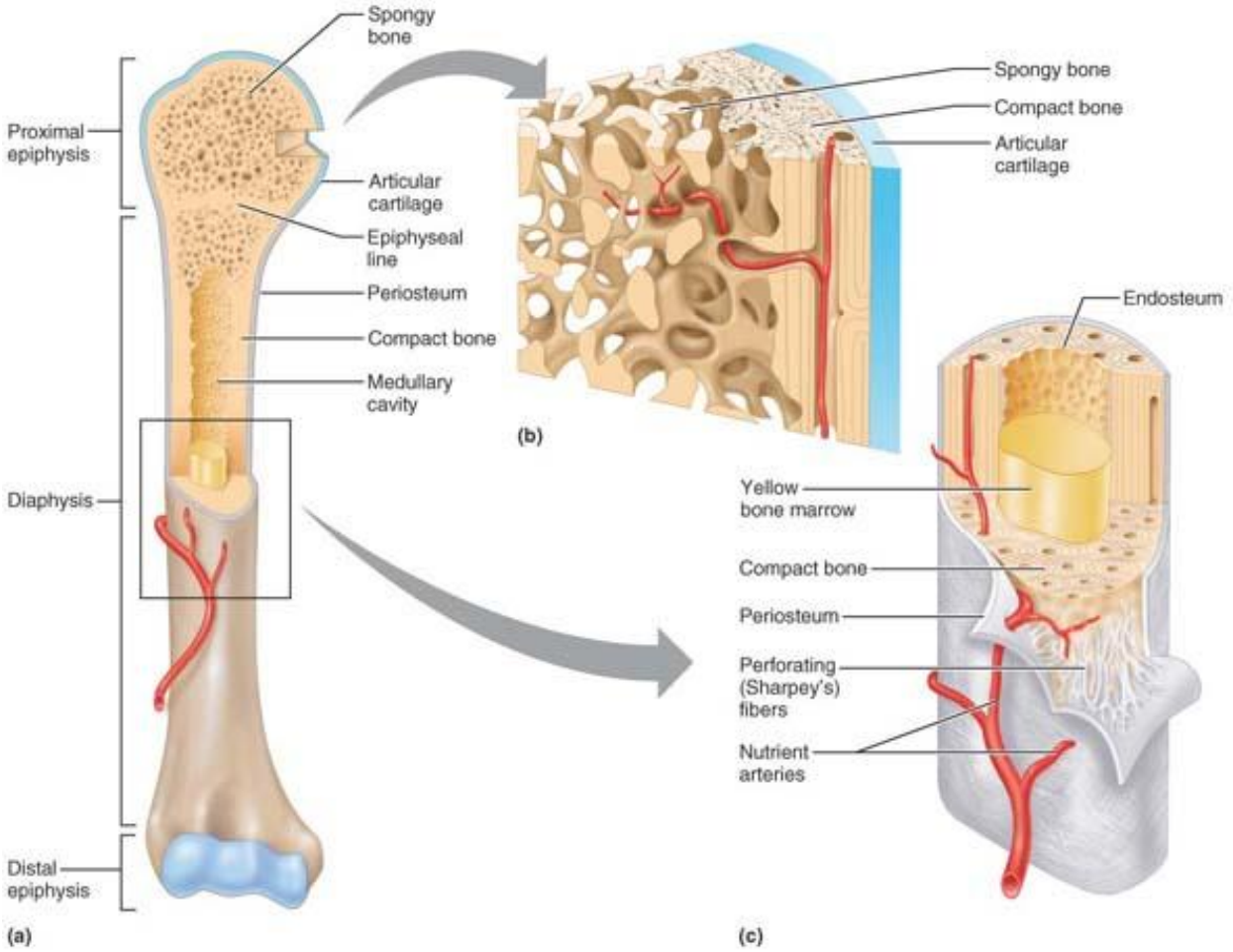

Figure 3: Gross anatomy of the long bone. (a) Long bone structure. (b) Cancellous bone structure. (c) Cortical bone structure.[5]

2.2 Biology of Fracture Healing

When bone experiences a load exceeding its ultimate tensile strength, fracture occurs. Fracture is defined as a breach in continuity of bone, either on a macroscopic or microscopic level. Fractures may heal via indirect or direct healing, depending on their relative stability.

2.2.1 Unstable Fractures

Unstable fractures heal via indirect healing, which is characterized by the formation of callus as a process intermediate before modeling into hard bone.[5] This is also the mode of healing for nonoperative fracture treatment, unstable internal and external fixation, along with the plate osteosynthesis of highly comminuted fractures.[9, 10] The amount of callus produced is inversely proportional to the stability of the fraction, as a less stable fracture results in increased callus formation, and vice versa.[11] This is dictated by interfragmentary strain.

Interfragmentary strain is the deformation which occurs at a fracture's bone fragment interface. This is a major influence in the progression of fracture healing and is calculated by dividing the displacement of the fracture gap by the initial gap width. Bone and callus formation cannot occur with an interfragmentary strain greater than two percent. To overcome high strain, muscles surrounding the bone first contract to begin resorption of the fragment ends. At strains between two and ten percent, a fibrocartilage forms and between ten and one-hundred percent a granulation tissue forms.[12] Once the tissues surrounding the fragment provide an interfragmentary strain below two-percent, callus formation may begin.[5] The timeline of unstable fracture healing is divided into three overlapping phases: inflammatory, repair, and remodeling.

2.2.1.1 Inflammatory Phase

Once the integrity of bone and its surrounding tissues are disrupted, the inflammatory phase begins and continues until the initiation of cartilage or bone formation. This typically lasts three to four days depending on the level of damage and magnitude of force causing the bone disruption.[5] Within hours after bone disruption, an extraosseous blood supply emerges from the surrounding tissues to begin the revascularization of the hypoxic fracture site. This forms a fibrin rich clot and initiates spontaneous healing. Growing evidence suggests that hematoma fosters the repair phase by releasing growth factors to stimulate angiogenesis and bone formation.[5] Vasoactive substances are released by mast cells and are believed to contribute to new vessel formation.[13] Macrophages also play a role in fracture repair as they release fibroblast growth factor (FGF), initiating fibroplasia both in soft tissues and in bone. As vasculature is reconstructed, internal, or medullary, blood flow resumes and the extraosseous blood supply diminishes. Mesenchymal stem cells (MSCs) from the cambium layer of the periosteum, endosteum, bone marrow, and adjacent soft tissues proliferate during this phase.[9] Unless infection, excessive motion, or extensive necrosis of the soft tissue is noted, the hematoma will resorb by the end of the first week after bone disruption. The end of this phase is marked by a decreased observation in pain or swelling.

2.2.1.2 Repair Phase

During the repair phase, hematoma is transformed into granulation tissue with assistance from capillary ingrowth, mononuclear cells, and fibroblasts. While interfragmentary strain remains high in this phase, the sustained formation of granulation tissue is explained by its ability to stretch to twice its length. The first observation of mechanical strength in the disrupted bone is observed during this phase as the formed granulation tissue has a tensile strength of 0.1 N/m^2. Granulation tissue helps reduce interfragmentary strain at the fracture site and in turn initiates cartilage formation.[5, 11] The tissue matures predominantly into Type I collagen fibers that have an ultimate tensile strength of 1-60 N/m^2 and can resist elongation to a maximum of 17%.[5] As the fibers mature, they organize into a diagonal pattern to allow for optimized elongation ability. Many elements including low oxygen tension, poor vascularity, growth factors, and interfragmentary strain influence the ability of the collagen fibers to develop into a cartilaginous callus. Proliferated MSCs present from the inflammatory phase are orchestrated by TGF-β and morphogenic proteins (BMPs) to differentiate into chondrocytes. This differentiation is essential to the maturation of collagenous fibers at the fracture gap into internal and external cartilaginous "soft callus" matrices, which are facilitated by angiogenesis and an intact periosteum. In well-vascularized unstable fractures, a bulging external callus is also found, increasing the injured bone's resistance to bending. An increase in proteoglycan concentrations in the fibrocartilage is observed, contributing to increased stiffness at the interfragmentary gap. This callus resists compression, but has a similar ultimate tensile strength and elongation before rupture as fibrous tissue (4-19 N/m^2, 10-12.8%). Once interfragmentary strain reduces to below ten percent, this cartilaginous matrix may mineralize, maturing into "hard callus" by endochondral ossification.[9, 11] In this process, chondrocytes calcify and degenerate, facilitate angiogenesis, and allow osteoblasts to lay down woven bone on the collagen framework left by the chondrocytes.

The length of time necessary to achieve union depends on the fracture configuration and location, the status of adjacent soft tissues, in addition to the patient's statistics. While bone union is achieved at the end of the repair phase, its existing structure at the fracture site does not resemble that of the original bone. At the end of the repair phase, however, enough strength and rigidity has been regained to allow a canine to begin low impact exercise. Table 2 describes the ultimate tensile strength and maximum elongation of tissues formed throughout the fracture healing process.

Table 2: UTS and Max Elongation of tissues throughout fracture healing.[5]

	UTS (N/m^2)	Max Elongation
Granulation Tissue	0.1	200%
Collagen Fibers	1-60	17%
Early soft callus	4-19	10-12.8%
Bone	130	2%

2.2.1.3 Remodeling Phase

In the final phase of fracture repair, hard callus undergoes a morphological adaptation to regain the optimal function and strength of intact bone. In humans, 6-9 years can pass until the process completes, and represents 70% of the total healing time. During this phase, the woven hard callus remodels into the required amount of lamellar bone and any excess callus is removed, thereby restoring the medullary canal and bone shape.[11] Bone is arranged in areas experiencing excess stress and removed from areas where there is too little, according to the accepted theory known as Wolff's Law which states that bone structure constantly adapts to the mechanical loads to which it is subject.

Figure 4 shows the phases and time distribution required to spontaneously heal bone. As previously described, the progression of soft to hard callus in spontaneous fracture healing is dependent on the fracture site being supplied with sufficient blood in addition to consistent increase in stability. Without these two factors, fibrous tissue will not advance to hard callus and will lead to an atrophic nonunion. This is typically remedied with the addition of bone grafts or removing the layer of both on the two apposed fracture ends to restart the healing process. If proper vasculature exists without interfragmentary motion control, the fracture will progress into a cartilaginous callus unable to stabilize the fragments and will further progress into hypertrophic nonunion. This is typically remedied with the addition of rigid fixation. When canine bone undergoes spontaneous bone repair, malunion is not uncommon.[5]

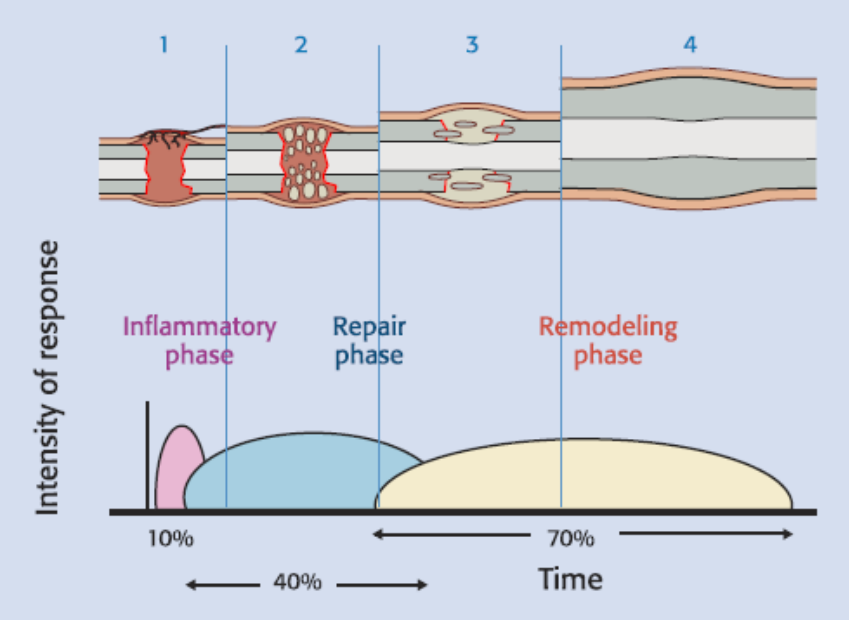

Figure 4: Phase Timeline of Spontaneous Healing.[5]

2.2.2 Healing Under Restricted Motion

Fractures controlled under restricted motion heal in a process intermediate to spontaneous healing of uncontrolled fractures and healing after absolute stabilization. To limit motion at the

fracture gap and minimize the likelihood of malalignment, pins and nails are often implanted. Healing of fractures under restricted motion begins with some resorption of the fragment ends. Primitive implantation methods advised reaming the medullary canal prior to implanting nails, thereby removing bone marrow and disrupting endosteal blood flow. This allowed for the largest possible nail diameter to be implanted in the medullary canal. The initial stability of these implants is attributed to the contact between the nail and the bone's inner cortex, in addition to the screws used to provide rotational stability. The process of reaming prior to implantation, however, decreases the blood supply available at the fracture site by 70%.[14] Since research has established that an appropriate blood supply is required for fracture healing, nailing methods and implants have been modernized to minimize disruption. This includes making optional the reaming of the medullary canal in addition to changes to implant geometry, which together have demonstrated only a 30% reduction in blood supply at the fracture site. Unreaming nails, however, do not offer the initial fixation stability of reaming nails. Some research has shown that the increased blood supply associated with unreamed implants may not correspond to improved healing times.[15] While the restricted motion from IM nailing demonstrates a significant improvement over spontaneous healing, the ossification associated with healing under restricted motion is only about 10% of that associated with plate or external fixator stabilization.[15] Advocates of unreamed nailing believe reaming of the intramedullary canal is detrimental as the endosteal blood flow will be disrupted and may potentially further damage the bone.[15, 16] Though studies have debated the healing success of reamed versus undreamed intramedullary nails, stable fixation remains the most effective form of fracture management as it facilitates direct healing.

External fixators may also be used to restrict motion and are applied using closed reduction techniques while further minimizing vasculature disruption and maintaining stability. The amount of callus formed is minimal but can vary greatly depending on the configuration of the fracture and the rigidity of the fixator frame applied.[5] Variation can occur if the implant is not placed on the tension side of the bone, fracture reduction is not perfect, or if the implant lacks rigidity. These factors are most relevant in fixation of comminuted fractures since fragment ends are more difficult to align properly and mechanical stability greatly influences the course of healing. While closed reduction external fracture fixators offer decreased callus formation, their structure may not provide adequate stability due to the moment created by implant being offset from the body. More importantly, a higher probability of infection exists as the implant must pass through the patient's dermis in multiple locations. Overall, while healing by restricted motion may pose benefits to the healing process over spontaneous healing, increased stability and lack of callus formation resulting from stable fracture fixation is optimal.

2.2.3 Stable Fractures

In 1949, Danis reported that a callus is not formed during bone healing when two bone fragments are apposed under a rigid plate and axially compressed.[5] Application of rigid, nongliding implants, such as compression plates and lag screws results in a stable bone fragment

interlocking connection. It was later confirmed by Schenk and Willenegger that healing under these conditions was the result of direct osteonal proliferation.[5, 17] This repair mode, termed "primary" or "direct" healing, refers to direct filling of the fracture site with bone, without the formation of periosteal or endosteal callus. Rigid fixation and precise reduction suppress the biological signals found through indirect healing methods which attract callus promoting osteoprogenitor cells to the fracture site.

Interfragmentary compression induced by a plating system creates differences in the biomechanical microenvironment within the fracture site and influences the progression of bone development.[5] Contact and compression areas are bounded regions separated by areas where fragments ends are separated by small gaps. A compression plate applied across a fracture site will create two different healing zones. The cortex directly under the plate will experience contact and compression characteristics triggered by the plating system. The far cortex will be exposed to forces in tension and will be subject to gap healing. Both contact and gap healing are mechanisms classified under direct fracture healing. Utilization of plating systems to facilitate primary healing remains the method of choice when fracture healing is required.[5]

2.2.3.1 Contact Healing

Contact healing in stable fractures is observed when the defect between bone ends is smaller than 0.01mm and the interfragmentary strain is less than 2%.[3, 5, 9, 12] Lamellar bone is directly formed as a result of primary osteonal reconstruction and is oriented in the normal axial direction. Cutting cones are cells which form at the ends of the osteons closest to the fracture site. These are seen in Figure 5, adapted from Rüedi et al.[5] Osteoclasts line the head of the cutting cones while osteoblasts line the tail. This enables bony union and Haversian remodeling to occur simultaneously.[5] Osteoclasts advance across the fracture site and create longitudinally oriented cavities in which the osteoblastic ends deposit osteoids. Cutting cone navigation has been reported across canine radial osteotomies under rigid fixation as early as three weeks after surgery. Cutting cones travel across fragments at a rate of 50-100 µm/day and become the "spot welds" which unite the fragment ends without the production of callus.[17] The bone formed during remodeling will be visible on radiographs until bone density at the fracture site reaches that of intact cortical bone.

2.2.3.2 Gap Healing

Direct healing at gaps between 800µm to 1mm occurs in a similar process to contact healing, though bony union and Haversian remodeling remain separate, sequential steps.[9] Healing starts with osteoblasts depositing layers of lamellar bone on both fracture surfaces, perpendicular to the long axis, until the ends unite.[9] This area, however, remains weak due to this bone orientation. Haversian remodeling initiates between three and eight weeks after surgery when osteoclasts form on both fracture ends and create longitudinally oriented resorption cavities. Longitudinally oriented lamellar bone is deposited into these cavities over time by the osteoblast tail of the cutting cone so anatomical and mechanical integrity of the cortex may be reestablished.[5]

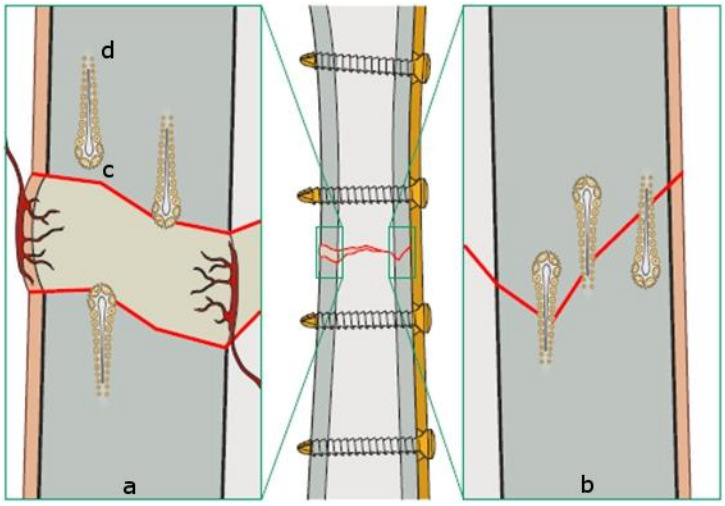

Figure 5: Cutting cones in stable fracture healing.[5]

(a) Gap healing. (b) Contact healing. (c) Osteoclast head. (d) Osteoblast tail.

2.2.4 Bone Response to Mechanical Loads

Contact and gap healing are facilitated by load transferred to the bone fragments. In 1892, Julius Wolff reported his research to explain how the orientation of trabeculae in the femur is established during development.[18] His findings matured into a general means to understanding the gross shapes and adaptations of bone. Often referred to as Wolff's Law, bones constantly grow and remodel to adapt to their mechanical environment.[4, 18-21]

The primary function of bone is to remain stiff and resist deformation from internal muscular and external forces.[18] To maintain its stiffness, bone strength can be increased with added bone mass, a changed geometry to redistribute the acting forces, or altering its microstructure through Haversian remodeling. Intrinsic factors including osteon density, mineral density, porosity, collagen fiber orientation, and histologic structure affect the strength of bone. Loading mode, duration, and rate of strain are extrinsic factors corresponding changes in bone strength. The combination of these intrinsic and extrinsic factors affects bone's mechanical properties and adaptations in response to loading. Bone is a viscoelastic material which responds to mechanical loads differently depending on their magnitude.

Wolff's hypothesis that osteocytes act as strain receptors and transducers has received the most attention in research.[18] When bone experiences a strain of sufficient magnitude to elicit a response, one of four outcomes may result. No osteogenic response may occur if the strain transduces a signal that is below a certain threshold or the receptor is inhibited as a result of aging. A sufficient signal will result in osteoblasts recruited in the periosteum or endosteum to initiate remodeling or osteoclasts recruited along the bone surface to initiate resorption. Finally, osteoclasts and osteoblasts can be activated sequentially to initiate Haversian remodeling, as described in Section 2.2.3.2.[18]

Though the methods of sensing mechanical loads by bone cells are not well understood, there are many indications that strain rate and magnitude are important stimuli effecting bone response.[18, 21, 22] One of the hypotheses regarding the mechanism of mechanotransduction which has received the most attention suggests that osteocytes are mechanosensors of shear stresses.[23] Osteocytes have radiating canaliculi which communicate with other osteocytes through transmitter proteins at gap junctions. Together, these osteocytes form a connected cellular network surrounding the periosteal and endosteal membranes. These cells further connect to osteoblasts lining the periosteum and endosteum which connect to preosteoblasts in the membrane. Together, this network effectively creates a nervous system in the bone which controls nutrient flow and initiates bone remodeling when activated.[18]

2.2.5 Stress Shielding

As described by Wolff's law, mechanical loading of bone stimulates the initiation of Haversian remodeling. One issue observed with the introduction of rigid fixation systems is bone refracture after implant removal. Researchers have attributed this to bone atrophy as a result of the fixation system bearing a majority of the load, and not the bone.[24] This phenomenon has been termed stress shielding.

Stress shielding is a common occurrence with rigid fixation systems and results in a loss of bone mass around the area where a plating system is applied.[12] The effects of this are apparent when a system is comprised of two or more components, as these components typically have different moduli of elasticity.[25, 26] An applied bone plating system, for example, creates a system comprised of the fractured bone, fixation plate, and plate screws as the components, which may all have different moduli of elasticity. When a load is placed on this system, the stiffer component bears more of the load, thus "shielding" the other components.[25] Research has suggested that fixation of fractured long bones with a plating system leads to osteoporosis and the possibility of fatigue fracture after its removal.[25] Immature bone formation and thinning of the cortical wall have been found at fracture sites shielded from loads by an apposed rigid plate.[25] As a system's material and geometry determine its stiffness, minimizing the effects of stress shielding will require a system's stiffness to be near that of bone. Preliminary clinical research, however, has shown promise in the use of internal fixators for stable fracture repair.[27]

A study conducted by Tonino et al. in the early days of rigid fixation compared the effects of stress shielding in canine femurs by fixing six canines of similar weight with two different implant systems: the right femur with one comprised of stainless steel (SS) and the left femur with one of polytrifluormonochloroethylene (PTFCE). After harvesting and evaluating the femora, the femora fixed with the SS implant had significantly lower bone mineral mass per centimeter.[25] This occurred due to both bone resorption and only partial mineralization of the newly formed bone. Microradiographs of the cross-sectional area of bone healed with the SS system had larger resorption cavities, thinner lamellae and less woven bone formation than that of the PTFCE plate. This can be seen in Figure 6, adapted from Tonino et al.

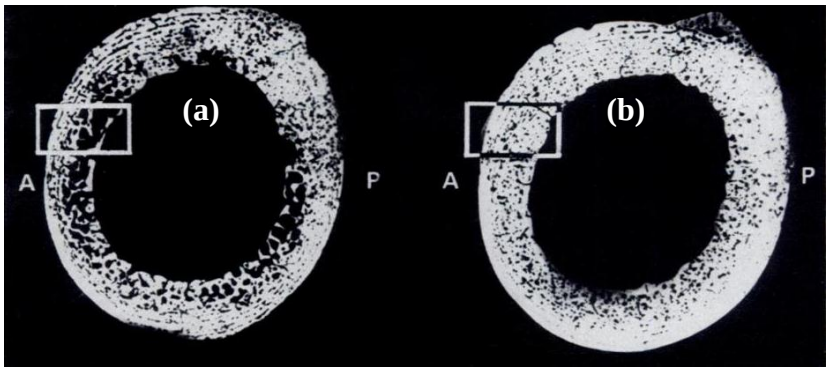

Figure 6: Microradiographs of plated femora. (a) SS plate (b) PTFCE plate.[25]

Mechanical testing confirmed these observations impacted the bone's strength as the femora healed with SS plates required a 30% lower force to fracture, 22% lower bending strength, and 20% lower modulus of elasticity than those healed with the PTFCE plate. The observed histological and mechanical differences are entirely due to the plate material as both systems had the same geometry and application area. It can therefore be concluded that the material composition of the SS plating system played a role in the stress shielding effects observed by the femora. Similar results have been reported by Diehl and Mittelmeier who observed a loss of function in tibias healed with stainless steel plating systems. They found the load required to fracture the bone to be one-third that of intact bone.[25] The effects of stress shielding are further amplified with systems disrupting bone's surrounding vasculature as this prevents bone growth beneath the plate. Recent plating system developments have attempted to address the issues surrounding stress shielding by changing plate material and geometry.

2.2.6 Fracture Types

Break in the continuity of bone is classified as a fracture. When caring for the diaphysis of long bones, two fracture types may be observed, undisplaced or displaced.[28] In undisplaced fractures, bony fragments are still in their anatomical position, have cracks present, and do not require any reduction.[28] Displaced fractures may be further classified into five categories: transverse, oblique, spiral, comminuted, and segmental. Transverse fractures are found perpendicular to the long axis of bone and may occur due to numerous factors. Failure may occur under tensile or bending loads, a direct strike to the bone, or an indirectly delivered force as may be seen from a fall from significant height. Trauma to the bone may result in the fracture becoming more comminuted with progressively greater force.[28, 29] Oblique fractures are characterized by an oblique line found at 30-45° from the long axis and are typically the result of combined bending and torsional forces.[28, 29] Bone failure as a result of torsional forces is a test of its mechanical properties in shear and tension. The torque moment creates a state of pure shear between parallel transverse planes and tension and compression forces at all angles in between. These forces both come to a maximum at 45° to the long axis of the bone, which when great enough to produce a fracture, result in a spiral shaped line.[29, 30] This type of fracture may be observed, for example, in cases where a canine paw becomes lodged while running,

indirectly distributing a torsional load to its long bones. A comminuted fracture is one where more than two bone fragments exist, typically including small wedges and small fragments which are nonreducible.[29, 31] Segmental fractures are a type of comminuted fracture where the fragments are whole and large enough to be anatomically reconstructed.[5] Figure 7 depicts these fracture types.

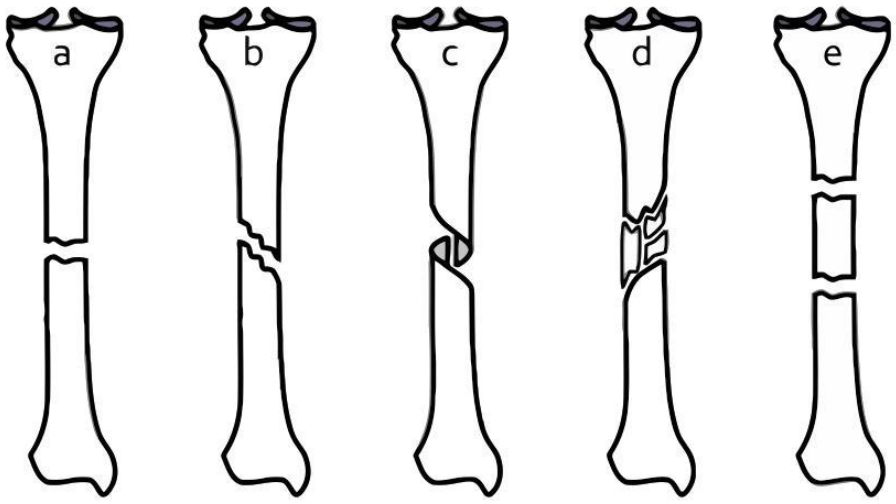

Figure 7: Fracture Types: (a) Transverse (b) Oblique (c) Spiral (d) Comminuted (e) Segmental.

2.3 Plating Systems

Screws and plates are used to achieve bony union of two or more fragment ends of a fracture, whether surgery is performed with Open Reduction Internal Fixation (ORIF) or Minimally Invasive Plate Osteosynthesis (MIPO) techniques. Depending on the type of fracture, different plates may be used to facilitate the proper healing function. Plates may accommodate conventional or locking screws. Multiple screw types may be used to attach a plate to bone. These include cortical and cancellous screws with self-tapping or standard threads, and may have locking heads. There are two plate types which can be applied: conventional and locking.

2.3.1 Screws

When choosing screws for plate application, veterinarians are recommended to utilize a screw diameter should not exceed 40% of the fractured bone diameter to prevent a decrease in bone strength.[5] Conventional or locking head screws may be chosen for implantation depending on the plate being applied. A standard screw is depicted in Figure 8 and a locking head screw in Figure 9. Conventional screws are adapted to accommodate both cancellous and cortical bone. Cancellous screws have a relatively thin core with wide and deep threads, while cortical screws have a relatively thicker inner core with shallower threads. The increased ratio of the outer diameter to inner core of the cancellous screws allow for a significantly greater holding power in the trabecular bone of the metaphyses and epiphyses. Cortical screws are typically used in bone diaphyses. They can be fully threaded when used to fix plates to bone or partially

threaded when used as a lag screw. Lag screws are used when interfragmentary compression between bone fragments is required.[5]

2.3.1.1 Self-Tapping Screws

Self-tapping screws are designed to be screwed into bone after a pilot hole has been drilled. Self-tapping screws cut a thread into bone as they are being fastened. While self-tapping screws may be removed and reinserted, they are best used in applications where applied only once since an inadvertent misalignment after removal will destroy the previously cut thread and may cause premature failure of the plate.

2.3.1.2 Standard Screws

Standard screws are used in conventional plates and when a need to replace or reposition the screw along the healing process is anticipated. A pilot hole is first drilled into the bone and then threads are cut into the hole using a tap corresponding to the threads on the screw being used. Standard screws may be removed and reinserted with ease and without fear of inadvertent thread damage.

2.3.1.3 Locking Head Screws

Locking head screws may have standard or self-tapping threads on their core in addition to having threads surrounding the head of the screw. The screw head locks into the plate hole threaded to accommodate them. The threads on the head incorporate a different pitch and diameter than those on the core and thus provide a greater resistance to pullout and the ability remove any compressive forces between the plate and the bone. This is essential in preventing the disruption of vasculature around the affected site. Furthermore, as plates may sometimes be contoured and angled to better fit their application, these screws guarantee the plate's location is undisturbed.

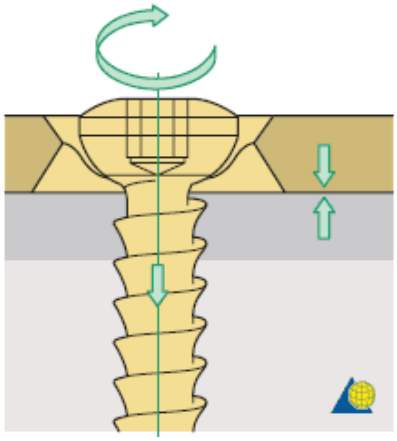

Figure 8: Conventional Screw.[32]

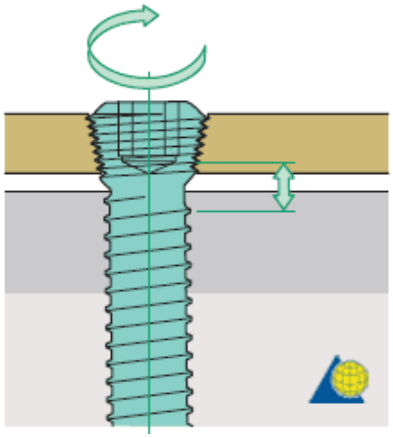

Figure 9: Locking Head Screw.[32]

2.3.2 Plates

Plates are designed to facilitate one or more of the following functions in fracture fixation: compression, neutralization, bridging, or buttress. Compression plating generates axial forces by use of a tensioning device or eccentrically loading screws. This mode is typically used in simple transverse fractures and those with low obliquity. If a diaphyseal fracture is fixed with a plate and screws to not produce any compressive axial forces, the system functions in a neutralization mode.[33] In addition, as lag screws may be used to fix fragments in comminuted fractures, a plate applied in neutralization mode protects the interfragmentary compression of the fragments from any rotational, bending, or shears forces when loaded.[5] A plate functioning as a buttress is applied to metaphyseal fractures to prevent the collapse of fragments when the articular surface is exposed to compressive forces.[5] A plate functioning as a bridge is applied when indirect reduction of bone is required, as in comminuted fractures. It functions as a splint to maintain correct length of the bone and normal joint alignment when fixing the fragment ends as it prevents axial deformity as a result of shear or bending forces.[5] Since the plate gets subjected to full weight-bearing forces, it is important that the soft tissue surrounding the fragments maintain their vascular supply as the success of indirect reduction is dependent on the formation of the bridging callus.[5] In all plates depicted below, the top panel shows the top surface of the plate, and the bottom panel shower the underside surface.

2.3.2.1 DCP

The dynamic compression plate (DCP) was first introduced in 1969 and featured unique hole geometry which allowed for axial compression by eccentric screw insertion and is available in stainless steel.[5, 34] The success of bone healing utilizing this plate is dependent on the friction between the plate and the bone to generate a rigid internal fixation. This plate may facilitate healing modes by compression, neutralization, bridging, or buttress. When the screw is inserted into the plate and tightened, the bone fragment moves relative to the plate and consequently compresses the fracture ends axially. The shape of the holes allows for a 25° inclination of the screws longitudinally, and 7° transversely.[5] DCP's plate holes are symmetric and evenly distributed, allowing for versatile and eccentric placement of screws. This allows compression at any part of the plate and is advantageous in segmental fractures. Different drilling guides are available for different plate sizes and for the facilitation of eccentric and neutral screw loading. This plate can be seen in Figure 7.

Recent studies have shown that implementing the DCP plating system may be detrimental to bone healing. Use of this system is now associated with a surgical technique that causes the plate to disrupt the blood supply underneath the plate, thus leading to delayed healing, nonunion, or an increased chance of bacterial infection.[35] Compromising the periosteal blood supply is a key disadvantage of using this system, and a factor which should be taken into consideration by the surgeon before deciding on an implant system.

Figure 10: Dynamic Compression Plate

2.3.2.2 LC-DCP

The low contact dynamic compression plate (LC-DCP) seen in Figure 11 is an advancement of the DCP system and is available both in stainless steel and titanium.[5] The LC-DCP was developed to alleviate some of the disruption to the periosteum seen with the DCP system. The geometry of the LC-DCP system accomplishes this by allowing 50% less contact with the bone that would otherwise be achieved with the DCP plate.[35] This geometry improves cortical perfusion and integrity of vasculature beneath the plate. The scalloped configuration of the plate's underside facilitates this and more evenly distributes load across the bone, allows contouring of the plate easier, and minimizes the possibility of damaging the screw holes when being contoured.[5, 35] When used in a buttress or bridging configurations, the plate geometry facilitates a distribution of load results in a minor elastic deformation of the plate without stress concentration at any of the screw holes, as would be present in DCP.[5] While this is an improvement from the DCP plating system, LC-DCP still requires compressive axial forces along the bone fragments and periosteum to facilitate proper healing.

LC-DCP has similar characteristics to DCP. LC-DCP's plate holes are symmetric and evenly distributed, allowing for versatile and eccentric placement of screws. This allows compression at any part of the plate and is advantageous in segmental fractures. Screws may be placed up off-axis up to 7° transversely and 40° longitudinally, allowing more screw angulation freedom than DCP. The screws may be placed similarly to the DCP to facilitate compression, neutral, bridging, and buttress healing modes.[5] Similar to the DCP, various drilling guides are available for various screw loading techniques. As both DCP and LC-DCP plates both have the potential to disrupt vascularity, their efficacy may vary between patients.

Figure 11: Low Contact Dynamic Compression Plate

2.3.2.3 LCP

The locking compression plate (LCP) is a unique implant as it incorporates the vascularity-preserving underside geometric advantages of the LC-DCP system while eliminating the need for compressive forces to be applied to the bone. This is achieved when using locking

head screws, though LCP is a combination hole plate which accommodates standard screws as well.[36] One-half of each hole is designed to accommodate the standard DCP and LC-DCP screws for fragment compression while the other half accommodates the locking head screws, advantageous for angular stability and removal of compressive forces from the bone fragment surfaces. As locking head screws have a larger core diameter, their use increases bending and shear strengths while displacing the load across a larger area across the bone. Use of locking head screws reduces the priority of perfectly contouring the plate due to the angular stability produced.[36] This plate is illustrated in Figure 12.

In vitro biomechanical testing was conducted in a study by Aguila et al. comparing the LC-DCP and LCP plates when fixed to 14 pairs of femora with a 20mm osteotomy gap. No significant difference in structural stiffness of both plates was found in four-point bending. The LC-DCP system was found to be significantly stiffer when tested in cyclic torsion.[36]

Figure 12: Locking Compression Plate

2.3.2.4 SOP

The string of pearls (SOP) plating system, illustrated in Figure 13, is a newer, stainless steel locking plate system designed both for veterinary and human use. Though it is a locking plate, it is secured using standard screws. Holes in the spherical "pearls" of the plate have threads which correspond to those on the core of the screws. As the screw is secured to the plate, it threads into the pearls and thus allows the screw to be properly torqued while removing any compressive force acting on the bone. The SOP system is similar to that of the LCP as they both locking plates which serve to minimize damage to the periosteal blood supply and minimize the need for plate contouring to the bone. The SOP plate is comprised of cylindrical internodes connecting the spheres, which have a greater moment of inertia over the DCP, LC-DCP, and LCP plating systems due to their geometry. The internodes are 5mm in diameter while the spheres are 8mm in diameter for all plate lengths. These cylindrical components allow the plate to have up to six degrees of rotational freedom when contouring is necessary.[37] The design of these components also prevents potential deformation of the screw holes when being contoured, a drawback to the flat locking plate systems.

In a four-point bending study conducted by Ness, the SOP plating system attained a higher bending stiffness, bending structural stiffness, and bending strength than the DCP system.[37] Further testing was conducted comparing bent, twisted, and contoured SOP plates to the untouched DCP plate. The results of these tests demonstrated that the twisted and contoured SOP plate maintained higher strength and stiffness properties. No significant difference was

found between the mechanical properties of the bent SOP plate and the untouched DCP plate.[37] Another study conducted by Ness evaluated the outcome of humeral fracture repair in canines with a mean weight of 22.8 kg where two SOP systems were applied to the fracture. Postoperative analysis of the thirteen canine humeri demonstrated satisfactory function of the repaired limb in 12 of the 13 canines.[38] Additional surgery due to complications was recorded in four canines, three of which demonstrated satisfactory function after healing. Refracture was only evident in one canine. No screw loosening, backing out, or breakage was observed in the 115 SOP screws used for fracture fixation.[38] While the functional outcome following surgery was excellent in most cases, no bone density analysis was performed analyzing the healed bone.

Figure 13: String of Pearls Plate.

2.3.2.5 Fixin

Fixin is a novel locking plate system which incorporates a bushing insert between the screw-plate interfaces. It facilitates locking by creating a friction fit between the conical bushing and screw head as the bushing threads screw into the plate and the screw threads into the fractured bone. The bushing's titanium make-up allows for easier removal of the implant as the any concern of removal complications resulting from cold welding, cross threading, or damage to the hexagonal screw recess previously reported with other locking plate systems.[39] This combination of features allows the Fixin plating system to be angularly stable, simple to apply, and easy to remove when necessary.

The Fixin plate is made of stainless steel and has threaded holes for the titanium bushing inserts. The screws used in this plating system are typically stainless steel, self-tapping, and are used in a locking mode. They have a larger core diameter to increase bending and shear strength while also improving load distribution along the bone. The head of the screw incorporates a conical surface matching that of the titanium insert, allowing stability through friction, microwelding, and elastic deformation.[39] While no previous studies have been found evaluating the stability and stiffness of this system, typical patients are canines and felines weighing up to 10kg. This is illustrated in Figure 14.

Figure 14: Fixin Plate

2.3.2.6 ALPS

The Advanced Locking Plate System (ALPS) is a novel system incorporating a uniform cross-sectional moment of inertia along the entire length of the plate due to its geometry where the screw hole sections are wider than those connecting them.[40] The profile of this plate also allows for improved periosteal blood flow in comparison to standard plates as there is minimal contact with the bone.[40] The scalloped geometry and titanium makeup allow for increased resistance to infection and deceased healing time as contact with the bone is decreased.[40] The screw holes on the plate allow for standard screws to be placed in various angulations, or locking head screws in fixed angulation. The locking mechanism of the hole functions by engaging the threads on the screw shaft. As the screw reaches its last few threads by the screw head, the thread diameter is reduced and the plate is pulled toward the bone when the locking mechanism is fully engaged.[40] The conical interface between the screw heads and plate hole also allows both screw types to be held in a stable position.

The manufacturer of this plating system, Kyon Pharma Inc., claims the strength of their ALPS10 plating system is higher than that of the 3.5 DCP system.[41] In a study case report written by Inauen et al., an ALPS5 plate was implanted into a two-year old feline to repair the left hind limb lameness caused by a separation in an arthrodial joint of its foot. Five days post-surgery, the owner reported no apparent lameness, and unrestricted activity was allowed.[40] The surgeon had initially advised two weeks of cage rest followed by three weeks of restricted activity. Clinical examination six weeks after surgery proved the feline was without lameness and its left tarsus was stable and not swollen.[40] Furthermore, radiographs depicted uneventful healing. As a result of this study, the ALPS system is shown to be effective in conditions where standard compression plates may be applied for healing.[40] ALPS10 and ALPS11 are depicted in Figure 15 and Figure 16.

Figure 15: Advanced Locking Plate System #10

Figure 16: Advanced Locking Plate System #11

2.3.3 Fixing Plates to Bone

In summary, conventional plates require compressive forces to be applied to the bone fragments, require contouring to the bone, and may disrupt the bone's surrounding vasculature

depending on the geometry of the plate's underside. Locking plates do not require compressive forces to be applied to the bone and also do not require exact contouring to the bone to facilitate adequate healing and as a result of no compressive forces being applied to the bone, the bone's surrounding vasculature is preserved. However, due to their geometry and the method of application, locking screws cannot be applied eccentrically in these plates to provide compression at the fracture site.

When plating systems are required to heal bone fracture, Open Reduction Internal Fixation (ORIF) or Minimally Invasive Plate Osteosynthesis (MIPO) techniques may be employed to secure plates to bone. To allow proper alignment, ORIF utilizes direct reduction techniques as the fracture site and surrounding tissues are exposed. This is typically achievable with transverse, oblique, segmental, and comminuted fractures with one to three reducible fragments.[5, 28] This treatment allows fragments to be perfectly aligned, but comes at the cost of increase healing time due to the disruption of surrounding tissues. Plates fixed to these fracture types will act in compression or neutralization modes. MIPO utilizes indirect reduction techniques to align fracture fragments without exposing the fracture site or disrupting the periosteum, thus maximizing the healing potential of the fracture site.[42] Reduction instruments are inserted through skin incisions made near the fracture to align the fragments.[42] After proper alignment, a plate is inserted through the incisions. Incisions are then made over the area of the plate where screws are inserted. This is typically performed in undisplaced or highly comminuted fractures.[42] Plates fixed to these fracture types will act in bridging or buttress. Fractures reduced by direct reduction will be healed via direct healing.[5, 9] As anatomical reconstruction is not possible in fractures reduced by indirect reduction techniques, these fractures will heal via indirect healing.[5, 9] The correct plating system to stabilize a fracture is dependent on the required fixation mode.

Plate size is typically dependent on the diameter of the fractured bone and the patient's weight, but is chosen at the surgeon's discretion. Screw size is dependent on the requirements of the plate being applied as the screw holes accommodate a certain size. After choosing the appropriate plate and screw, a pilot hole is drilled for the chosen screw size using a drill bit and drill sleeve for accurate alignment. While conventional plating systems allow the surgeon to angulate the applied screws when inserted, studies have shown that insertion perpendicular to the plate provides the highest resistance to pullout in normal bone and forty degrees off-axis the lowest.[43] Different types of drill guides may be used to facilitate the intended function of the plating system. These include a universal guide to center the drill in the plate hole for a Neutrally applied screw for Neutralization, Bridging, and Buttress modes and an eccentric guide to offset the drill to enable Compression mode.[5] Figure depicts the difference in screw application using the two guides. When securing holes in an eccentrically drilled screw hole, the fragment ends of the fracture being secured glide toward each other and apply a compressive force at the fracture site. This is only possible in fractures that are transverse or minimally oblique, to ensure the fragment ends do not slide when exposed to compressive axial forces along the bone.

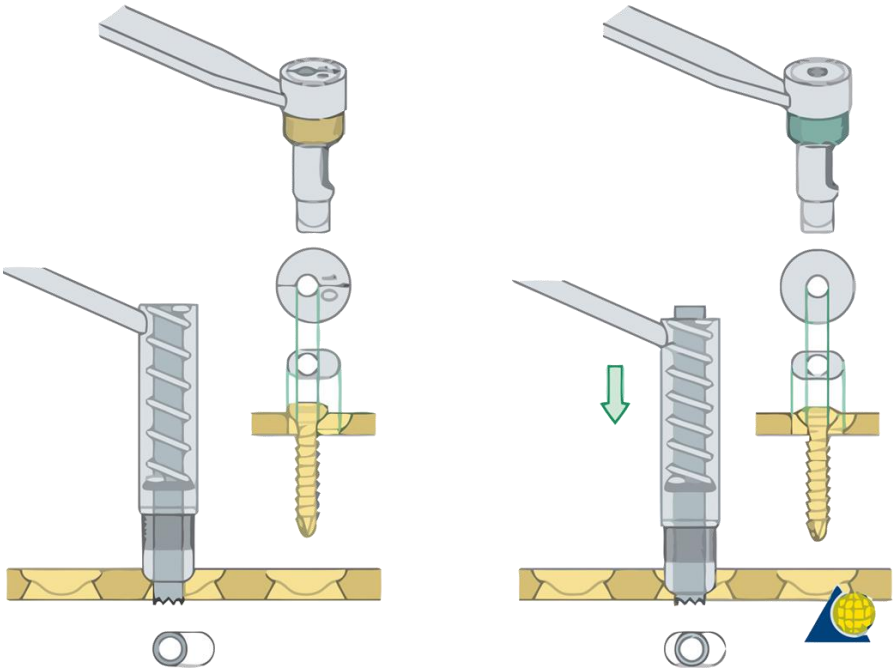

Figure 17: Eccentric Drill Guide (Left). Universal Drill guide (Right).

The hole depth is measured and the correct screw length is used. If the correct length is unavailable, the next longer screw is chosen. If a standard screw is being applied, threads are first tapped in the hole and the screw is then inserted through the plate and bone and tightened with a torque-limiting screwdriver. This process is repeated for the remaining screw locations chosen by the surgeon to fit the plate to the bone. To ensure axial alignment of the plate to the bone, screws are first applied at the ends of the plate most distal to the fracture site. Screws are then applied to the holes most proximal to the fracture and then to the remaining holes chosen to secure the plate to the bone.[5] Alternatively, if the alignment is straightforward, the surgeon may choose to first fix the plate to the bone at the holes most proximal to the fracture gap, and then alternate sides moving toward the end of each plate. Regardless of the procedure used, screw torque is confirmed after all have been seated. These two securing methods are labeled as “A” and “B” in Figure 18.

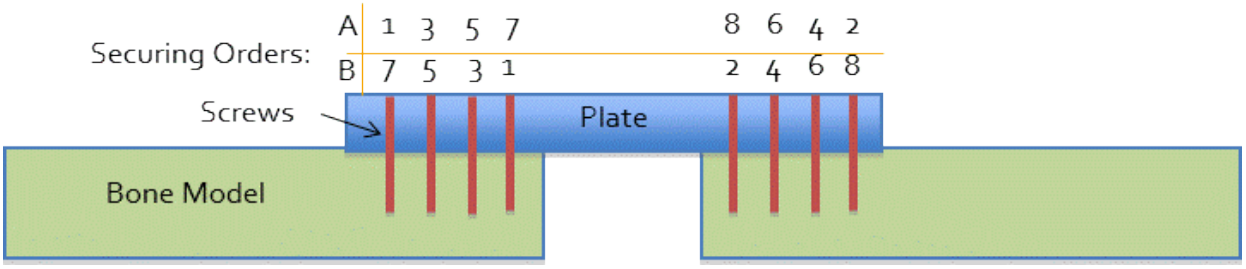

Figure 18: Screw Securing Orders "A" and "B".

2.4 Bone Loading

There are four predominant mechanical testing methods used in the evaluation of bone and plating systems: tension, compression, bending, and torsion. These sufficiently calculate various mechanical properties of bone.

2.4.1 Tension

Tensile testing is a simple method of determining the mechanical properties of both cortical and cancellous bone, though the specimen required is usually large. Prior to testing, specimens are modified to form a dog bone-like shape to ensure a uniform strain in central portion of the specimen. This test is not physiologically relevant as in vivo bone is not primarily loaded in tension, though it may still be used to calculate Young's modulus, ultimate strength, and yield strength.[6, 30]

Only a limited number of studies evaluate the tensile properties of healing bone. In one study, bone healing was investigated in an osteotomy of the diaphysis of the right sheep metatarsal as a function of gap size and stability. Specimens containing callus were evaluated nine weeks after surgery and were found to have a decreasing tensile strength with greater initial interfragmentary gap.[44] For example, a one millimeter initial gap corresponded to a tensile strength eight times lower than normal bone; a six millimeter gap resulted in a tensile strength 36 times lower than normal bone.

2.4.2 Compression

Compression testing is more commonly used to test cancellous bone as this is its most physiologically relevant loading mode. Compression tests are advantageous as they require smaller specimens compared to tensile tests, thus simplifying the mechanical testing. Most importantly, compression testing more closely simulates in vivo loading conditions, especially in vertebrae.[6]

Similar to tensile testing, few studies have reported compressive properties of healing bone. The same study analyzing tensile properties of healing bone collected from a transverse osteotomy in the midshaft of sheep metatarsal nine weeks after surgery reported compressive testing results. Testing showed a great variation in mean indentation stiffness depending on callus location, gap size, and stability.[44] A similar technique was used in a study using the canine femoral osteotomy model. Specimens showed an increase in indentation stiffness from 2% to 25% from two to twelve weeks after surgery. The change in local stiffness over time also correlated significantly to the increase in maximum torque and torsional stiffness.[45]

2.4.3 Bending

Bending tests can be performed either in three-point or four-point loading modes. Three-point bending involves a simply supported beam with one load applied between the supporting ends. Four-point bending applies two loads between the supporting ends. Bending tests allow tensile stresses to be present on one side of the specimen while the other side experiences

compressive stresses. As bone is usually weaker in tension than in compression, failure most commonly occurs on the tensile side of the specimen.[6] Bending is an essential test when evaluating bending strength and stiffness properties of long bones.[6, 7]

Three-point bending is a common test, but causes a high shear stress near the middle section of the specimen. With the addition of a second, equally-spaced, load applied to the specimen, pure bending is achieved in the middle section of the specimen without the presence of transverse shear stresses. Stress, strain, and Young's modulus can be calculated as well, in addition to structural stiffness of the bone. A study conducted on healing metatarsal bone nine weeks after surgery evaluated its bending stiffness and showed that bending stiffness increased in specimen with smaller gap sizes and higher fixation stability.[6, 44]

2.4.4 Torsion

Torsion tests are an effective way of measuring biomechanical properties of bone in shear. When loaded, shear stress varies from zero at the center of the specimen, to the maximum at the surface.[6] Shear stress and shear modulus are properties which can be calculated from acquired torsion data.[46] Depending on the requirements of the test, structural strength, fatigue strength, and stiffness can be calculated. This is depicted in Figure 19(c),(d).

A study conducted by White et al. defined four different stages of fracture in torsion during the process of bone healing. Using the rabbit tibia as a model, partial and full failure was found to occur through the original fracture site during low and high callus stiffness. Paavolainen et al. performed a study analyzing the mechanical properties of tibio-fibular bone fixed with a DCP plate. It was found that the torsional stiffness, strength, and toughness of healing bone peaks between six and nine weeks after surgery. Waris performed a similar study where a DCP plate was fixed to rabbit tibio-fibular bones. It was found that the torque moment at fracture, energy absorption, rigidity, and angular deformation increased from 3 to 12 weeks after surgery.

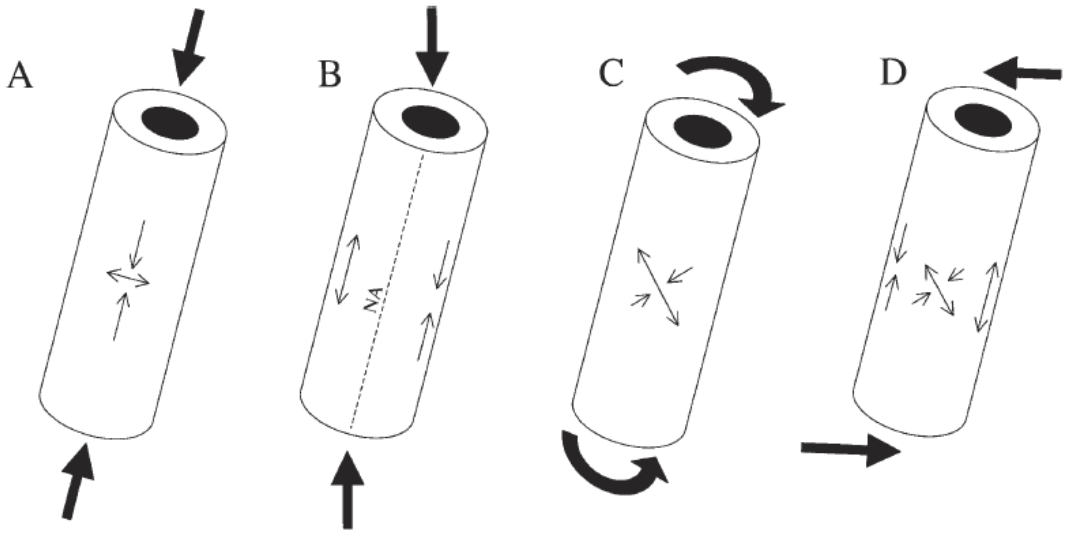

Figure 19: Bone Loading. (a) Axial tension/compression. (b) Bending. (c) Torsion. (d) Shear. Adapted from Athanasiou et al.[6]

2.4.5 Plating System Load Distribution

As a result of applying an internal fixation system to bone, additional forces and stresses interact with the system and are dependent on the design of the system and the loading mode. These load distributions are an important consideration when designing an implantable plating system.

When subjecting bone to axial compression and bending loads, additional force interactions are present in the system. Figure 20 depicts the forces associated with applying a conventional plate, as observed by the additional forces at the plate/bone, plate/screw, and screw/bone interfaces due to the compression and friction forces created. The additional forces present in fractures secured with a locking plate system, as seen in Figure 21, are at the screw and bone interface as no contact or compression is required between the plate and the bone.

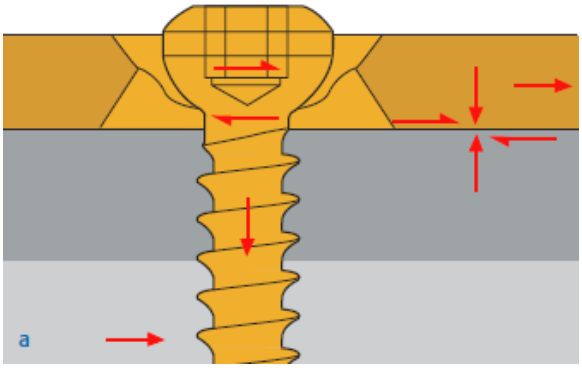

Figure 20: Axial and Bending Load Distribution for Conventional Plating Systems.[5]

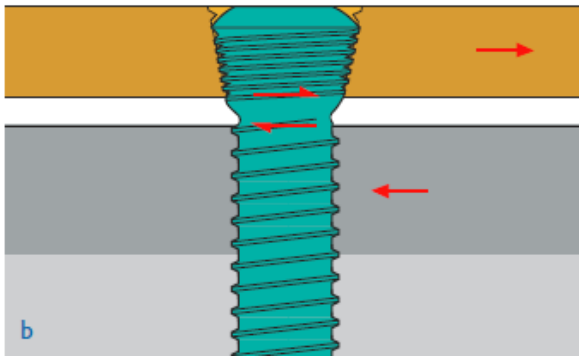

Figure 21: Axial and Bending Load Distribution for Locked Plating Systems.[5]

Similarly, when subjecting the systems to torsional loads, Figure 22 and Figure 23 are adapted from Gautier and Sommer and depict the additional force interactions in these systems.[47]

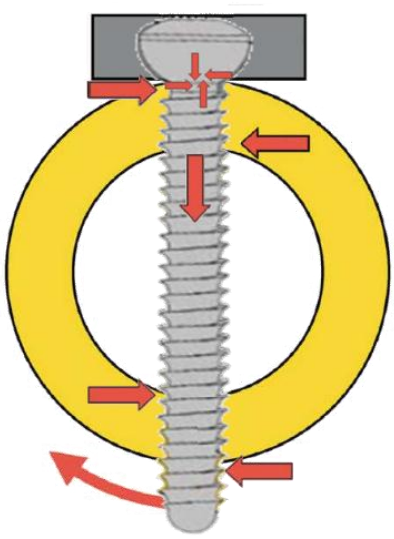

Figure 22: Torsion Load Distribution for Conventional Plating Systems. Adapted from [47].

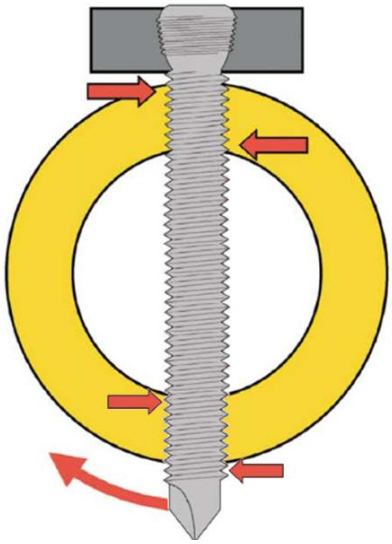

Figure 23: Torsion Load Distribution for Locked Plating Systems. Adapted from [47]

2.5 Bridging the Gap

Unlike medical devices for humans, no regulations exist in the Federal Food, Drug, and Cosmetic Act under the FDA requiring evidence of the safety and effectiveness of veterinary devices. Although several studies evaluate the functionality of one or two plating systems, no research has been conducted evaluating the mechanical properties of each plating system in a standardized fashion. Mechanical and clinical evaluation of plating system mechanics and bone healing effectiveness will allow for a better understanding of system behavior in vivo and will pronounce their benefits and faults. Evaluation of the eight most prevalent plating systems will help veterinary surgeons better treat their canine patients with the optimal device for the fractured bone by identifying plating characteristics which both support and inhibit fracture healing.

3. Goals

The most prominent loading modes experienced by bone are bending and torsion. To simulate this loading, two types of mechanical tests will be performed: four-point bending and torsion. Mechanical tests will be conducted simulating a comminuted femoral fracture with a plating system bridged across the gap. To diminish any variation with regard to bone geometry, implant placement, implant shape, and gap size, a standardized model must be used. Through the normal gait of canines, numerous forces act upon their bones translating primarily to a combination of bending and torsional forces. Though the exact mode and intensity of loading is not known, it is important to analyze the response of the plating systems to these loading types.[48, 49] As described in ASTM F382, Standard Specification and Test Method for Metallic Bone Plates, cyclic loading should allow for one million cycles to be placed on the plating system without causing failure. Though it is important to analyze the cyclic loading properties in each loading mode, testing machine limitations will allow us to only conduct cyclic loading in torsion. The only previously conducted testing on these plating systems evaluated their single cycle to failure properties in torsion. In this evaluation, we will determine the various mechanical properties of these seven plating systems when simulating a comminuted fracture utilizing a synthetic bone model.

3.1 Specific Aim 1

Evaluate the mechanical properties of eight plating systems in single cycle to failure four-point bending.

Utilizing ASTM F382 as guidance, four-point bending tests will be conducted to evaluate the mechanical properties of the various plating systems. The bending stiffnesses and strengths will be calculated for each construct and compared to determine if any significant differences exist. Furthermore, failure modes of each plating system will be noted. Due to limitations in the equipment used for the acute four-point bending tests, cyclic loading will not be performed at this time.

3.2 Specific Aim 2

Evaluate the fatigue strength of seven plating systems in cyclic torsional loading.

A previous evaluation has identified the acute failure torque in these systems.[50] Utilizing the staircase method, samples will be cyclically torqued for evaluation. This will allow us to ultimately determine the fatigue strength of each plating system utilizing probability plots and Dixon-Mood analysis. Furthermore, failure modes of each plating system will be noted.

4. Experimentation

Acute failure properties were evaluated for eight plating systems using four-point bending tests. Seven plating systems were evaluated for their fatigue strength using cyclic torsion tests. While limited biomechanical data exist for a few of these systems, no data exist evaluating them in a standardized manner. Samples were assembled in a fashion to simulate a comminuted fracture utilizing a synthetic bone model as the fractured bone fragments and plating systems to span the fracture gap.

4.1 Bone Model

To remove variability encountered with cadaveric bone, a synthetic bone model was used in the mechanical testing. Short-fiber filled hollow epoxy (SFE) cylinders were previously validated to simulate the mechanical properties of bone.[51] This study compared the elastic modulus, maximum stress, and yield stress of synthetic bone models of various dimensions to published pit-bull and greyhound femur, humerus, and tibia results.[8] Based on their results, the bone model with a 20mm outer diameter and 3mm wall thickness best represented these mechanical properties of native bone. The model used is depicted in Figure 24.

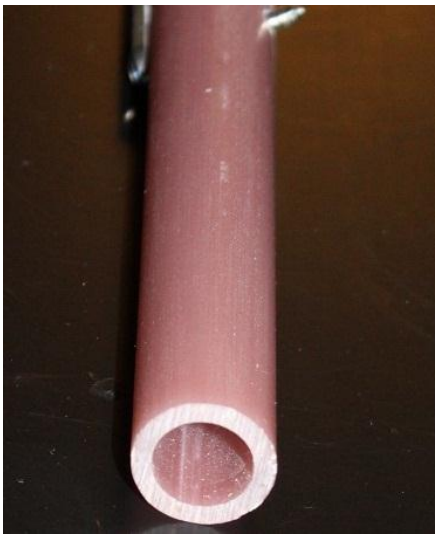

Figure 24: Bone Model Cross-Section.

4.2 Plates and Screws

Eight different plating systems were evaluated when used as a bridging plate and tested in acute four-point bending, while only seven of these plating systems were evaluated in cyclic torsion. While both SS and TI LC-DCP systems were evaluated in four-point bending, only the SS LC-DCP system was evaluated in torsion due to limited sample quantities. These systems included two conventional, four locking plates, and one combination standard/locking hole plate. These plates were secured to the bone model with the appropriate screws corresponding to the manufacturer's specifications. These included standard and locking screws for both monocortical and bicortical purchase. Table 3 below summarizes the properties of the plates and screws used. It should be noted that only the locking holes were used in the combination hole LCP plate. In

addition, bicortical screws were used secure the ALPS plates at the hole most distal to the fracture gap on both bone model segments and monocortical screws were applied to the remaining holes. For all systems, stainless steel plates were mated to stainless steel screws while titanium plates were mated to titanium screws. Although, these plating systems differ in their screw hole spacing, screw size, and number of screws used to secure the plate to the bone, all available screw holes on the plate are used when assembling the samples. As this method is followed for all plating systems, it maintains uniformity in the sample assembly and allows for a comparison to be made between all plating systems without accounting for screw density. Screw density is the quotient formed by the number of screws inserted and the total number of plate holes, typically recommended to be below 0.5.[5] For plates smaller than twelve holes, screws should be applied to at least three holes per fragment.

Table 3: Plate and screw system features.

Plate	Screw/Plate Size	Plate Hole	Screw type	Cortex Penetration	Plate/Screw Material
DCP	3.5mm	Conventional	Standard	Bicortical	SS
LC-DCP	3.5mm	Conventional	Standard	Bicortical	SS/Ti
LCP	3.5mm	Conv/Locking	Std/Locking	Bicortical	SS
SOP	3.5mm	Locking	Standard	Bicortical	SS
Fixin	3.0/3.5mm	Locking	Locking	Bicortical	SS
ALPS10	2.7mm	Locking	Locking	Mono/bicortical	Ti
ALPS11	4.0mm	Locking	Locking	Mono/bicortical	Ti

4.3 Assembly tools

Numerous tools were required to assemble all the samples. Two custom jigs were designed and manufactured to aid the veterinarians in uniformly assembling test samples. A drilling guide was fabricated to stabilize the bone models while aligning and fastening a plating system. A one-inch long SFE tube was used between the bone fragments to maintain a fixed distance between the bone models. The gap created is larger than that observed in previous tests, thus testing the construct more strenuously and mimicking a bridging osteosynthesis.[36, 52, 53] These are seen in Figure 25. A torque-limiting screwdriver, drill, and the required drill bits and bit sleeves were also used to aid in assembly. All samples were assembled by a veterinarian to ensure compliance with manufacturer and surgical specifications.

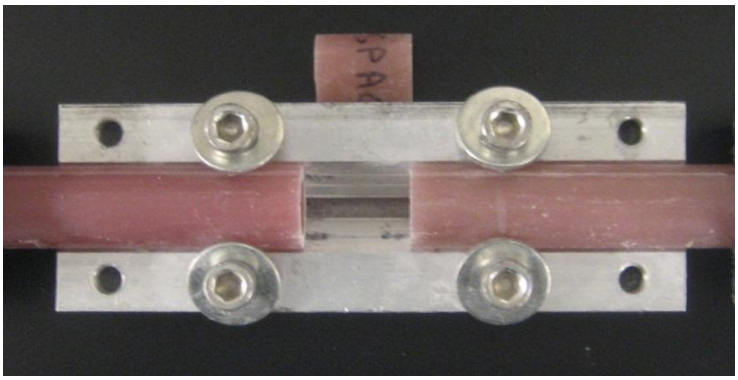

Figure 25: Drilling Guide and Spacer.

A centering jig was developed to ensure bone models are properly centered when potting bone models for torsion samples. This is pictured in Figure 26.

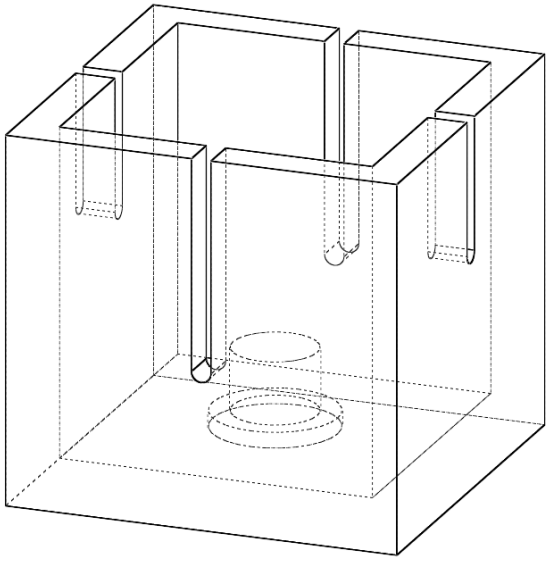

Figure 26: Centering Jig.

4.4 Aim #1 Experimentation

4.4.1 Sample assembly

For each sample, two six-inch bone models were placed into the drilling guide, spaced using a one-inch SFE tube, and secured with the method described in 2.3.3. While smaller gaps were utilized in previously conducted studies, a larger gap may better accentuate the differences between plating systems.[53] The spacer was then removed, thus simulating a comminuted fracture. Plates were centered on the bone models to ensure equal plate contact on each bone model. Furthermore, all screw holes on the plate in contact with the bone models were fastened. The DCP, LC-DCP, LCP, and Fixin plates were secured to the bone models using three bicortical screws in each bone model segment. The SOP plate was secured to the bone models using four bicortical screws in each bone model segment. The ALPS10 and ALPS11 plates were

secured with one bicortical screw on each bone model segment at the furthest position from the fracture gap. Three monocortical screws were used to secure the plate at the remaining screw holes on each bone model segment. All screws were loaded neutrally and a torque limiting screwdriver was used to ensure the insertion torque applied to each screw was standardized to 2.5 N-m.

4.4.2 Initial Mechanical Testing

Initial testing was conducted using an Instron 5544 electro-mechanical testing machine. The loading anvils were placed distal to the screw most proximal to the fracture gap on each bone model segment. The bottom support anvils were placed at their furthest position allowed by the grip. The sample was preloaded to 5N and loaded at a rate of 0.1mm/sec until reaching the deflection limit of the machine. After conducting a single test, interference between the top loading anvils and plating system screws were noted to cause undesirable deflection and fracture of the sample's screws in the sample. Figure 27 depicts this deflection on a Fixin plating system. Furthermore, as screw spacing differs between plating systems, the constant adjustment of loading anvil placement would be detrimental to maintaining a controlled environment.

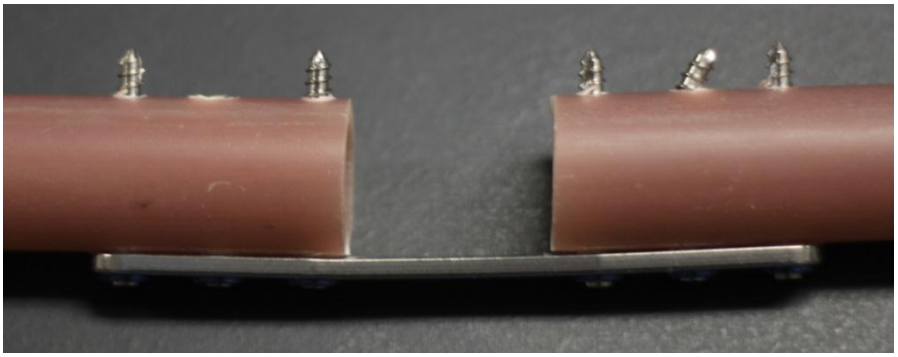

Figure 27: Fixin Screw Deflection.

4.4.3 Final Testing

Acute, single cycle to failure tests were conducted using the same Instron 5544 testing machine utilizing ASTM F382 as guidance.[7] The top loading anvils were spaced 14cm apart to be distal to the distal-most screw on the sample with the longest bridging plate. The bottom support anvils were placed 24cm apart, corresponding to the widest position allowed by the grip. Each sample was manually centered in the test fixtures, preloaded to 5N, and loaded at a rate of 0.1mm/sec until reaching the deflection limit of the machine. Load and displacement data were recorded at 10Hz. Four samples were tested for each plating system, totaling 32 samples. Figure 28 depicts a properly installed sample in the test fixture.

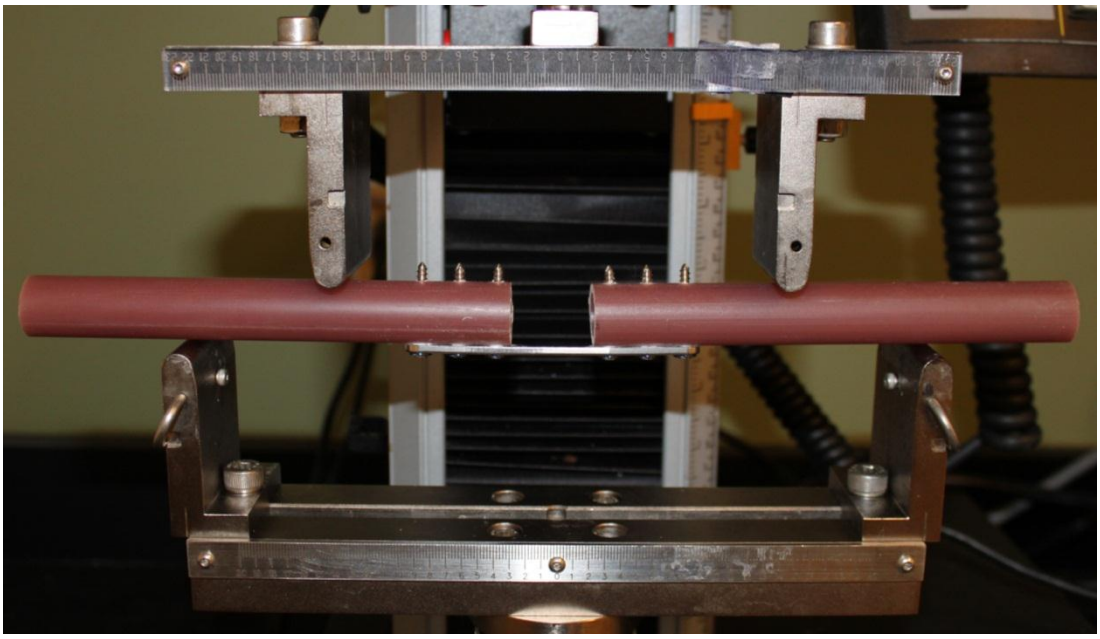

Figure 28: Properly Installed Four-Point Bending Test Sample.

4.4.4 Aim #1 Results

After mechanically testing all the samples, the acquired data are evaluated to extrapolate the bending stiffness, bending structural stiffness, and bending strength. Bending stiffness is defined as the maximum slope of the linear-elastic portion of the load-displacement curve for each sample. Bending strength is defined as the bending moment needed to generate a 0.2% offset displacement in the sample. Finally, the bending structural stiffness is a normalized effective bending stiffness taking the test setup configuration into consideration.

To calculate the various mechanical properties, anvil span measurements must first be noted. Loading span, *h*, is defined as the distance between one bottom support anvil and the nearest top loading anvil. Center span, *a*, is defined as the distance between the top loading anvils. Both span measurements are used in their millimeter form. These values correspond to 50mm and 140mm, respectively, according to our test setup. Figure 29 is adapted from ASTM F382 and depicts these measurement locations.[7]

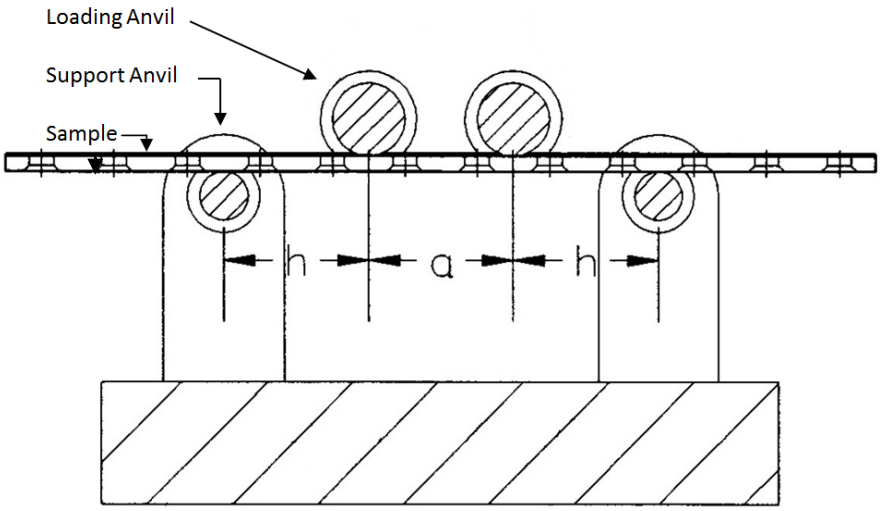

Figure 29: Anvil Span Measurement Locations. Adapted from ASTM F382.[7]

Graphs are first generated for each sample plotting load over displacement, a sample of which is seen in Figure 30. Before making any calculations, a linear regression, represented by segment OM, is performed on the region of the graph most closely representing linear-elastic deformation in the system. A line with slope equal to that of the regression is plotted at a 0.2% offset to the linear regression to ensure calculations are based on a failure load in the plastically deformed area of the plot. This is represented as segment BN, which intersects the load-displacement curve at point P, labeled as the proof load, and is the load after which plastic deformation occurs.

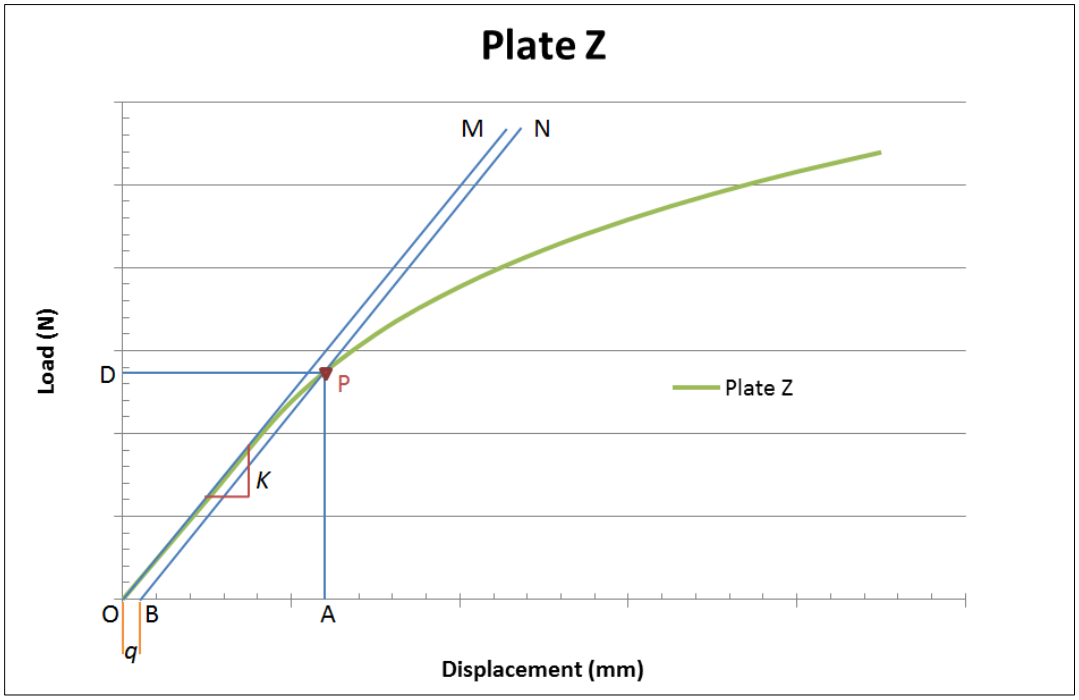

Figure 30: Sample Load-Displacement Curve.

The slope of segment OM is equal to the bending stiffness of the plating system, represented as *K* in the equations below. Using Equation 1, the offset value, *q*, is first determined in order to draw segment BN and determine the proof load. Because grip setup remains the same throughout the testing process, the calculated offset value of 0.028mm is used in calculating proof load for all samples. Using Equation 2, bending strength is now calculated. The final calculated mechanical property, bending structural stiffness, is calculated to normalize the stiffness data based on test setup configuration. The evaluated plating systems have different geometries and screws required to secure the plate to the bone, however, the test configuration does not change, and therefore we expect the normalized stiffness calculation for each system to be of similar order to its bending stiffness. Equation 3 is used to calculated this with *a*, *h*, and *K* as inputs.

Equation 1: Offset Displacement Calculation.

$$q = 0.002 \times a$$

Equation 2: Bending Strength Calculation.

$$bending\ strength = \frac{P \cdot h}{2}$$

Equation 3: Bending Structural Stiffness Calculation.

$$bending\ structural\ stiffness = \frac{(2 \cdot h + 3 \cdot a) \cdot K \cdot h^2}{12}$$

The calculated mechanical properties are then analyzed using a one-way ANOVA with Tukey pairwise comparison to compare the values between all plating systems. Statistical significance will be set at $p<0.05$.

4.5 Aim #2 Experimentation

The up-and-down, or staircase, method was used to evaluate each plating system. Staircase testing is used to evaluate the fatigue strength of a material at a specific fatigue life.[54] In our application, a starting load is first chosen and torqued to a specified number of cycles. If the sample fails before reaching the predetermined number of cycles, the sample is designated as a failure and a subsequent sample is tested at a load decreased by a constant value. If a sample does not fail it is designated as a runout and a subsequent sample is tested at a load increased by the same constant value. This process is repeated for all samples. To ensure accurate results, it is recommended to test at least fifteen samples.[55]

4.5.1 Sample Assembly

The assembly of the torsion samples was similar to that of the four-point testing samples, however, an additional step of potting one end of each bone model segment in fiberglass resin was added prior to application of the plating system. The jig depicted in Figure 26 above was first used to center the bone model segment prior to potting it in fiberglass resin. A two-inch tall

and two-inch square PVC tube was inserted into the jig along with a bone model segment over the centering nub. Two pins were then inserted perpendicularly through adjacent faces of the PVC tube and bone model segment to keep the bone model segment centered upon removal from the jig. When removed, this setup was placed on a sheet of cellophane wrap and the tube was filled with resin to facilitate ultimate stability while testing. After the resin fully cured, the respective plate was secured to the bone models with the method described in Section 4.4.1. The length of the bone model segment varied between plates to allow a fixed distance between the distal-most screw to the fracture gap and the top of the potting fiberglass resin. Table 4 below lists the bone model segment lengths for all plating systems and Figure 31 depicts multiple views of a complete bone model segment.

Table 4: Bone Segment Lengths

Plating System	Bone Segment Lengths (mm)
DCP	123
LCP	122
Fixin	118
ALPS10	130
ALPS11	134
SOP	130
LC-DCP	123

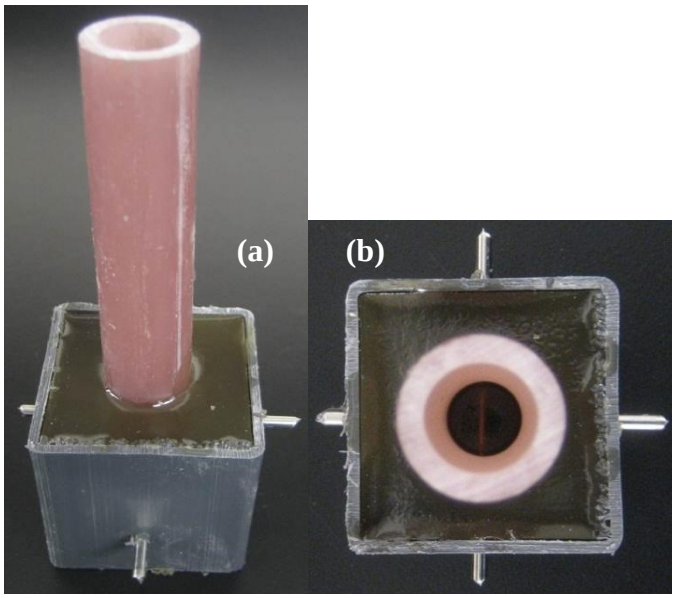

Figure 31: Complete Torsion Bone Model Segment (a) Front View (b) Top View.

4.5.2 Initial Mechanical Testing

Initial testing was conducted using a MTS 858 Mini-Bionix hydraulic testing machine, utilizing the sample assembly methods from the four-point bending tests described in Section 4.4.1 and machine grips from previously conducted acute torsion testing. This setup did not

include potted bone model ends, and was secured in the grip using screws to provide stability through a friction fit. This setup is seen in Figure 32.

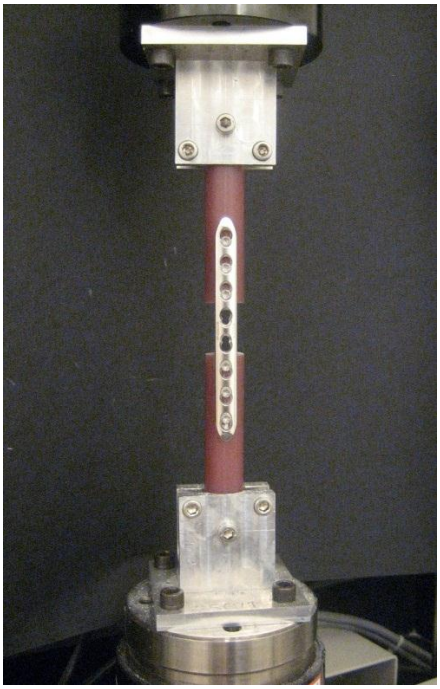

Figure 32: Initial Torsion Test Setup.

Initial testing was conducted cycling the samples at 1Hz torqued to 60% of the plating system's failure torque in both positive and negative directions, as determined through prior testing. The maximum torque value from each positive and negative cycle was recorded. It was found that the grips used to secure the constructs allowed slight movement in the construct when cyclically tested, thus leading to inaccurate acquisition of data. Figure 33 plots the maximum positive torque values and corresponding angles recorded during a portion of the test. Though the torsion testing was torque driven, slip within the grip did not allow the specified torque value to be consistently attained. In an effort to reduce any slip throughout the test, the ends of the sample were potted in fiberglass resin and new machine grips were manufactured.

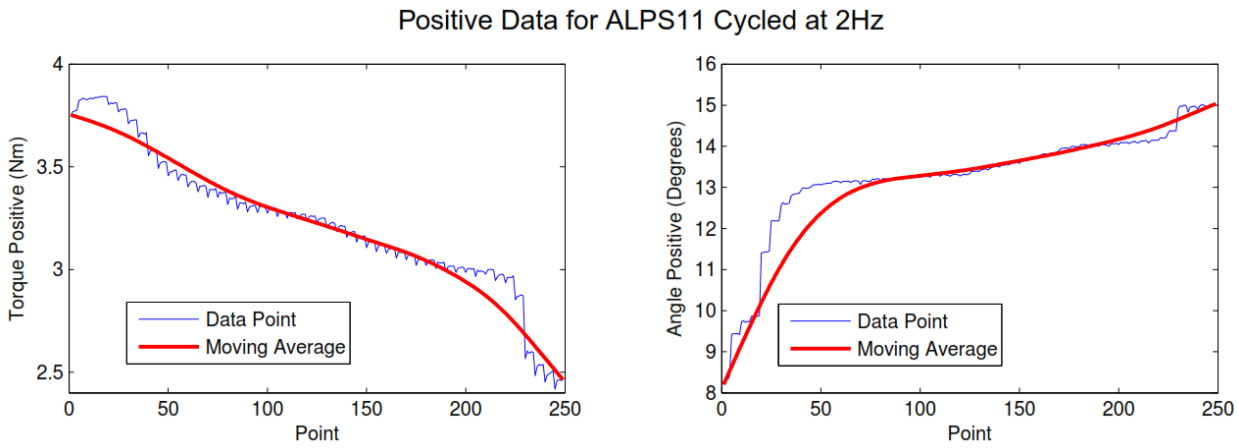

Figure 33: Positive Cycle Data for ALPS11 Cycled at 2Hz.

4.5.3 Final Testing

Samples for final testing were assembled using the jig described in Section 4.5.1. A pair of grips were designed and manufactured to accommodate the new sample assemblies in the testing machine. These grips are made of aluminum and their geometry allows for a close fitting sample. Screws are tightened on each face of the jig to provide supplementary stabilization prior to testing. Figure 34 depicts a properly installed sample end in the jig.

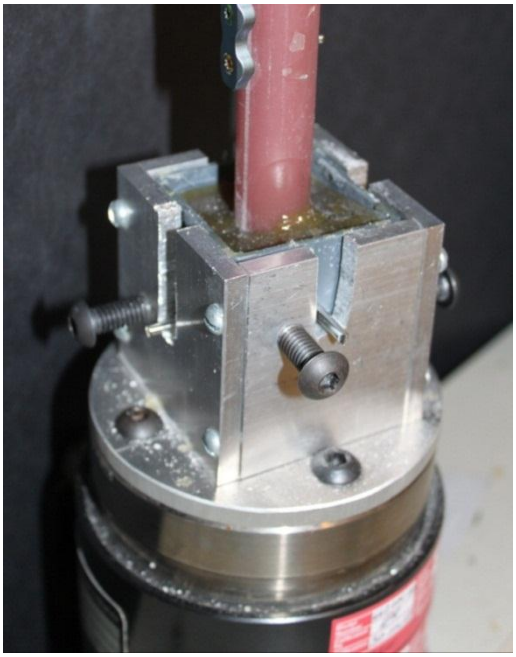

Figure 34: Assembled Bone Segment End.

No standard currently defines a method to evaluate fatigue properties of plating systems in torsion. Based on previous research and accelerated methods of analyzing material fatigue properties, sixteen samples of each plating system were tested in torsion using the staircase method to determine their respective fatigue strength.[54, 56-58] The first sample of each plating

system was cycled at 1Hz to 60% of its previously determined acute failure torque, and all samples were cycled 15,000 times.[50] After implanting a plating system, the patient is recommended to remain under cage rest for the first six to eight weeks with activity limited to five minutes a day. Based on gait analysis, 15,000 cycles represents an estimated number of strides a canine will load onto the healing bone during six weeks of limited activity.[59] As seen in previous studies, samples were torqued about the center axis of the bone model.[52, 60, 61] One cycle is defined as torqueing the sample from its neutral position to the specified torque in the positive direction, returning past the neutral position to the specified torque in the negative direction, and back to its neutral position. The cycling torque for subsequent tests was increased by 10% if run-out was achieved or decreased by 10% if the sample failed. To assist in determining run-out or failure, maximum torque and angular displacement were recorded and plotted for each half cycle of the test. After collaborating with veterinarians, three failure criteria were defined before initiating the tests. Failure was considered if total angular rotation progressively increased by at least 25% of its original value at the end of the test. This was chosen as any higher angular rotation would have a greater chance of improperly healing. When viewing the plot of total angular rotation per each half cycle, abrupt increases in angular rotation were translated to sample failure as this depicts fracture in the system. Finally, if any visual fracture of the bone plate, bone screws, or bone model were observed, the test was terminated early and the sample was labeled as a failure. These criteria were established to ensure evaluation of the plating systems with no addition fracture points or deformation. All samples and data were also evaluated with veterinarians to confirm run-out and failure presence. Sixteen samples were tested for each plating system.

4.5.4 Results

After testing is complete for each plating system sample, the acquired data and physical integrity of the construct are analyzed to determine run-out or failure. When data portray sample failure or fracture to the sample causes a premature end to the test, the construct is visually inspected to determine the root cause. We expect to visualize failure in the form of screw pullout, screw failure, bone model fracture, bone model failure, and plate failure. Screw pullout is defined as the loosening or backing out of a screw from the plate as a result of cyclic loading. Screw failure is defined as breakage of screws into two or more pieces. Bone model fracture is defined as an intact construct only containing cracks on the bone model. Finally, bone model failure is defined as breakage of a bone model into two or more pieces.

After testing is complete for each of the sixteen samples tested per plating system, a chart is developed summarizing each the run-out and failure points at the various load levels. A sample chart is seen in Figure 35.

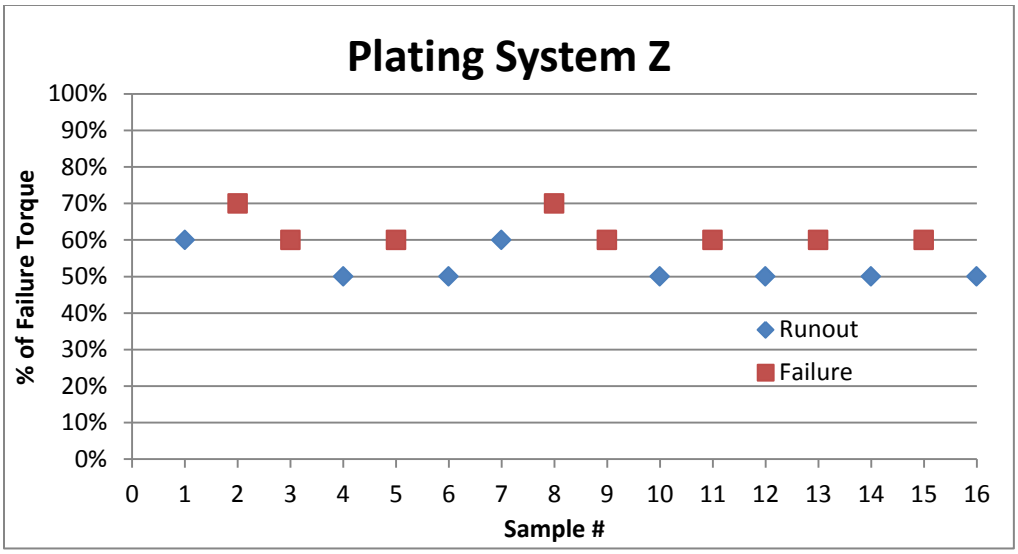

Figure 35: Sample Plating System run-out and Failure Summary.

An estimate of the mean fatigue strength of each plating system is calculated using a probability plot. For each tested torque level, the percentage of failed samples is first calculated from the summarizing charts. These values are then plotted on a torque level versus failure percentage graph. A vertical line is drawn at the 50% value and a linear regression is performed on the plotted data points. The value at the intersection of the linear regression with the vertical 50% line corresponds to the estimated mean fatigue strength of the plating system. Furthermore, the slope of the regression line corresponds to the standard deviation of this estimate. A sample plot is pictured below in Figure 36.

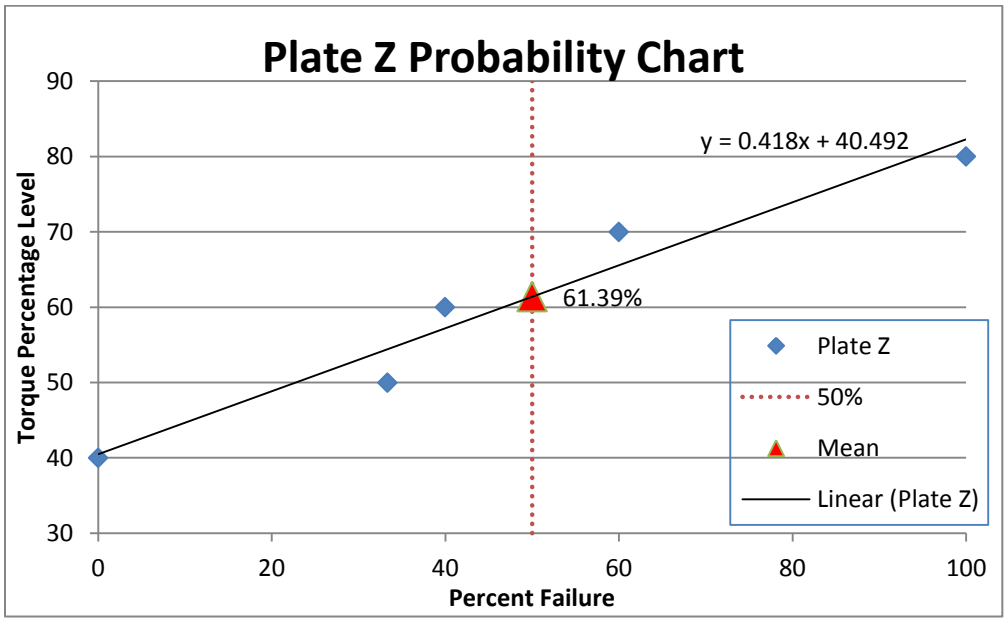

Figure 36: Sample Probability Plot.

The Dixon-Mood method is the more common technique used to estimate the mean and standard deviation of fatigue strength.[54, 57] Enumerating run-outs and failures of each plating system is first completed. The more prominent occurrence is used to perform the calculations. In the event that the number of run-outs equals the number of failures, either group may be used as they will yield the same results. Equation 4 below defines the variables A, B, and C required in the Dixon-Mood equations.

Equation 4: A, B, and C variables for Dixon-Mood Equations.

$$A = \sum_{i=0}^{i_{max}} m_i \quad , \quad B = \sum_{i=0}^{i_{max}} i m_i \quad , \quad C = \sum_{i=0}^{i_{max}} i^2 m_i$$

Load level is denoted as the integer parameter i in these equations with i_{max} corresponding to the highest stress level in the staircase. Stress level $i = 0$ corresponds to the lowest stress level where run-out is observed if a majority of samples in the plating system failed. Conversely, $i = 0$ would correspond to the lowest stress level where failure is observed if a majority of samples in the plating system achieved run-out. For example, if 9 of 16 samples failed with the lowest survival load at 40% of the plating system's failure torque, $i = 0$ would correspond to the 40% level. If the step level in the staircase was 10% and the highest load level was 90%, i_{max} would equal five.

Equation 5 below defines the Dixon-Mood equation for mean fatigue strength in which A, B, and C are inserted. Fatigue strength is defined as μ, initial load level is S_0, and step size is s. The plus sign in the equation is used when failures are the more prominent occurrence while the minus sign is used when the opposite holds true.

Equation 5: Dixon-Mood Equation for Mean Fatigue Strength.

$$\mu = S_0 + s \cdot \left(\frac{B}{A} \pm 0.5 \right)$$

The Dixon-Mood method for calculating standard deviation is defined below in Equation 6 as variable σ.

Equation 6: Dixon-Mood Equation for Standard Deviation.

$$\sigma = 1.62 \cdot s \cdot \left(\frac{A \cdot C - B^2}{A^2} + 0.029 \right) \quad if \quad \frac{A \cdot C - B^2}{A^2} \geq 0.3$$

$$or$$

$$\sigma = 0.53 \cdot s \quad if \quad \frac{A \cdot C - B^2}{A^2} \leq 0.3$$

A table is created to more simply calculate the A, B, and C values which will be inserted into the Dixon and Mood equations for mean fatigue strength and standard deviation. Load levels are placed in descending order in column i. A second column is created noting the occurrences in

the group being counted, defined as *n*. A third column displays the load level multiplied by the number of occurrences. Finally, a fourth column displays the load level, squared, and then multiplied by the number of occurrences. The final row in each of the three right-most columns contains a summation of the column's contents and correspond to the A, B, and C values. A sample of this table is seen below in Table 5. For modeling purposes, three load levels are used.

Table 5: Sample Dixon-Mood Variable Calculation.

Plate Z	Load Range	*i*	*n*	*i*n*	i^2*n
Failure	**80%**	2	2	4	8
Prominent	**70%**	1	3	3	3
	60%	0	2	0	0
	Totals:		**A = 7**	**B = 7**	**C = 11**

An alternative method to calculate standard deviation, based on that obtained from the Dixon-Mood equation, has been developed by Svensson and Lorén.[56, 62] This method was developed to better reflect the calculated standard deviation in tests which included fewer than 30 samples. This is seen in Equation 7.

Equation 7: Svensson-Lorén Standard Deviation Adjustment.

$$\sigma_{SL} = \sigma_{DM} \frac{N}{N-3}$$

5. Results

5.1 Four-point Bending

Raw data were recorded as comma separated variables. Three variables were reported: time, displacement, and force. This data were analyzed using Microsoft Excel 2010, MATLAB R2010b and Minitab Release 16. Calculations were made with the assistance of the ASTM F382 standard test methods for metallic bone plates. These methods describe the process for testing metallic bone plates via four-point bending and extrapolation of bending stiffness, bending structural stiffness, and bending strength properties as described in Section 4.4.1. The load required to achieve plastic deformation in each plating system ranged from 150.0N to 580.4N. The bending stiffness of each plating system ranged from 37.2N/mm to 98.2N/mm. The bending strength of each plating system ranged from 3.8N-mm to 12.5N-mm. The bending structural stiffness of each plating system ranged from 4.03Nm^2 to 10.64Nm^2. The load-displacement curves with calculated proof load are summarized in Appendix A. The mean and standard deviation of these mechanical properties were calculated for each plating system and are summarized in Table 6 below while the calculated data are elaborated in Appendix B. A one-way ANOVA with Tukey pairwise comparison was conducted to determine which plating systems had significantly different means when comparing their bending stiffness, bending strength, and bending structural stiffness.

Table 6: Four-Point Bending Mechanical Property Summary.

Plating System	Bending Stiffness (N/mm)		Bending Structural Stiffness (N-m^2)		Bending Strength (N-mm)	
	Mean	SD	Mean	SD	Mean	SD
DCP	71.0	15.2	7.7	1.7	9.6	2.1
LCDCP	57.3	1.3	6.2	0.1	8.5	0.4
Ti-LCDCP	44.2	2.6	4.8	0.3	6.1	0.6
LCP	66.7	6.6	7.2	0.7	6.7	2.1
ALPS10	40.0	1.9	4.3	0.2	5.1	1.2
ALPS11	76.3	1.8	8.3	0.2	11.6	0.6
SOP	80.4	12.5	8.7	1.4	11.6	1.7
Fixin	44.4	2.8	4.8	0.3	7.3	1.4

When comparing bending stiffnesses, DCP was significantly different from Ti LC-DCP, ALPS10, and Fixin. LC-DCP was significantly different from SOP. Ti LC-DCP was significantly different from LCP, ALPS11, and SOP. LCP was significantly different from ALPS10 and Fixin. ALPS10 was significantly different from ALPS11 and SOP. Finally, ALPS11 and SOP were both significantly different from Fixin. This is summarized in Table 7.

When comparing bending strengths, DCP was significantly different from Ti LC-DCP, ALPS10, and Fixin. LC-DCP was significantly different from SOP. Ti LC-DCP was significantly different from LCP, ALPS11, and SOP. LCP was significantly different from ALPS10 and Fixin. ALPS10 was significantly different from ALPS11 and SOP. Finally, ALPS11 and SOP were both significantly different from Fixin. This is summarized in Table 7.

When comparing bending structural stiffnesses, DCP was significantly different from ALPS10. LC-DCP was not significantly different from any plating system. Ti LC-DCP, LCP, and ALPS10 were significantly different from ALPS11 and SOP. ALPS11 and SOP were significantly different from Fixin. This is summarized in Table 7. The elaborated ANOVA and Tukey pairwise comparison output from Minitab is included in Appendix C.

Table 7: Four-Point Bending Tukey Analysis Summary

Plating System	Bending Stiffness			Bending Structural Stiffness			Bending Strength		
SOP	A			A			A		
ALPS11	A	B		A	B		A		
DCP	A	B		A	B		A	B	
LCP	A	B		A	B			B	C
LCDCP		B	C		B	C	A	B	C
Fixin			C			C		B	C
Ti-LCDCP			C			C		B	C
ALPS10			C			C			C

Plating systems which don't share grouping letters are significantly different.

5.2 Torsion

Raw data were recorded in comma separated variable format reporting time, maximum torque, and maximum angle at each half cycle. Using Microsoft Excel, graphs for maximum torque and maximum angle for each half cycle were developed for each plating system to assist in determining failure modes of the samples and ensuring the specified torque was reached. To determine if the sample exceeded the failure specification for angular rotation, total angular rotation was extrapolated at the 1000^{th}, $5{,}000^{th}$, $10{,}000^{th}$, and $15{,}000^{th}$ cycle. This rotation was not calculated below the 1000^{th} cycle to allow the construct to settle.[53] If the total increase in angular displacement between the $1{,}000^{th}$ and $15{,}000^{th}$ cycle was greater than 25%, the subsequent test was cycled at the torque value 10% lower than that of the evaluated test or 10% higher if the contrary occurred. Based on previously conducted acute failure tests, Table 8 below was developed to summarize the different torque values which may have been tested. Appendix C elaborates the extrapolated angular rotation for each sample.

Table 8: Plating System Torque Values.

Plating System Torque Values (N-m)										
	100%	90%	80%	70%	60%	50%	40%	30%	20%	10%
SOP	8.66	7.79	6.93	6.06	5.20	4.33	3.46	2.60	1.73	0.87
LCP	8.53	7.68	6.82	5.97	5.12	4.27	3.41	2.56	1.71	0.85
ALPS11	8.35	7.52	6.68	5.85	5.01	4.18	3.34	2.51	1.67	0.84
DCP	8.32	7.49	6.66	5.82	4.99	4.16	3.33	2.50	1.66	0.83
LC-DCP	7.58	6.82	6.06	5.31	4.55	3.79	3.03	2.27	1.52	0.76
Fixin	6.80	6.12	5.44	4.76	4.08	3.40	2.72	2.04	1.36	0.68
ALPS10	5.68	5.11	4.54	3.98	3.41	2.84	2.27	1.70	1.14	0.57

When total angular displacement increased by 25% throughout the test, bone model fracture, at minimum, was evident. When tested samples failed before reaching 15,000 cycles, samples were visually inspected to determine the cause of failure. Screw fracture was evident across all plating systems. Multiple plating systems also experienced bone model fracture and failure. Screw pullout was only evident on one plating system, as was plate fracture. Table 9 summarizes the number of occurrences for each construct failure mode.

Table 9: Plating System Failure Mode Occurrences.

		Screw Pullout	Screw Fracture	Bone Model Fracture	Bone Model Failure	Plate Failure
DCP	Occurrences		3	3	4	
LCP			7	2		
Fixin			8			
ALPS10		1	1			6
ALPS11			5		7	
SOP		1	9			
LC-DCP			1	3	5	

The run-out and failure data points for samples of each plating system were plotted to note any visible trends in the data and are included in Appendix D. Appendix E includes the summarized angular rotation, in degrees, for each plating system across four points throughout the cycle. Probability plots were developed as one method of quantifying the estimated mean fatigue strength and standard deviation of each plating system. These can be seen in Appendix F.

The previously described Dixon-Mood equations were also used as an equivalent method for calculating mean fatigue strength and standard deviation. Mean fatigue strength was calculated in terms of each plating system's acute failure torque percentage and absolute torque value in both methods. The highest mean fatigue strength in terms of percentage of acute failure torque of the plating system able to survive at its highest percentage of acute torque was observed in the ALPS10 plating system. The lowest was seen in the SOP plating system. Dixon-

Mood calculations estimate the mean fatigue strengths of the ALPS10 and SOP plating systems to be 76.4% and 43.6% of their acute failure torques, respectively. When comparing absolute torque values in Dixon-Mood calculations, we found that the DCP plating system maintained the highest estimated mean fatigue strength at a torque of 5.4N-m. The Fixin plating system maintained the lowest torque at 3.5N-m. Probability plot data showed ALPS10 as the strongest at 72.9% and SOP the weakest at 44.2% of their acute failures torques. DCP maintained the highest estimated mean fatigue strength with a torque of 5.4N-m and Fixin the lowest at 3.5N-m. Table 10 below elaborates the results obtained from both Dixon-Mood and probability plot calculations, including standard deviation, in descending order of magnitude. The green cells note the highest estimated mean fatigue strength and orange cells note the lowest. These calculations are elaborated in Appendix G.

Table 10: Mean Fatigue Strength Calculations.

	As Percentage of Acute Failure Torque (%)				As Absolute Torque Value (N-m)			
	Dixon-Mood		Probability Plot		Dixon-Mood		Probability Plot	
Plating System	Mean Fatigue Strength	SD	Mean Fatigue Strength	SD	Mean Fatigue Strength	SD	Mean Fatigue Strength	SD
ALPS10	76.4	16.3	72.9	28.6	4.3	0.9	4.1	1.6
DCP	65.0	8.6	65.0	30.0	5.4	0.7	5.4	2.5
LC-DCP	62.5	15.7	61.4	41.8	4.7	1.2	4.7	3.3
ALPS11	57.5	3.5	58.5	18.4	4.8	0.4	4.9	1.5
Fixin	51.3	4.3	50.8	19.6	3.5	0.4	3.5	1.3
LCP	47.9	3.8	46.8	22.8	4.1	0.5	4.0	1.9
SOP	43.6	5.3	44.2	22.1	3.8	0.5	3.8	1.9

The Svensson-Lorén adjustment for standard deviation was also calculated for each plating system whose results met the criteria in Equation 4. Table 11 summarizes these calculations for each plating system. σ_{DM} is the Dixon-Mood calculated standard deviation and σ_{SL} is the Svensson-Lorén adjusted value.

Table 11: Dixon-Mood and Svensson-Loren Standard Deviation Comparison.

Dixon-Mood and Svensson-Loren Standard Deviation Comparison				
Failure Torque As:	**Percentage (%)**		**Absolute Value (N-m)**	
Plating System	σ_{DM}	σ_{SL}	σ_{DM}	σ_{SL}
ALPS10	16.3	20.1	0.9	1.1
ALPS11	3.5	4.3	0.4	0.5
DCP	8.6	10.6	0.7	0.9
Fixin	4.3	5.3	0.4	0.4
LCP	3.8	4.7	0.5	0.6
LC-DCP	15.7	19.3	1.2	1.5
SOP	5.3	6.5	0.5	0.6

6. Discussion

6.1 Four-Point Bending

A few observations were made about the effect of bending forces on tested constructs. With exception to Fixin, which has a flat underside, all plating systems have uniquely scalloped or curved undersides with distinct lateral geometries. These features, in combination with evenly spaced screw holes spanning across the entire length of the plate, influence the areas of deformation in each plate when exposed to bending forces. These geometries can be observed through two general design concepts. While not always the case, plates may incorporate wide sections to accommodate screws with narrow connecting features. Furthermore, plates can have scallops or other unique underside geometries in combination with a thicker profile at screw holes and thinner profile at connecting segments. Deformation is guided to these narrower and thinner sections as their smaller cross-sectional area results in a lower moment of inertia. This lower moment of inertia corresponds to lower resistance to bending. Figure 37 below shows a sample of each bone construct when loaded to the machine's deflection limits via four-point bending. Deformation is evident along the screw holes on the plate. These observations are similar to those found in a study conducted by DeTora and Kraus.[35]

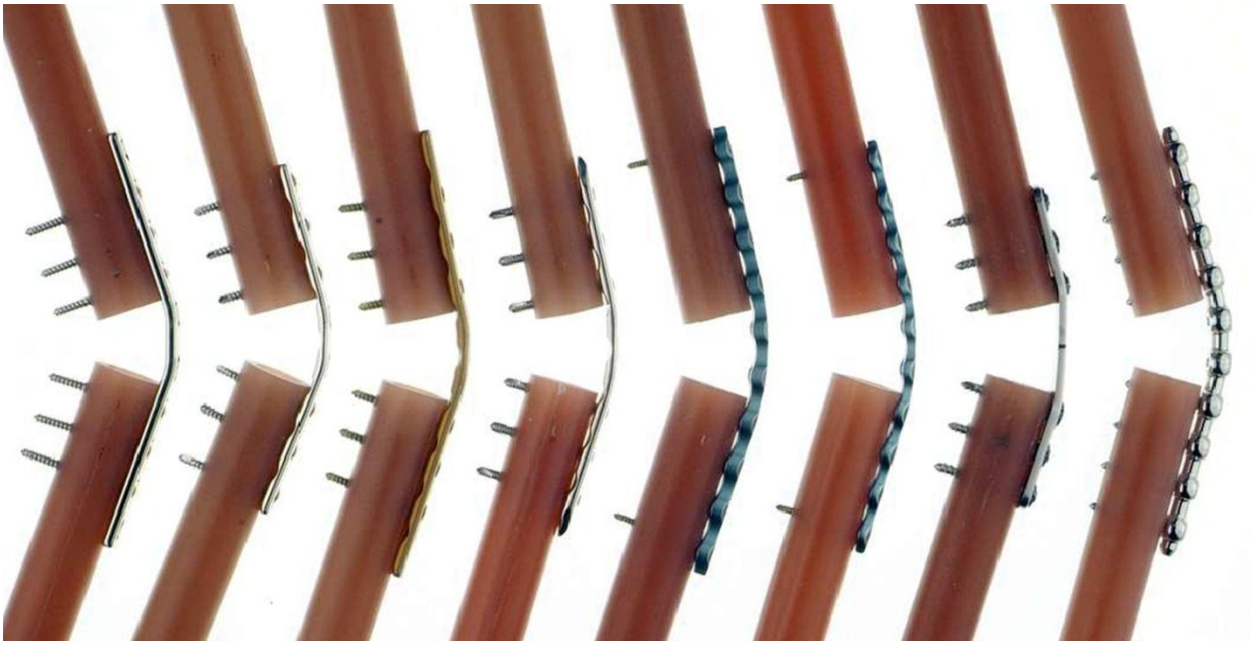

Figure 37: Four-point bending plate deformation. From left to right: DCP, LCP, SS LC-DCP, Ti LC-DCP, ALPS11, ALPS10, Fixin, and SOP.

With exception to the Fixin plating system, no fracture was found to any plate, screw, or bone model. Due to the geometry of the Fixin plate, we found that loads applied to the system during four point bending induced a minor crack at the interface between the bone model and plate at the fracture gap in one sample and catastrophic bone model fracture in a second sample. This can be seen in Figure 38 and Figure 39. We attribute this partly to its flat underside as this

creates a greater contact point with the bone model and near uniform lateral geometry. Screw holes along the entire plate length seen in other systems help guide deformation to them when under load. The Fixin geometry does not facilitate plate bending along the middle section of the plate and thus deforms at the interface with the bone model.

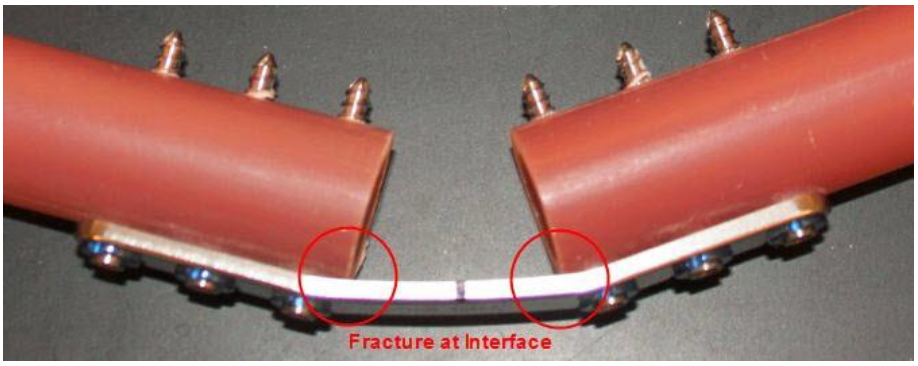

Figure 38: Fixin Bone Model Fracture and Plate Deformation at Plate/Bone Model Interface.

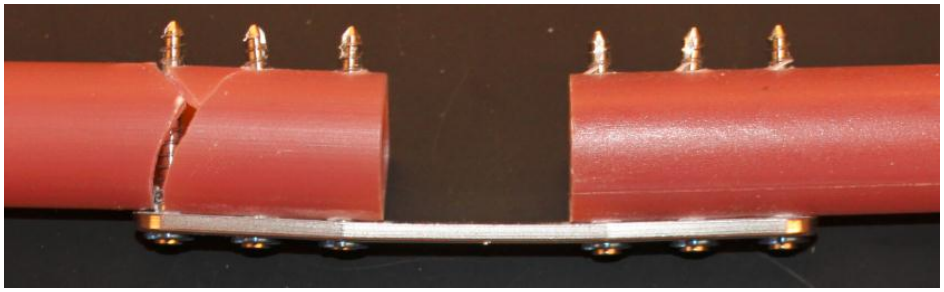

Figure 39: Fixin Bone Model Failure.

Quantitative analysis of four-point bending results shows that the SOP plating system had the highest bending stiffness, bending strength, and bending structural stiffness values. This result was expected as SOP appears to have the largest cross sectional area measurement of all plating systems and centroid furthest away from the loading axis. The rigidity in this system results in it absorbing a majority of the load, and therefore may represent a case of stress shielding if implanted into a patient with similar bone geometry to the bone model used. ALPS10, on the other hand, had the lowest values. It is further noted that the two plating systems with the lowest values for all calculated properties were Ti LC-DCP and ALPS10. This is expected as both systems are made up entirely of titanium. In addition, the narrow sections connecting the screw holes on these plates also have smaller dimensions, and therefore lower moment of inertia.

When comparing the mechanical properties of the Ti LC-DCP and SS LC-DCP systems, it was found that all calculated values for the stainless steel version were about 1.3 times higher than that of the titanium system. As the geometry of the plates and screws of these systems are identical, this difference can be attributed solely to the system's material. It was also found that the ALPS10 and ALPS11 plates had significantly different mechanical properties, as expected

considering their difference in size. As seen in the results, ALPS10 has half the bending strength and bending structural stiffness of ALPS11.

When comparing mechanical properties across systems, an interesting observation is noted between the SS LC-DCP and LCP plating systems. Though the bending stiffness of the SS LC-DCP system is lower than LCP, it maintains a higher bending strength due to its higher proof load. The load-displacement curve of SS LC-DCP has a broader linear-elastic region than other plating systems. We are unsure why this difference occurs, but it remains unique to this system.

The Tukey Pairwise Comparison of the plating systems provides alignment with previous research for a few of the plating systems. DeTora and Kraus found no significant difference in bending stiffness between DCP, LCP, and LC-DCP when subjecting only the plate to four-point bending loads.[35] Aguila et. al found no significant difference in bending structural stiffness between LCP and LC-DCP when subjecting the plating system and bone model to four-point bending loads.[36] Previous research indicates significantly different bending properties between SOP and DCP when subjecting only the plate to four-point bending loads, however, this does not align with our data indicating no significant difference.

Although plates with different materials and components of varying geometries were tested, the bending strength of the SS LC-DCP plating system did not prove to be significantly different than that of any other plating system when tested in single cycle to failure four-point bending according to the Tukey pairwise comparison. While this may give the impression of a well-balanced system, four-point bending fatigue testing will confirm if its use of standard screws is a detriment to its effectiveness.

6.2 Torsion

Multiple failure modes were observed when cyclically loading the torsion samples. These included screw failure, screw pullout, bone model fracture, bone model failure, and plate failure. It was apparent that screws failed on samples from all plating system. Furthermore, when cycling the ALPS10 plating system at both 80% and 90% of its acute failure torque, plate fracture was observed three times at each level. When catastrophic failure in a system did not occur, hairline fractures were noted on the bone models, typically emanating from the screw core and bone model interface. In addition, screw fracture or deformation may have occurred even if catastrophic failure was not observed, though visual inspection and the acquired data cannot confirm this. Screw pullout was also apparent on a minority of tested constructs, and occurred solely in locking systems. Although this observation was surprising, pullout only occurred in concert with screw fracture. We were able to confirm these through visual inspection of the construct after testing the sample. After analyzing all the data, we were able to determine that these nondestructive fractures typically correlated to abrupt increases in angular rotation. An example of this is seen in Figure 40 where ALPS10 failed progressively across the 15,000 cycles at which it was loaded. The graph is marked to depict the abrupt increases. We also found that some samples failed in more than one mode. Bone model failure was observed in conjunction

with screw failure seven times. Four of these occurrences were observed with the ALPS11 plating system. We attribute these occurrences to both the larger geometry of ALPS11 in addition to its use of the same screw size as the smaller plate in its family, ALPS10. Screw failure was observed combined with screw pullout once and with the SOP plating system. Though the SOP and ALPS plating systems use conventional screws, they incorporate threads in the plate holes, enabling them to be used as a locking plate. This is different from typical locking plate systems which utilize screw heads incorporating a different thread pitch and diameter than what is on the screw core. This greatly increases the chances of screws remaining locked when properly installed as their distinct and isolated threads each require a different number of revolutions to pull out to a certain distance.

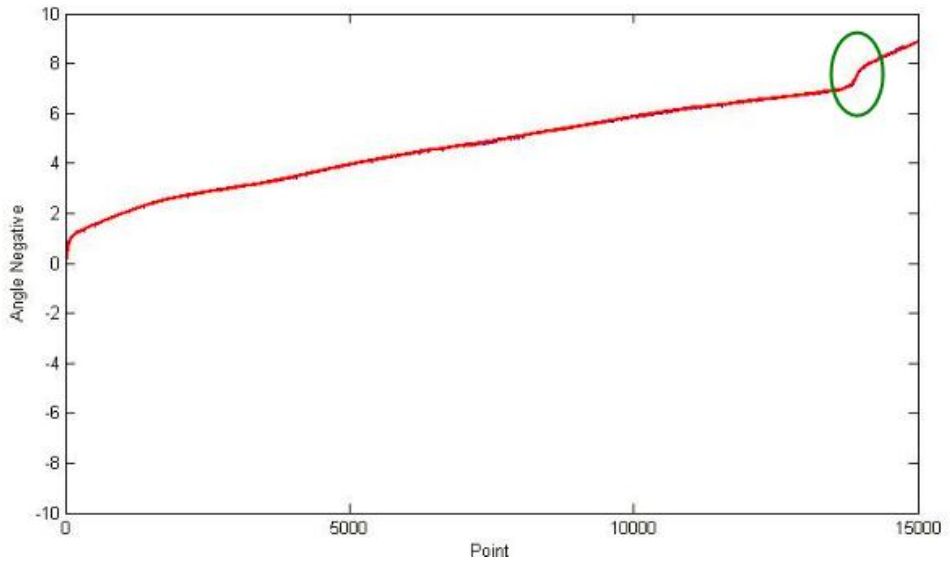

Figure 40: ALPS10 Progressive Failure.

Though qualitative analysis allows us to visualize different modes of construct failure, quantitative analysis allows us to better understand fatigue life of different plating systems. We found plating system mean fatigue strength to be ranked equally when evaluated with both Dixon-Mood and probability plot methods. This was expected despite the difference in evaluation methods. Based on percentage of acute failure torque, ALPS10 maintained the highest mean fatigue strength and SOP the lowest. This is not surprising as ALPS10 is comprised of titanium, a material which has half the tensile modulus of steel. This equates to an increased ductility thus corresponding to an increased angular rotation, confirmed by a previously conducted study.[50] SOP, conversely, is made of stainless steel and has a large cross-sectional geometry which places the plate further from the central loading axis than any other system. These correspond to SOP having a higher moment of inertia, corresponding to a decreased angular rotation. This is confirmed in Appendix H where the runout torque is plotted against the rotational displacement of the plating system. In addition to its low failure torque, each SOP failure was due to screw fracture where all screws on one fragment of the construct had sheared. Similar to the data we saw where SOP had the highest bending stiffness value, we believe the

failure mode of this system's fatigue testing in torsion further support the idea that this system has a high potential to cause stress shielding and be detriment to fracture healing. Although the Fixin plating system also failed due to screw fracture, we do not believe this is due to stress shielding. The shape of the plate deflects a majority of the angular rotation to the interface between the plate and the bone model and transfers much of this energy to the screws, thereby causing screw fracture across the tested cycle.

Higher angular rotation corresponds to a less stiff system and a lower angular rotation to a stiffer system. When the system is more ductile, as in the case with ALPS10, the plate is able to absorb more of the energy, thus removing some stresses present at the plate and screw interface. This corresponds to a lower susceptibility of screw fracture. Only one sample failed due to screw fracture with ALPS10, whereas it was the cause for failure in nine of the SOP samples. It is observed that the two plating systems comprised of titanium, ALPS10 and ALPS11, generally have a greater rotational displacement than the stainless steel plating systems across overlapping torque ranges. We are unsure of the impact of monocortical screw use in vivo as cyclic loading caused erosion of the bone model at the screw interface. By calculating the percentage of the failure torque a plating system is able to sustain, we can see how its material and geometry impacts its ability to be cyclically loaded.

When comparing absolute torque values, DCP proved to be the strongest and Fixin the weakest. We expected this considering the Fixin plating system has the smallest cross-sectional area of all plating systems. When comparing dimensions of the DCP, LCP, and LC-DCP plating systems, we found their width and height to be identical, though their screw hole patterns and underside geometries differed. We attribute the higher mean fatigue strength of the DCP construct to its greater cross-sectional area as its underside geometry is uniform when compared to the LCP and LC-DCP plating systems. This further allowed increased contact at the plate and bone model interface. While the DCP system employs the highest absolute fatigue strength, its clinical use may not be ideal due to non-locking screws and increased blood supply interference. We also note that DCP maintained the second strongest plating system when comparing percentage of acute failure torque, though ALPS10 maintained the median absolute torque value. By calculating the absolute torque values sustained by each system, we are able to compare them all regardless of their geometry. However, this cannot outline the effects of stress shielding as each plating system was able to maintain different angular rotations.

LCP and LC-DCP have similar, though not equal, failure torques. Based on the measured angular rotation in each construct at equal load levels, as seen in Appendix E:, LCP demonstrates a higher total angular rotation in comparison to LC-DCP and therefore a lower resistance to cyclic torsion loading. This aligns with previous research indicating LCP is less resistant to cyclic torsion loads in comparison to LC-DCP when secured to a bone model.[53] Depending on the activity level of the patient, angular rotation of the system can play a role in fracture healing. Although activity should be restricted during the first six to eight weeks after implantation, those

that are more active and able to transfer higher loads to the fractured bone may benefit from a stiffer plate to limit angular rotation as excessive movement can lead to delayed or non-union.

Probability plots and the Dixon-Mood method are the only methods of analyzing staircase data. The accuracy of probability plots are directly proportional to the number of torque levels at which the samples have been tested as the calculated mean fatigue strength is dependent on the goodness of fit of the linear regression. Estimated mean fatigue strength using both probability plots and Dixon and Mood equations seem to be similar, though the calculated standard deviations vary greatly. Unfortunately, we are unable to statistically quantify the correlation between the values acquired through the two evaluation methods. We believe that the probability plots have a higher standard deviation due to the low number of tested torque levels. While standard deviation calculated from the Dixon-Mood equations appear to be more accurate, the research of Svensson and Lorén makes particular note to the need for more accurate standard deviation calculations when testing small sample sizes. This is the motive behind the supplementary calculation to the Dixon-Mood results. It is evident from the Svensson-Lorén results that a higher standard deviation is calculated in all applicable plating systems in comparison to the values acquired from the Dixon-Mood methods. This is expected as smaller sample sizes may not always portray an accurate population mean and standard deviation. Testing of supplementary constructs will allow us to create a more accurate calculation of both fatigue strength and standard deviation.

A once-inch gap was chosen for the constructs to mimic a bridging osteosynthesis for a comminuted fracture. This gap, in addition, more severely tests the differences in plate geometry and securing methods due to the increased plating area lacking an interface with the bone model. A limitation of this test setup is that the loading axis lies along the center of the bone model. If each construct was assembled to mimic the true loading axis for each construct based on the applied plating system's geometry, more physiologically accurate results would be acquired. By torqueing the plating systems along the center axis of the bone model, we were able to maintain a uniform testing field throughout all samples, in addition to more severely stressing the plating systems. The more physiologically accurate torqueing axis would be shifted away from the bone center and toward the plate at a distance dependent on the plate's centroid. Furthermore, this setup does not portray the true effect of internal and external forces acting upon a fractured bone as they typically act in a combination of torsion, bending, and shear modes and not pure torsion.[48, 49] Thus, the calculated fatigue strength of these plating systems represents the worst-case torsion loading conditions.

6.3 Cinical Relevance

Stiffness and relative rigidity of these plating systems provide a good indication of systems which may contribute more to stress shielding than others, based on the results of our quantitative analyses for both loading modes. However, based on our observations, plating systems offer various design features which may promote or reduce healing ability.

Features reducing the contact area between the plate and the bone result in preserving the blood supply at the fracture site and thus promote proper healing. The plates incorporating these features include SS LC-DCP, Ti LC-DCP, LCP, ALPS10, ALPS11, and SOP. Furthermore, locking plates provide the least disruption of the blood supply since no contact is required between the plate and the bone.

As observed in the Fixin plating system, lacking screw holes across the entire length of the plate deflects loads to the plate and bone interface rather than distributing the load more evenly across the entire plate length. This feature, in addition to Fixin's underside geometry posing a high risk of disrupting the blood supply at the fracture site reduce its ability to properly heal fractures.

Deformation in the other systems was relatively uniform, though most apparent along the screw holes. ALPS10 and ALPS11 deformed most uniformly across the entire length of the plate due to its unique geometric features. Based on the evaluated bending properties of these two plating systems, ALPS11 maintains the second highest values and ALPS10 the lowest, thus representing nearly the entire range of tested systems. Therefore, based on what we have observed with regard to the bending profiles of the ALPS10 and ALPS11 plates, implementing this design to create a range of stiffness properties based on the size of the patient and severity of the fracture would be beneficial.

The unique geometry of the SOP system allows for it to be contoured with six degrees of freedom when necessary without deforming the screw holes. However, due to the size of this system, a majority of the load is absorbed by the plate and the stresses transferred to the screws, leading to screw failure. Unless unique contouring is required or the geometry is updated to better distribute the load, implanting an SOP system may not be the ideal choice for promoting proper healing.

7. Conclusions

This focus of this study was to evaluate the mechanical properties of seven plating systems using acute four-point bending and cyclic fatigue torsion test methods. The combination of these forces has been shown to represent more than 90% of loads acting on a fracture, though their exact mechanisms are not known.[48, 49] Based on the analyzed test data we are able to conclude that the SOP system has the highest acute bending mechanical properties and ALPS10 the lowest. Analysis of the cyclic torsion fatigue data allows us to conclude that the ALPS10 system is able to maintain the highest percentage of its failure torque when tested to 15,000 cycles and SOP the lowest. Furthermore, the DCP system is able to maintain the highest absolute torque value across 15,000 cycles and Fixin the lowest. The absolute torque data gives us an idea of how the plating system's material and geometry influence its cyclic behavior, although this alone cannot determine the superior plating system as it does not account for effects of stress shielding.

Based on qualitative analysis of the plating systems, several design features are beneficial to the healing of fractures. By incorporating screw holes along with a unique geometry along the entire length of the plate, plating system deformation as a result of bending loads can be made more uniform and deflected away from the plate and bone interface. In addition, as preserving the periosteum of the of the bone is critical to the reconstruction of bone, conventional plating systems which reduce the contact with bone and locked plating systems which do not require contact with bone are able to achieve this. Finally, although not preferred, if a complex plate contour is required to properly heal bone, the pearls and internodes of the SOP plating system offer a unique approach to contouring a plate without risk of deforming the screw holes.

The conducted mechanical evaluation is the start of better understanding plate mechanics. To further develop and understand the mechanical properties of these plating systems, it is recommended to perform fatigue life testing with both loading conditions. This should entail cyclic testing in both torsion and four-point bending to at least one million cycles per sample. This is recommended by ASTM F382 to accurately compare a plating system's geometric and material properties to its ability to resist fatigue. While the quantitative testing is an excellent start to the evaluation of bone plating systems, we are still unable to make conclusions about their effectiveness in vivo as biological responses were not examined. Controlled testing in vivo will allow for more accurate determination of the shortcomings of each system in addition to providing a more accurate understanding of a plating system's mechanical and biological response. Controlled in vivo testing will allow conclusions to be made regarding each system's effectiveness.

When considering application of a plating system on a comminuted canine femoral fracture, the results reported in this study should be interpreted in concert with cyclic four-point bending results and veterinary requirements.

Bibliography

1. Tan, S.L. and Z.J. Balogh, *Indications and limitations of locked plating.* Injury, 2009. **40**(7): p. 683-691.
2. Zlowodzki, M., et al., *Operative treatment of acute distal femur fractures: systematic review of 2 comparative studies and 45 case series (1989 to 2005).* J Orthop Trauma, 2006. **20**(5): p. 366-71.
3. Miller, D.L. and T. Goswami, *A review of locking compression plate biomechanics and their advantages as internal fixators in fracture healing.* Clinical Biomechanics, 2007. **22**(10): p. 1049-1062.
4. Carter, D.R., *Mechanical loading histories and cortical bone remodeling.* Calcified tissue international, 1984. **36**: p. 19-24.
5. Rüedi, T.P., et al., *AO principles of fracture management*. Vol. 1. 2007: George Thieme Verlag.
6. Athanasiou, K.A., et al., *Fundamentals of biomechanics in tissue engineering of bone.* Tissue engineering, 2000. **6**(4): p. 361-381.
7. *ASTM Standard F382, 2008e1, "Standard Specification and Test Method for Metallic Bone Plates," ASTM International, West Conshohocken, PA, 2008.*
8. Kemp, T., et al., *Functional trade-offs in the limb bones of dogs selected for running versus fighting.* Journal of experimental biology, 2005. **208**(18): p. 3475-3482.
9. Marsell, R. and T.A. Einhorn, *The biology of fracture healing.* Injury, 2011. **42**(6): p. 551-555.
10. Perren, S.M., *Evolution of the internal fixation of long bone fractures: the scientific basis of biological internal fixation: choosing a new balance between stability and biology.* Journal of Bone and Joint Surgery-British Volume, 2002. **84**(8): p. 1093.
11. Jahagirdar, R. and B.E. Scammell, *Principles of fracture healing and disorders of bone union.* Surgery (Oxford), 2009. **27**(2): p. 63-69.
12. Ramakrishna, K., et al., *Design of Fracture Fixation Plate for Necessary and Sufficient Bone Stress Shielding.* JSME International Journal Series C Mechanical Systems, Machine Elements and Manufacturing, 2004. **47**(4): p. 1086-1094.
13. Lindholm, R., et al., *The mast cell as a component of callus in healing fractures.* J Bone Joint Surg Br, 1969. **51**(1): p. 148-55.
14. Pape, H.C., et al., *Effects of intramedullary femoral fracture fixation: what is the impact of experimental studies in regards to the clinical knowledge?* Shock, 2002. **18**(4): p. 291-300.
15. Court-Brown, C.M., et al., *Reamed or unreamed nailing for closed tibial fractures. A prospective study in Tscherne C1 fractures.* J Bone Joint Surg Br, 1996. **78**(4): p. 580-3.
16. Haas, N., et al., *A new solid unreamed tibial nail for shaft fractures with severe soft tissue injury.* Injury, 1993. **24**(1): p. 49-54.
17. McKibbin, B., *The biology of fracture healing in long bones.* J Bone Joint Surg Br, 1978. **60-B**(2): p. 150-62.
18. Pearson, O.M. and D.E. Lieberman, *The aging of Wolff's "law": ontogeny and responses to mechanical loading in cortical bone.* Am J Phys Anthropol, 2004. **Suppl 39**: p. 63-99.
19. Besdo, S., *Determination of dynamically adapting anisotropic material properties of bone under cyclic loading.* J Biomech, 2011. **44**(2): p. 272-6.

20. Robling, A.G., D.B. Burr, and C.H. Turner, *Partitioning a Daily Mechanical Stimulus into Discrete Loading Bouts Improves the Osteogenic Response to Loading.* Journal of Bone and Mineral Research, 2000. **15**(8): p. 1596-1602.
21. Burr, D.B., A.G. Robling, and C.H. Turner, *Effects of biomechanical stress on bones in animals.* Bone, 2002. **30**(5): p. 781-6.
22. Huang, C. and R. Ogawa, *Mechanotransduction in bone repair and regeneration.* FASEB J, 2010. **24**(10): p. 3625-32.
23. Datta, H.K., et al., *The cell biology of bone metabolism.* Journal of Clinical Pathology, 2008. **61**(5): p. 577-587.
24. Cordey, J., S.M. Perren, and S.G. Steinemann, *Stress protection due to plates: myth or reality? A parametric analysis made using the composite beam theory.* Injury, 2000. **31 Suppl 3**: p. C1-13.
25. Tonino, A.J., et al., *Protection from stress in bone and its effects. Experiments with stainless steel and plastic plates in dogs.* J Bone Joint Surg Br, 1976. **58**(1): p. 107-13.
26. Krishna, K.R., I. Sridhar, and D.N. Ghista, *Analysis of the helical plate for bone fracture fixation.* Injury, 2008. **39**(12): p. 1421-36.
27. Stoffel, K., et al., *Biomechanical testing of the LCP – how can stability in locked internal fixators be controlled?* Injury, 2003. **34, Supplement 2**(0): p. 11-19.
28. Levine, R.S., *Injury to the extremities.* Accidental injury: biomechanics and prevention. Nahum AM, Melvin J, eds. New York: Springer-Verlag, 1993: p. 460-492.
29. Pierce, M.C., et al., *Evaluating long bone fractures in children: a biomechanical approach with illustrative cases.* Child Abuse Negl, 2004. **28**(5): p. 505-24.
30. Turner, C.H. and D.B. Burr, *Basic biomechanical measurements of bone: A tutorial.* Bone, 1993. **14**(4): p. 595-608.
31. Kress, T., et al. *Fracture patterns of human cadaver long bones*. 1995.
32. *AO Surgery Reference*. [cited 2012 June 25]; Available from: http://www2.aofoundation.org.
33. Stiffler, K.S., *Internal fracture fixation.* Clinical Techniques in Small Animal Practice, 2004. **19**(3): p. 105-113.
34. Niemeyer, P. and N.P. Sudkamp, *Principles and clinical application of the locking compression plate (LCP).* Acta Chir Orthop Traumatol Cech, 2006. **73**(4): p. 221-228.
35. DeTora, M. and K. Kraus, *Mechanical testing of 3.5 mm locking and non-locking bone plates.* Vet Comp Orthop Traumatol, 2008. **21**(4): p. 318-22.
36. Aguila, A.Z., et al., *In vitro biomechanical comparison of limited contat dynamic compression plate and locking compression plate.* Vet Comp Orthop Traumatol, 2005. **18**(4): p. 220-6.
37. Ness, M.G., *The effect of bending and twisting on the stiffness and strength of the 3.5 SOP implant.* Vet Comp Orthop Traumatol, 2009. **22**(2): p. 132-6.
38. Ness, M.G., *Repair of Y-T humeral fractures in the dog using paired 'String of Pearls' locking plates.* Vet Comp Orthop Traumatol, 2009. **22**(6): p. 492-7.
39. Petazzoni, M., et al., *Fixin internal fixator: Concept and technique.* VCOT, 2009. **22**(4): p. 309-315.
40. Inauen, R., D. Koch, and M. Bass, *Arthrodesis of the tarsometatarsal joints in a cat with a two hole advanced locking plate system.* Vet Comp Orthop Traumatol, 2009. **22**(2): p. 166-9.
41. *Kyon Veterinary Surgical Products*. [cited 2012 May 1]; Available from: http://www.kyon.ch.

42. Apivatthakakul, T., C. Phornphutkul, and S. Patumasutra, *Idea and innovation: Simple minimally invasive plate osteosynthesis (MIPO) instruments.* Injury Extra, 2009. **40**(2): p. 39-44.
43. Patel, P.S.D., D.E.T. Shepherd, and D.W.L. Hukins, *The effect of screw insertion angle and thread type on the pullout strength of bone screws in normal and osteoporotic cancellous bone models.* Medical Engineering & Physics, 2010. **32**(8): p. 822-828.
44. Augat, P., et al., *Local tissue properties in bone healing: Influence of size and stability of the osteotomy gap.* Journal of Orthopaedic Research, 1998. **16**(4): p. 475-481.
45. Markel, M.D., M.A. Wikenheiser, and E.Y.S. Chao, *A study of fracture callus material properties: Relationship to the torsional strength of bone.* Journal of Orthopaedic Research, 1990. **8**(6): p. 843-850.
46. Jepsen, K.J. and D.T. Davy, *Comparison of damage accumulation measures in human cortical bone.* Journal of Biomechanics, 1997. **30**(9): p. 891-894.
47. Gautier, E. and C. Sommer, *Guidelines for the clinical application of the LCP.* Injury, 2003. **34 Suppl 2**: p. B63-76.
48. Stoffel, K., K. Klaue, and S.M. Perren, *Functional load of plates in fracture fixation in vivo and its correlate in bone healing.* Injury, 2000. **31, Supplement 2**(0): p. 37-86.
49. Gautier, E., S. Perren, and J. Cordey, *Strain distribution in plated and unplated sheep tibia an in vivo experiment.* Injury, 2000. **31**: p. 37-93.
50. Cabassu, J., et al., *Single cycle to failure in torsion of three standard and five locking plate constructs.* Veterinary and Comparative Orthopaedics and Traumatology, 2011. **24**(6): p. 418.
51. Acker ML, T.B., Kowaleski MP, Boudrieau RJ. *Structural properties of synthetic bone models compared to native canine bone.* in *European College of Veterinary Surgeons, 19th Annual Scientific Meeting*. 2010. Helsinki, Finland.
52. Fitzpatrick, D.C., et al., *Relative stability of conventional and locked plating fixation in a model of the osteoporotic femoral diaphysis.* Clinical Biomechanics, 2009. **24**(2): p. 203-209.
53. Filipowicz, D., et al., *A biomechanical comparison of 3.5 locking compression plate fixation to 3.5 limited contact dynamic compression plate fixation in a canine cadaveric distal humeral metaphyseal gap model.* Veterinary and Comparative Orthopaedics and Traumatology, 2009. **22**(4): p. 270-7.
54. Lin, S.K., Y.L. Lee, and M.W. Lu, *Evaluation of the staircase and the accelerated test methods for fatigue limit distributions.* International journal of fatigue, 2001. **23**(1): p. 75-83.
55. Lee, Y.L., *Fatigue testing and analysis: theory and practice*. Vol. 13. 2005: Butterworth-Heinemann.
56. Pollak, R.D., *Analysis of Methods for Determining High Cycle Fatigue Strength of a Material With Investigation of Ti-6Al-4V Gigacycle Fatigue Behavior*, 2005, DTIC Document.
57. Nicholas, T., *High cycle fatigue: a mechanics of materials perspective*2006: Elsevier Science.
58. Crow, E.L., F.A. Davis, and M.W. Maxfield, *Statistics manual: with examples taken from ordnance development*. Vol. 3369. 1960: Dover Publications.
59. Hottinger, H.A., et al., *Noninvasive kinematic analysis of the walk in healthy large-breed dogs.* Am J Vet Res, 1996. **57**(3): p. 381-8.
60. Heiner, A.D. and T.D. Brown, *Structural properties of a new design of composite replicate femurs and tibias.* Journal of Biomechanics, 2001. **34**(6): p. 773-781.

61. Yánez, A., J.A. Carta, and G. Garcés, *Biomechanical evaluation of a new system to improve screw fixation in osteoporotic bones.* Medical Engineering & Physics, 2010. **32**(5): p. 532-541.
62. Pollak, R., A. Palazotto, and T. Nicholas, *A simulation-based investigation of the staircase method for fatigue strength testing.* Mechanics of Materials, 2006. **38**(12): p. 1170-1181.

Appendix A: Four-Point Bending Force-Displacement Graphs

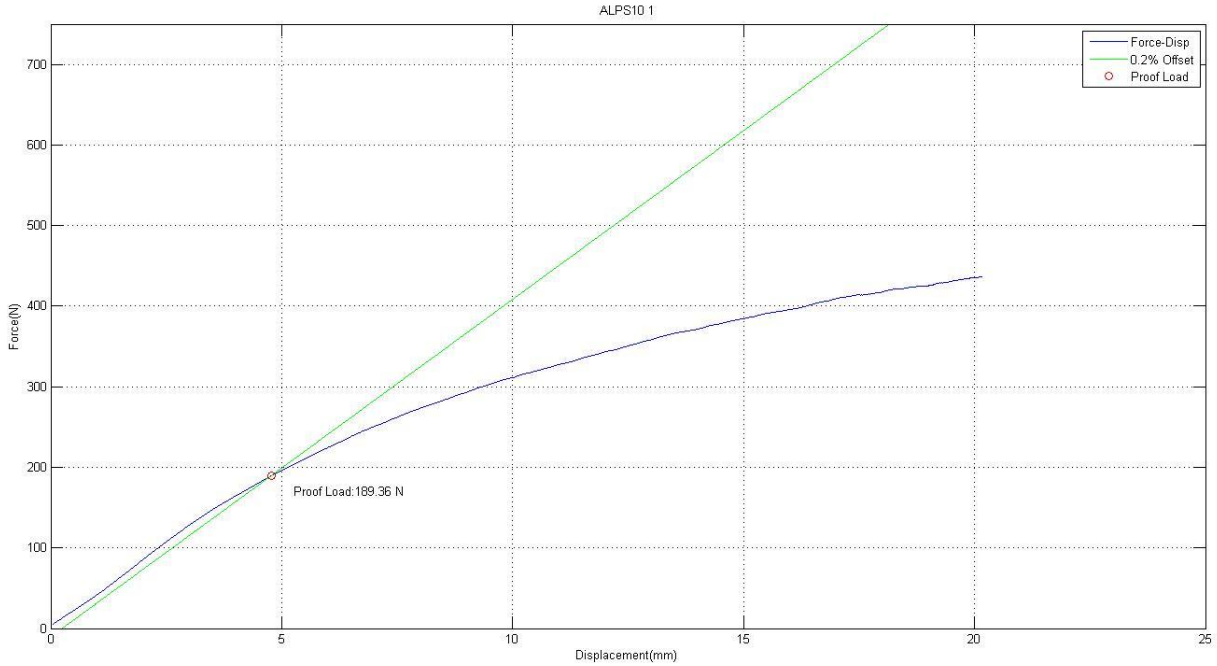

Figure A.1: ALPS10, Sample 1

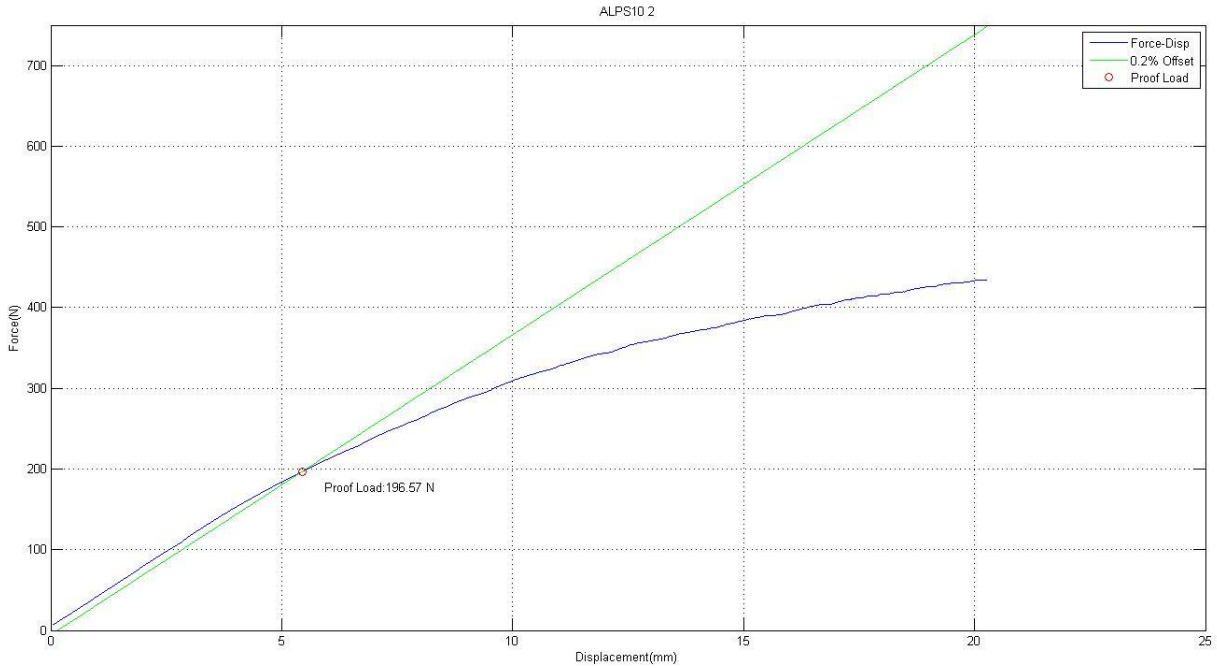

Figure A.2: ALPS10, Sample 2

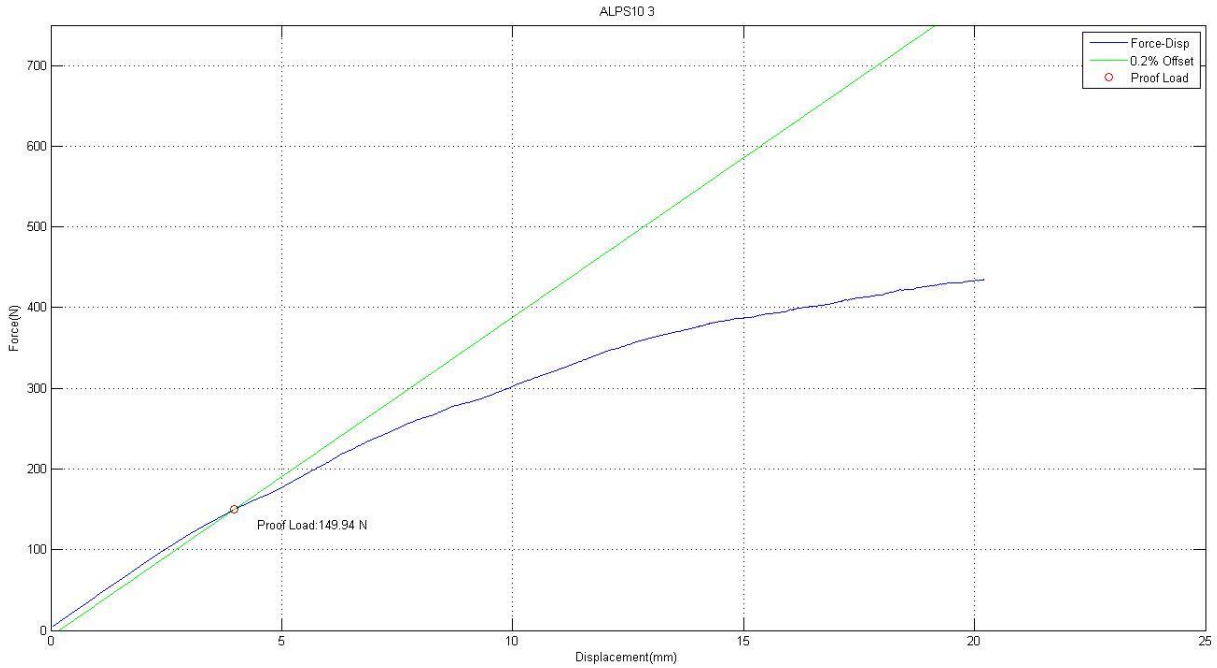

Figure A.3: ALPS10, Sample 3

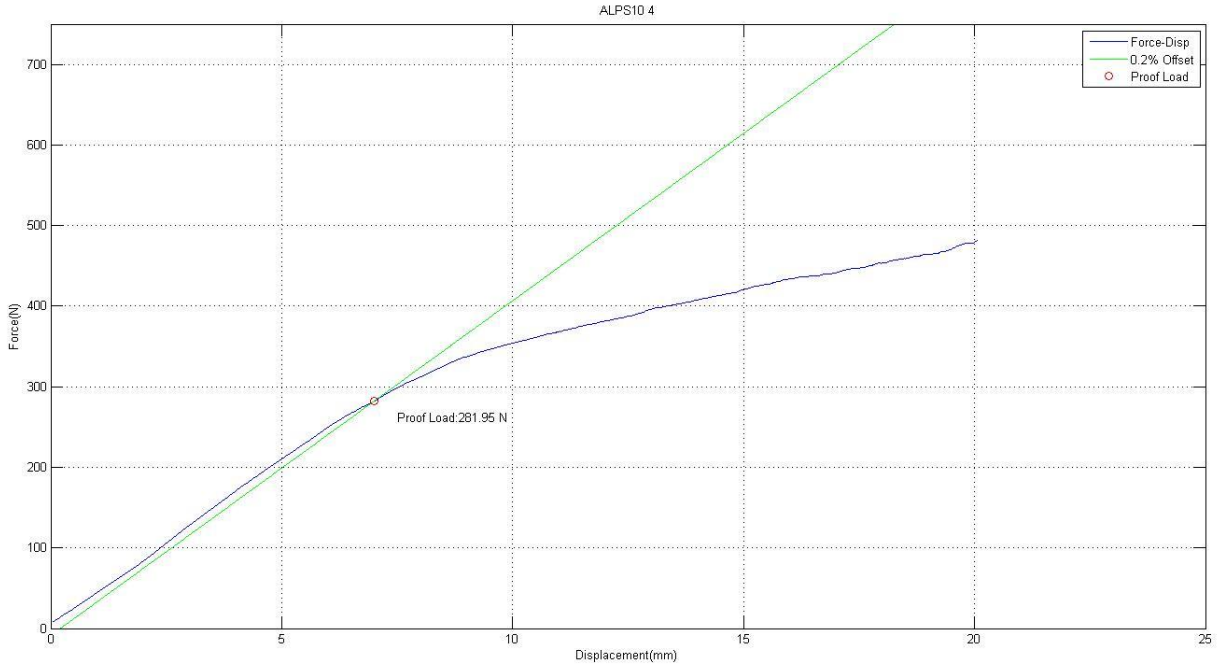

Figure A.4: ALPS10, Sample 4

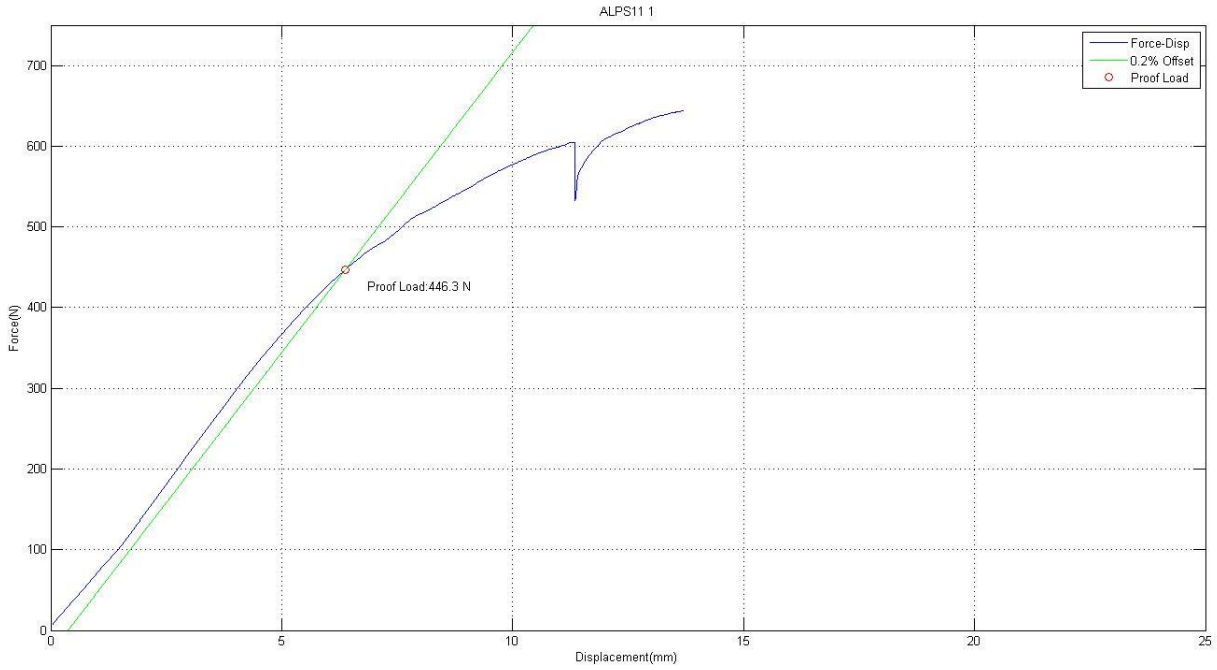

Figure A.5: ALPS11, Sample 1

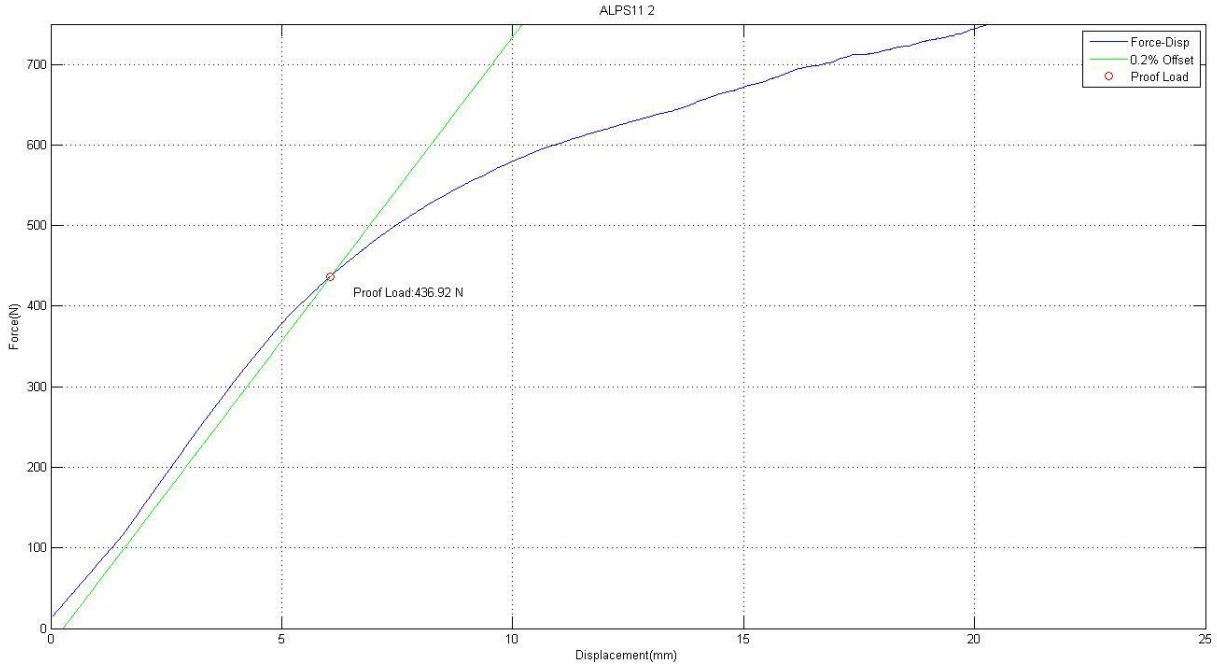

Figure A.6: ALPS11, Sample 2

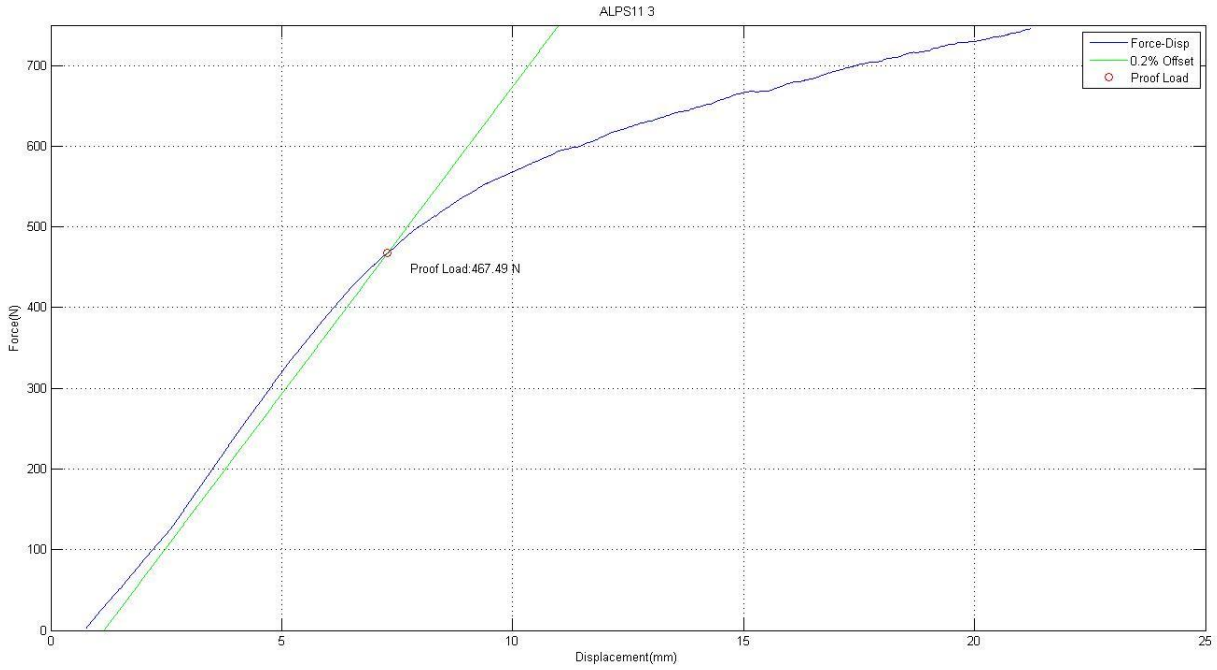

Figure A.7: ALPS11, Sample 3

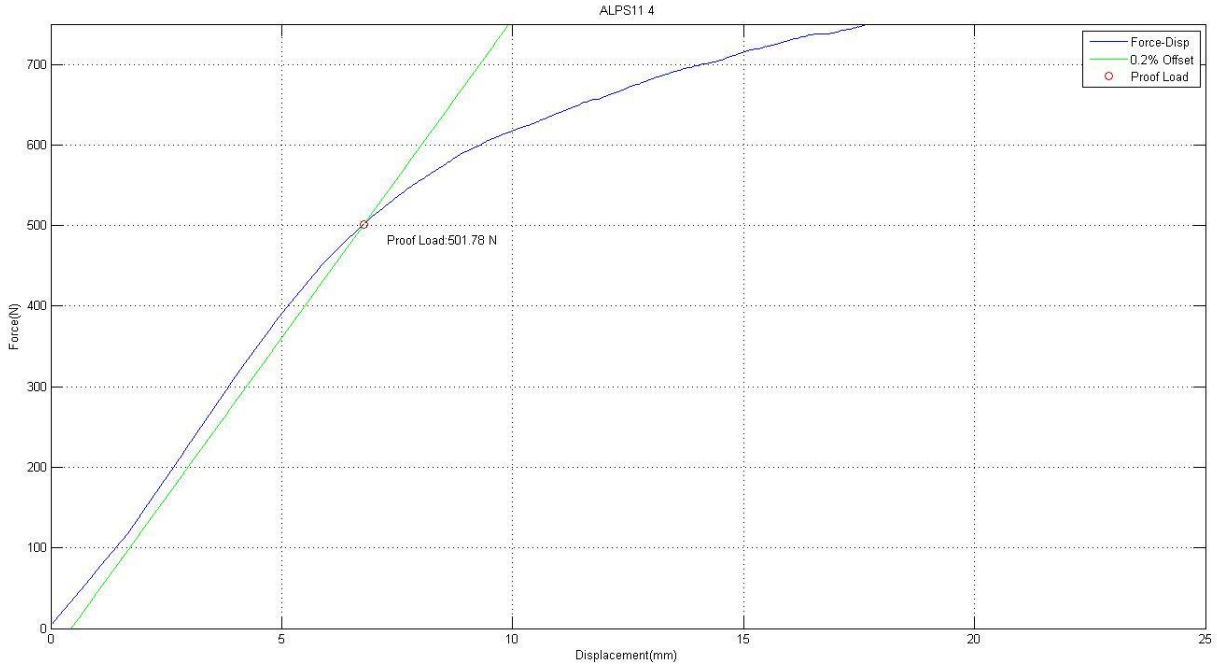

Figure A.8: ALPS11, Sample 4

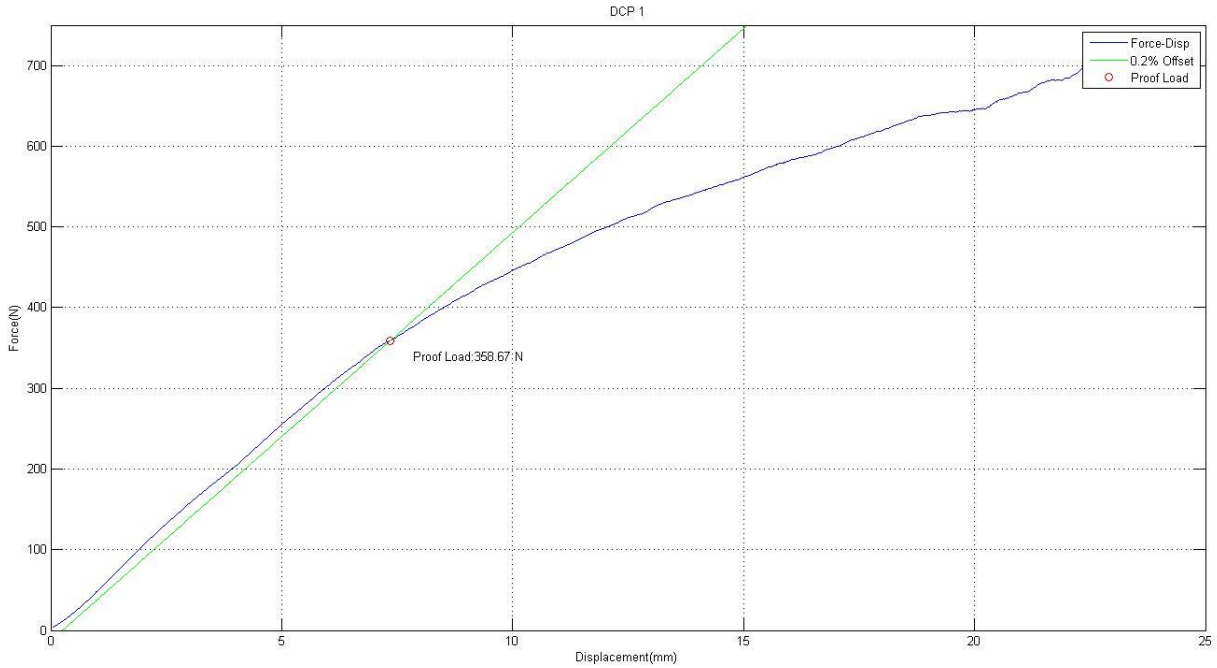

Figure A.9: DCP, Sample 1

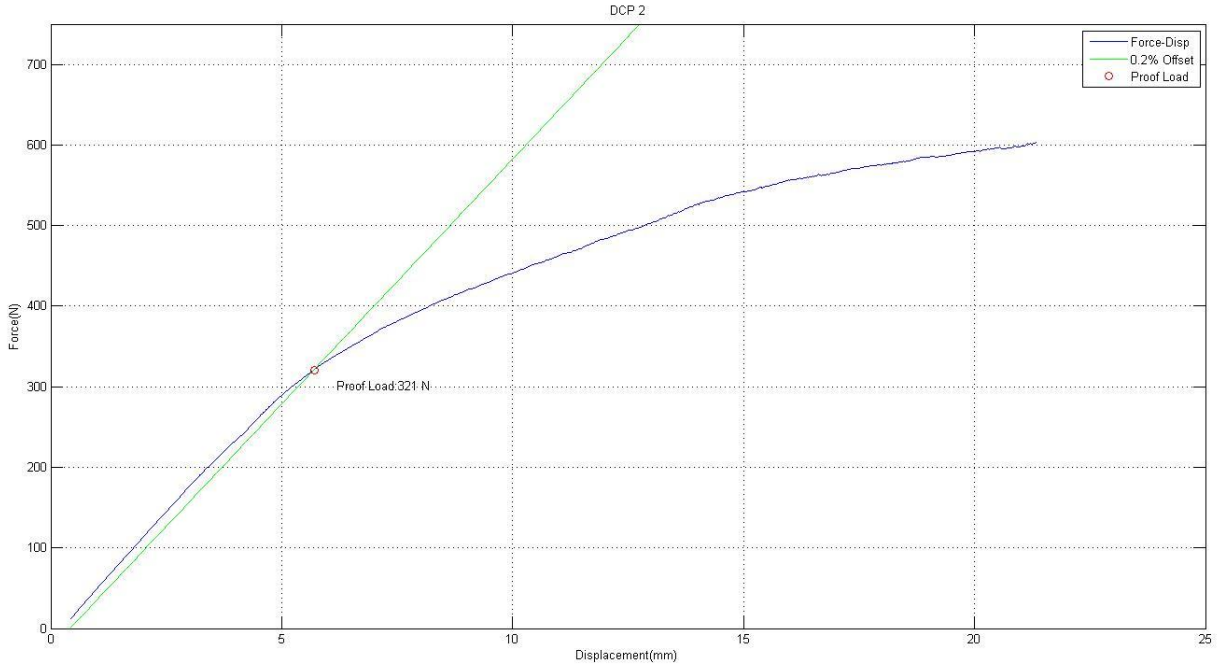

Figure A.10: DCP, Sample 2

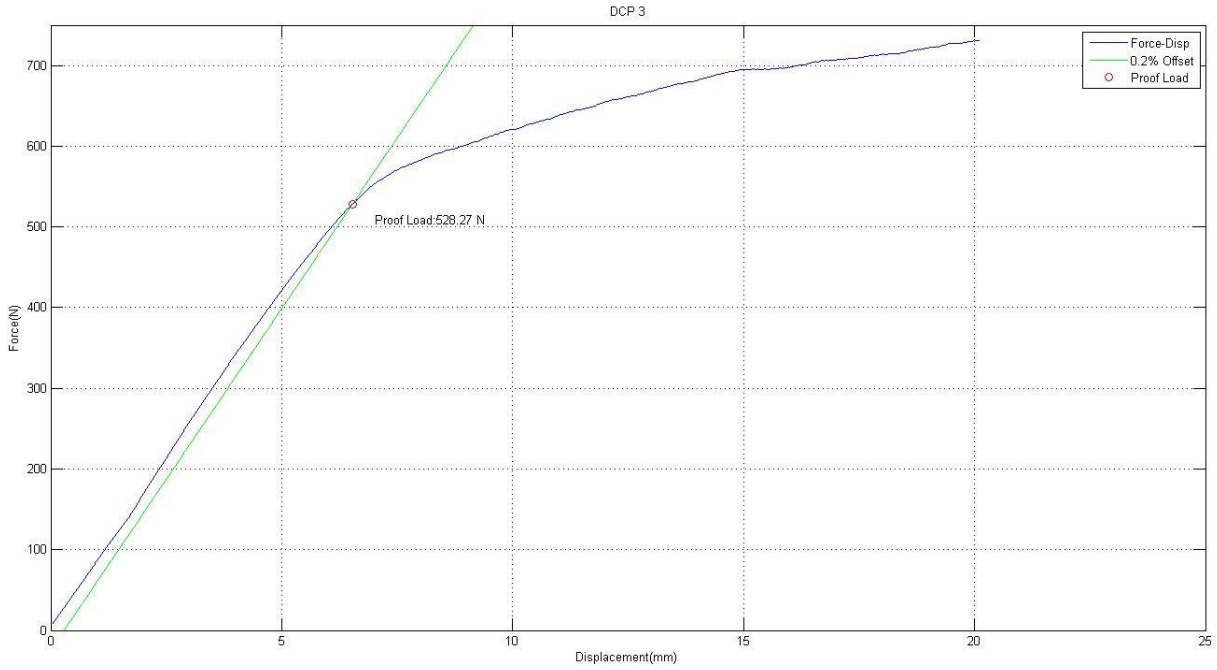

Figure A.11: DCP, Sample 3

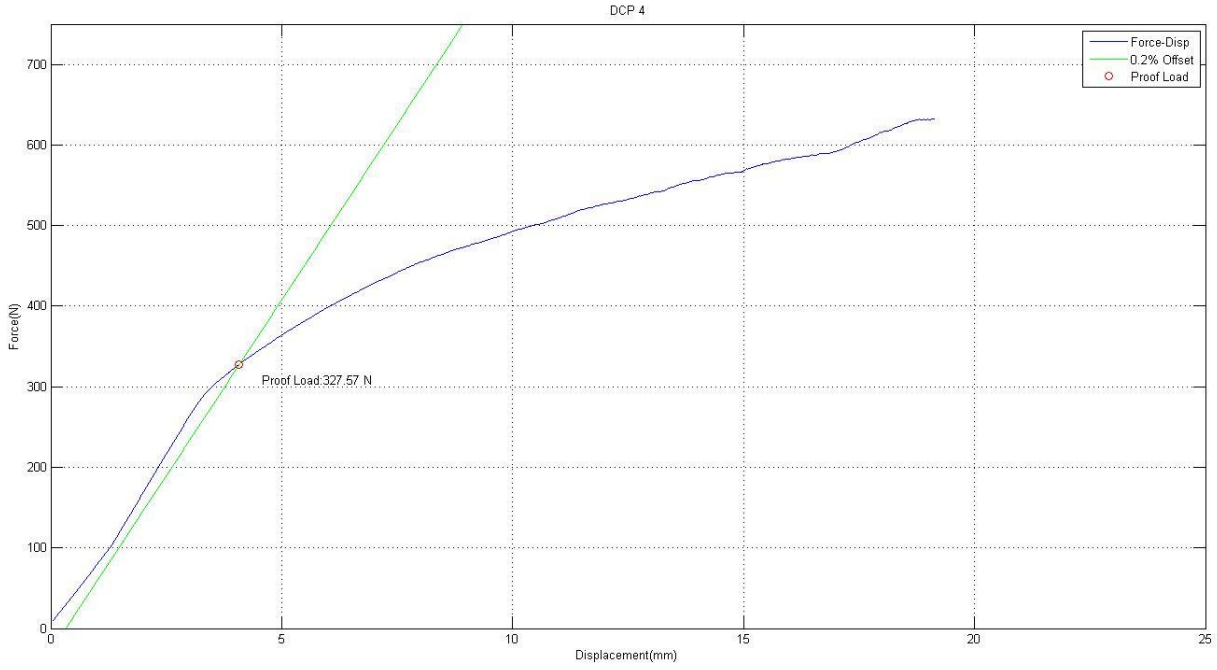

Figure A.12: DCP, Sample 4

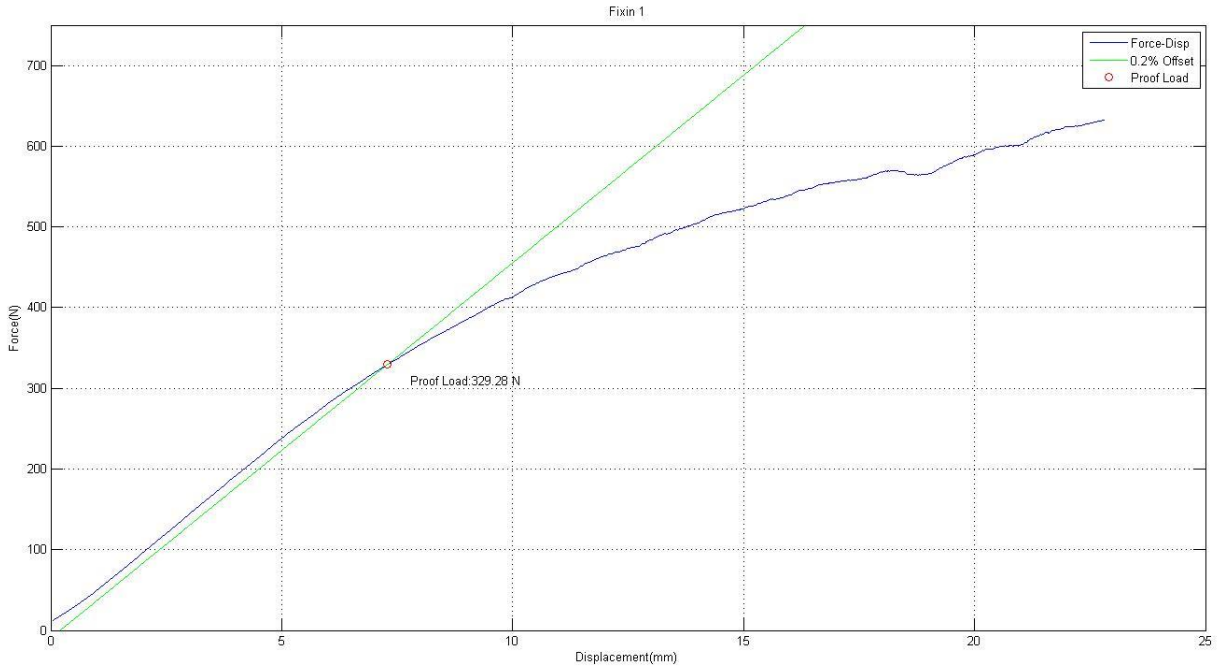

Figure A.13: Fixin, Sample 1

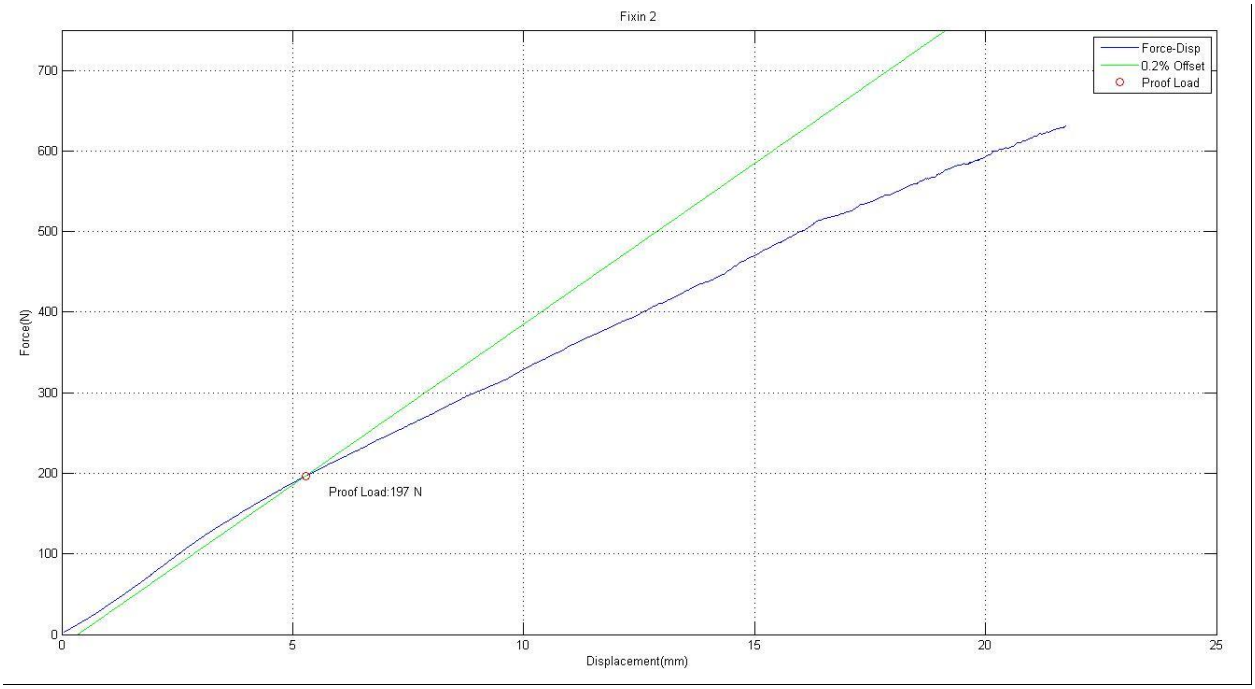

Figure A.14: Fixin, Sample 2

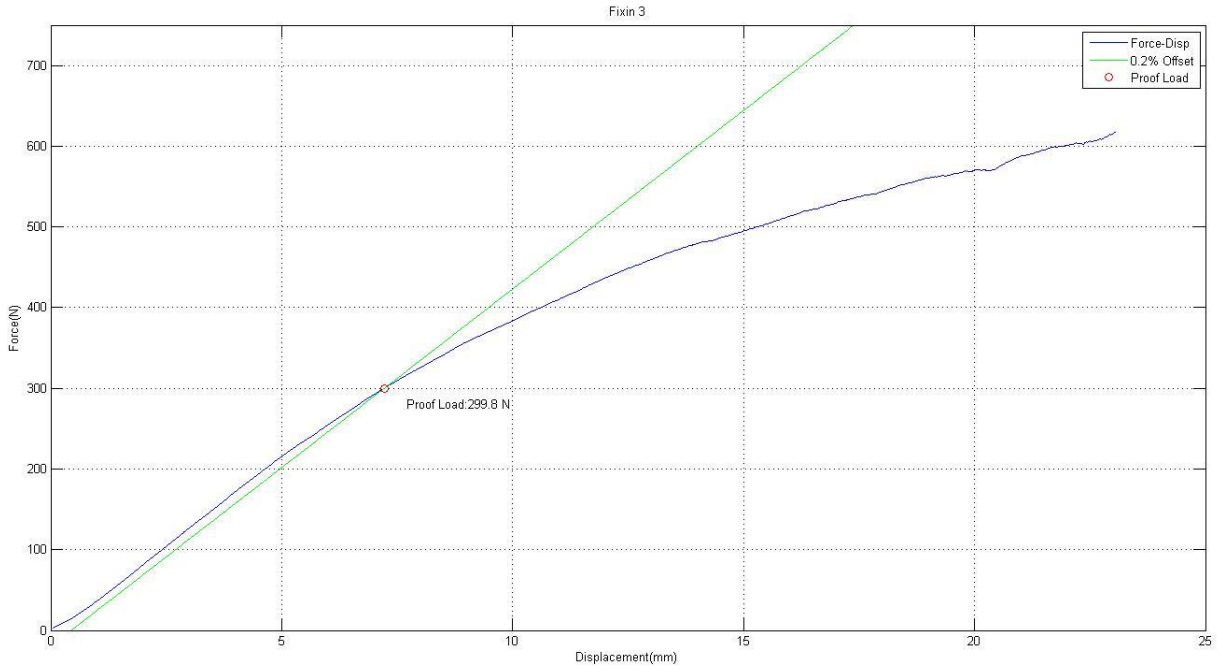

Figure A.15: Fixin, Sample 3

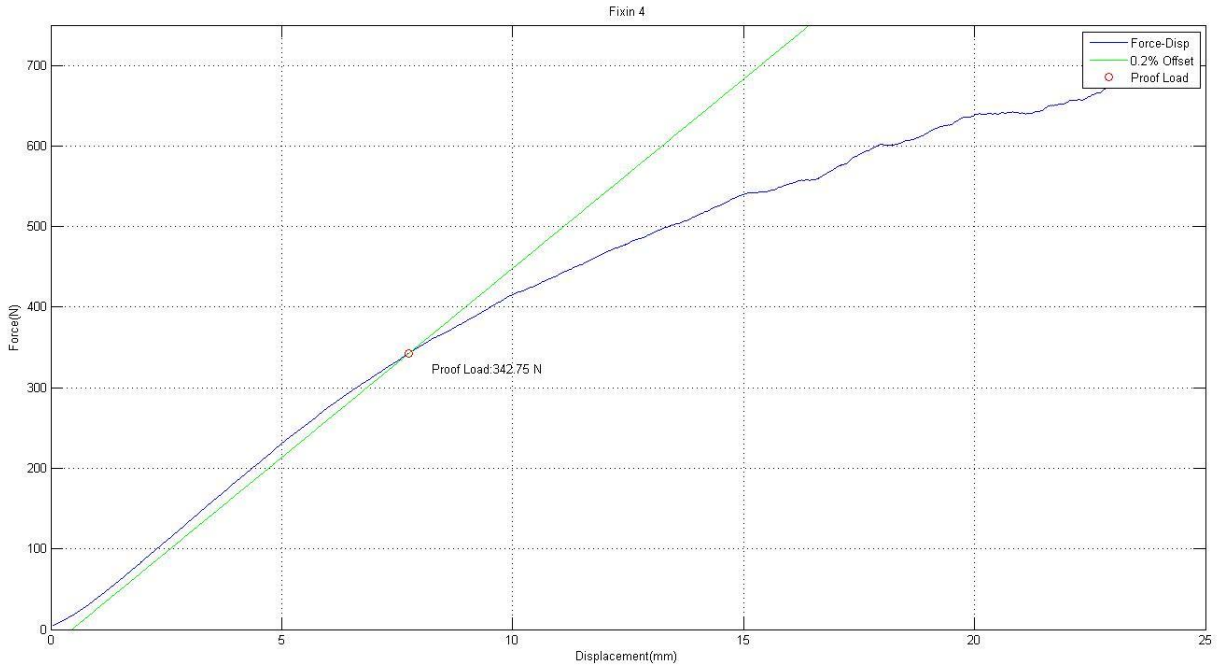

Figure A.16: Fixin, Sample 4

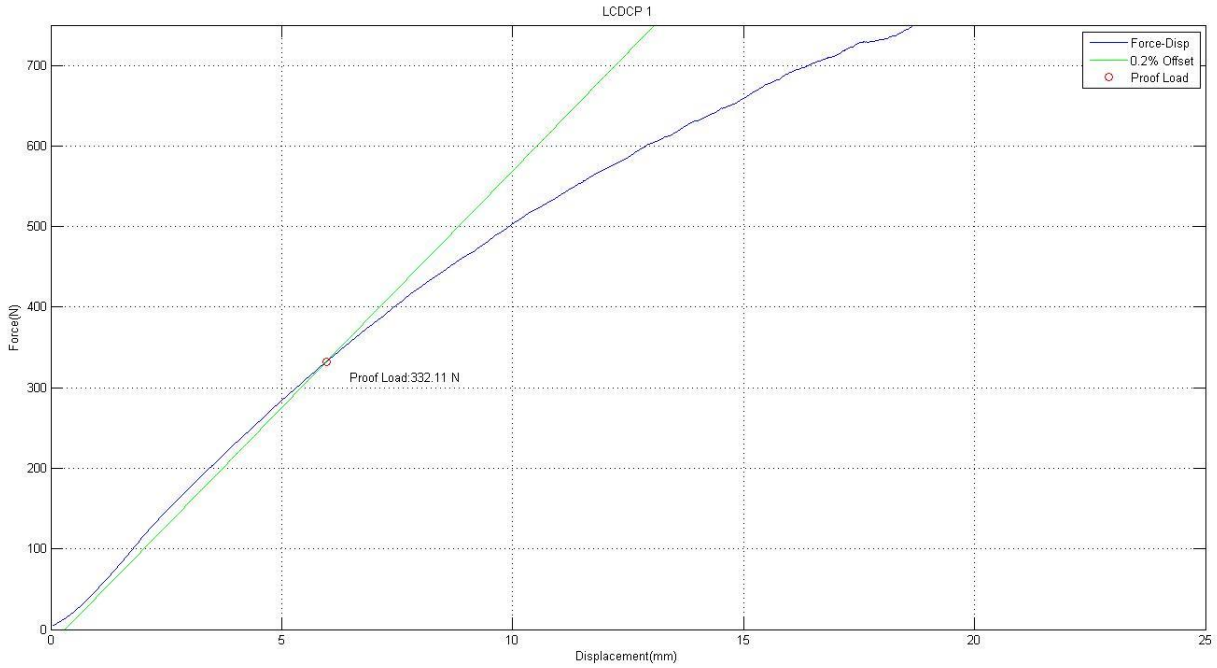

Figure A.17: SS LC-DCP, Sample 1

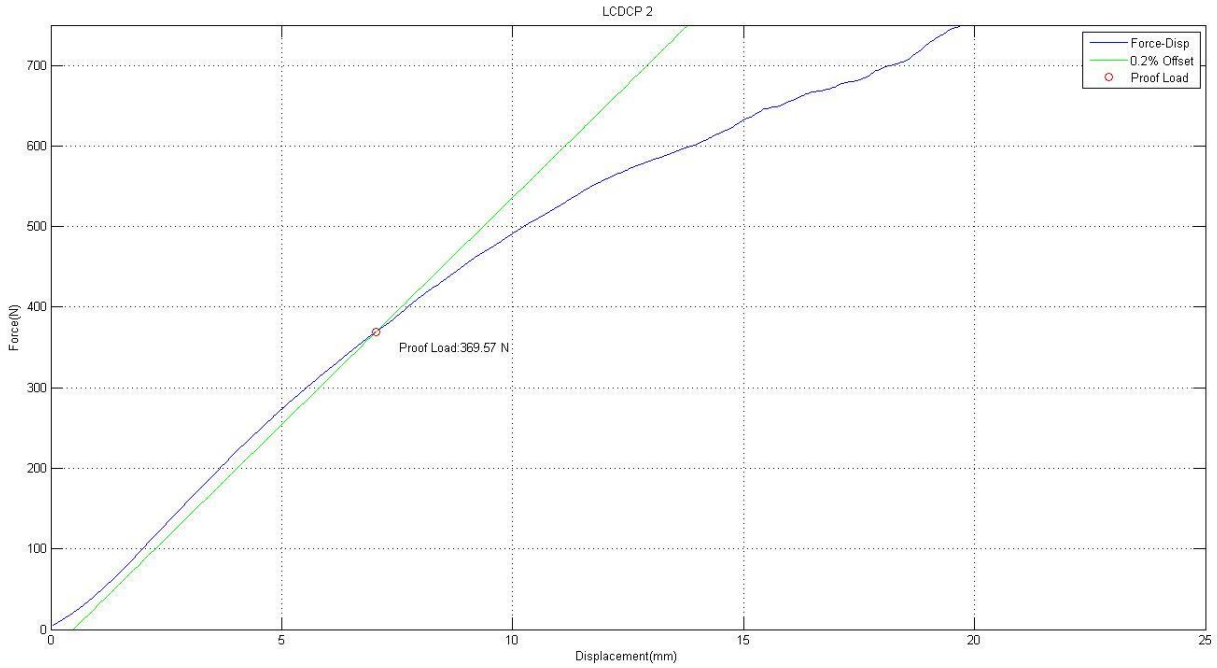

Figure A.18: SS LC-DCP, Sample 2

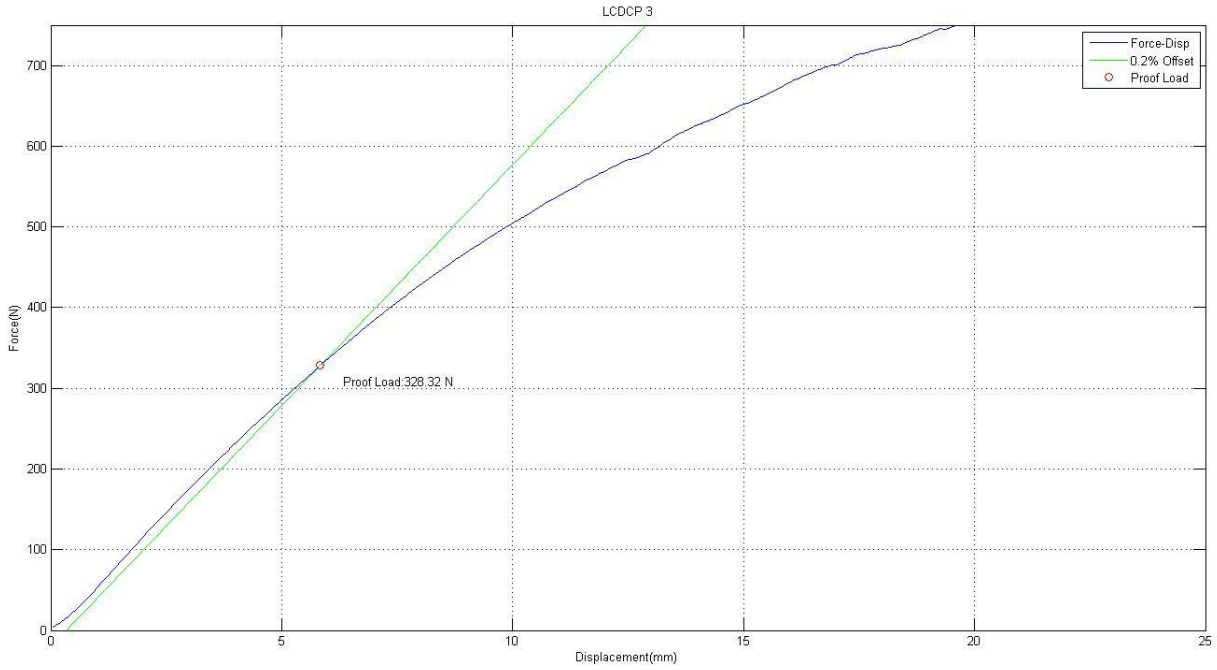

Figure A.19: SS LC-DCP, Sample 3

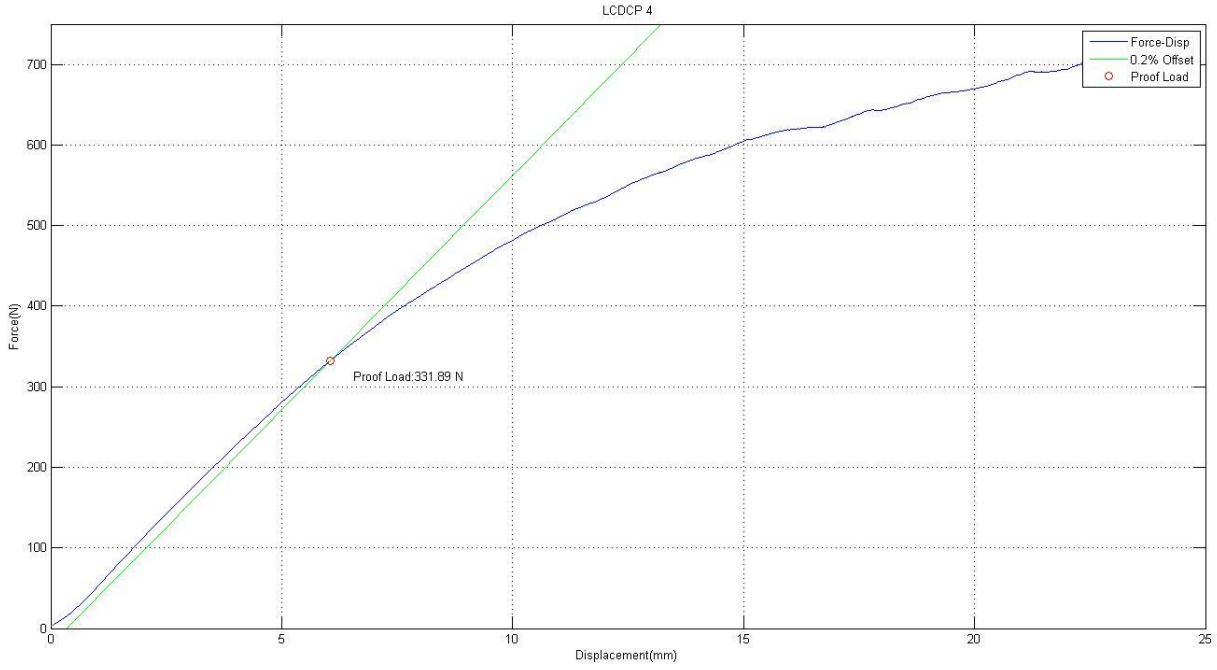

Figure A.20: SS LC-DCP, Sample 4

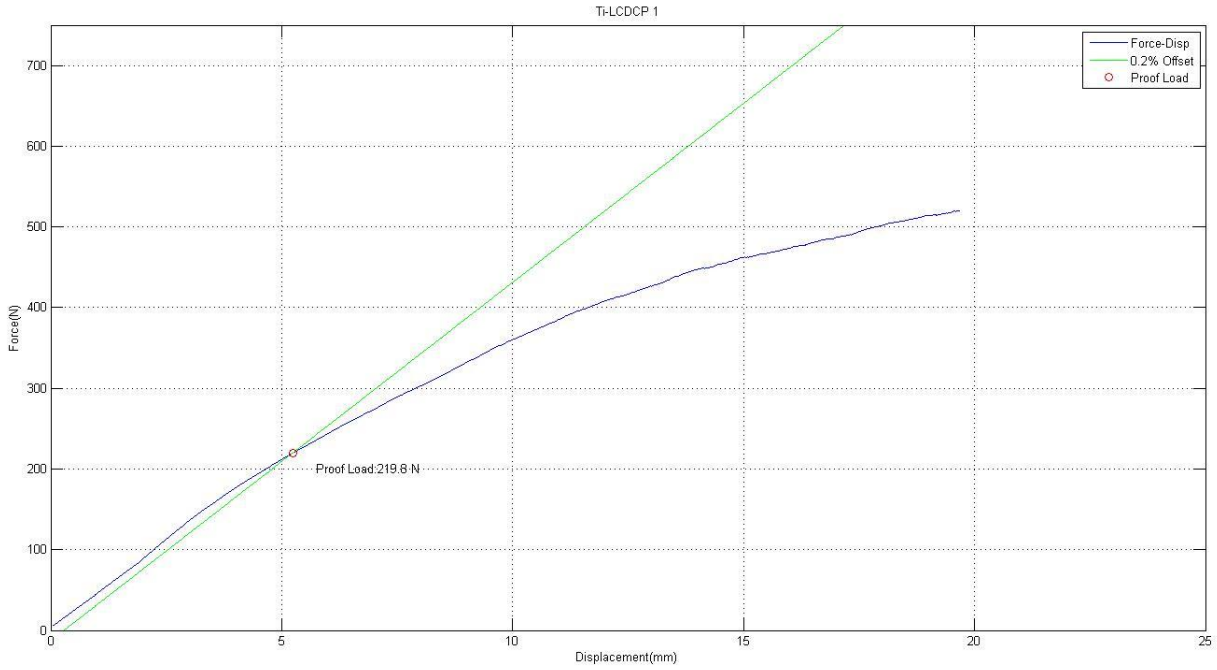

Figure A.21: Ti LC-DCP, Sample 1

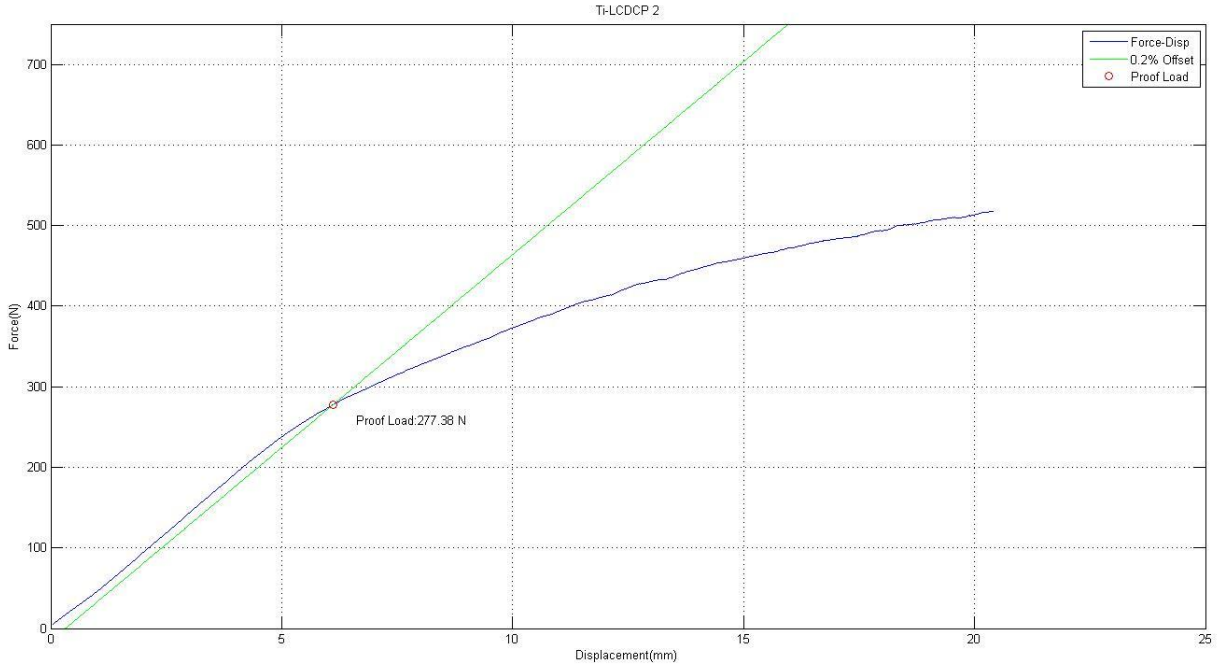

Figure A.22: Ti LC-DCP, Sample 2

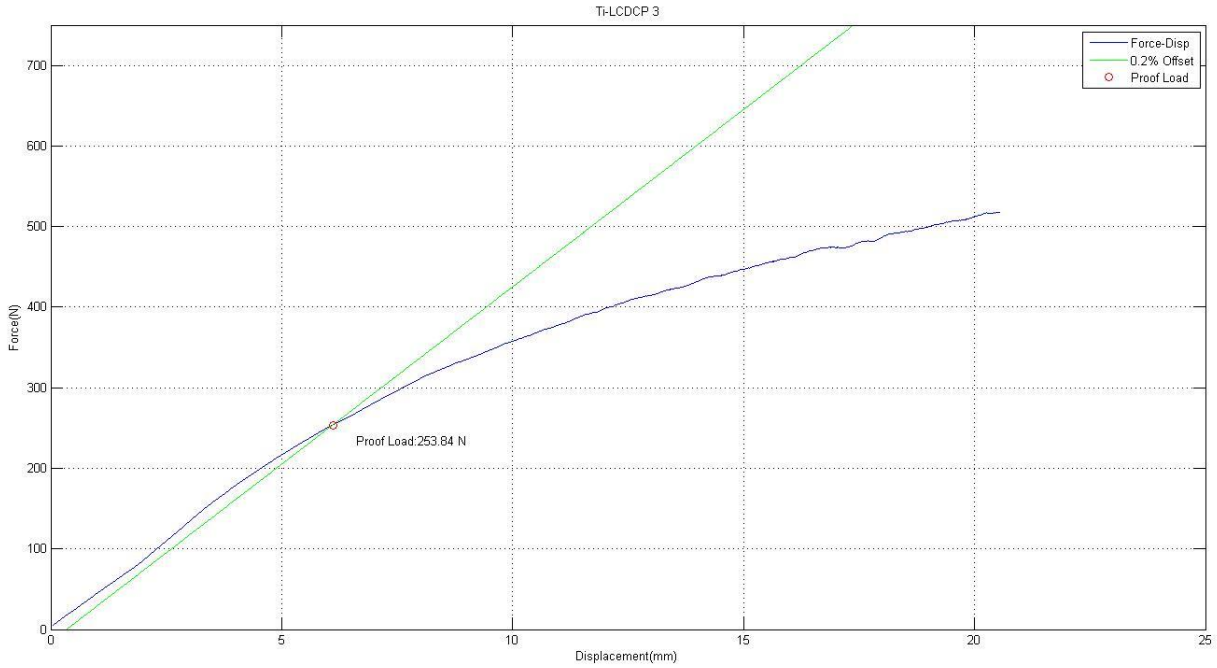

Figure A.23: Ti LC-DCP, Sample 3

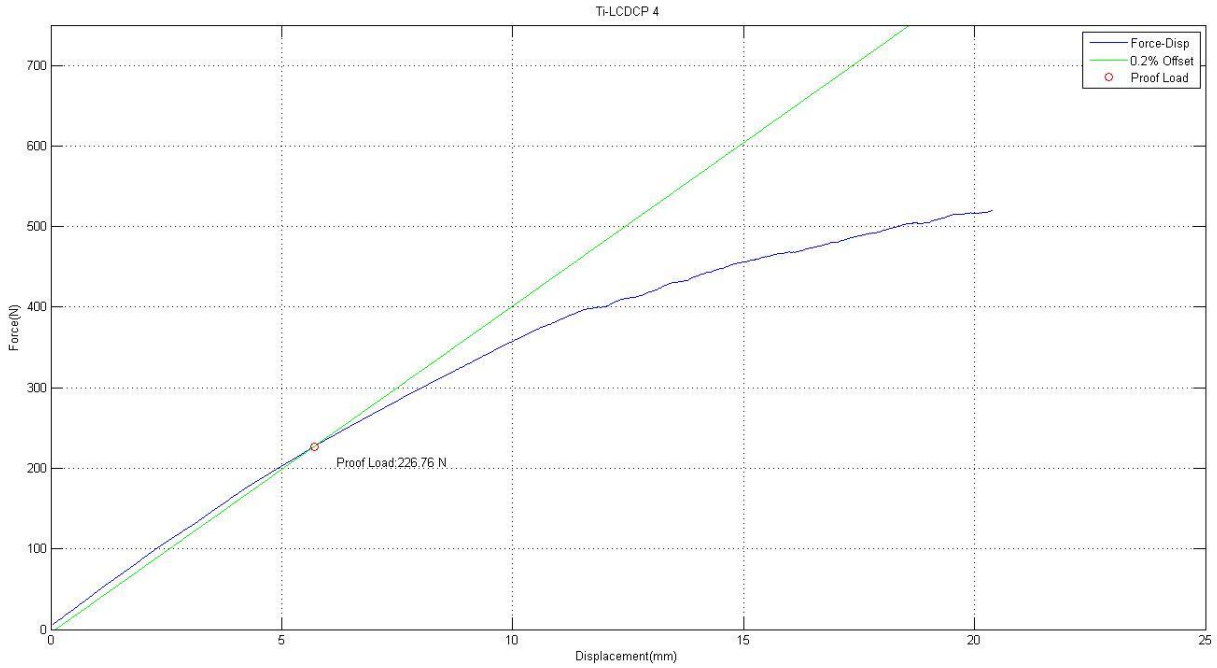

Figure A.24: Ti LC-DCP, Sample 4

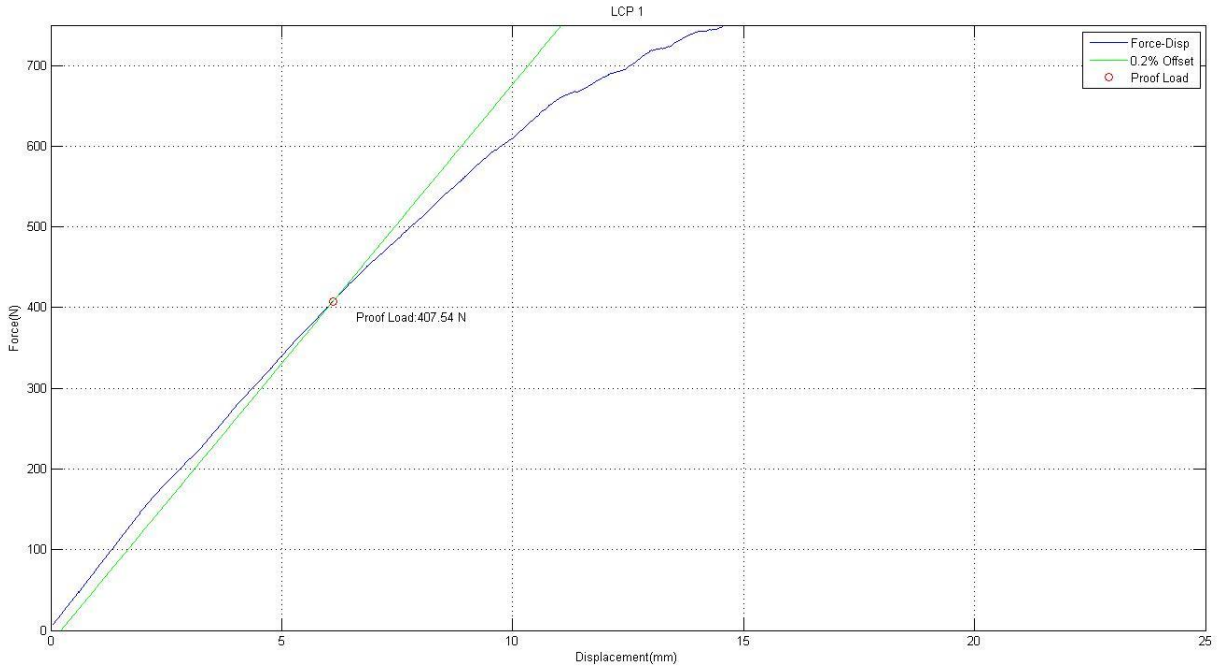

Figure A.25: LCP, Sample 1

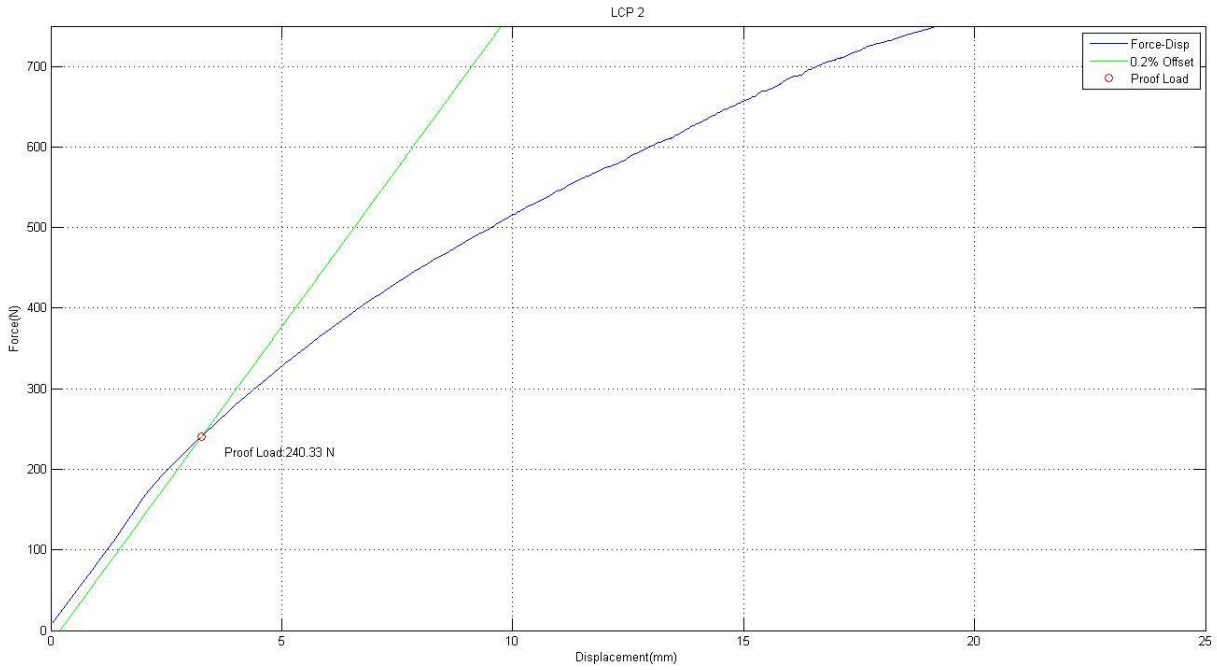

Figure A.26: LCP, Sample 2

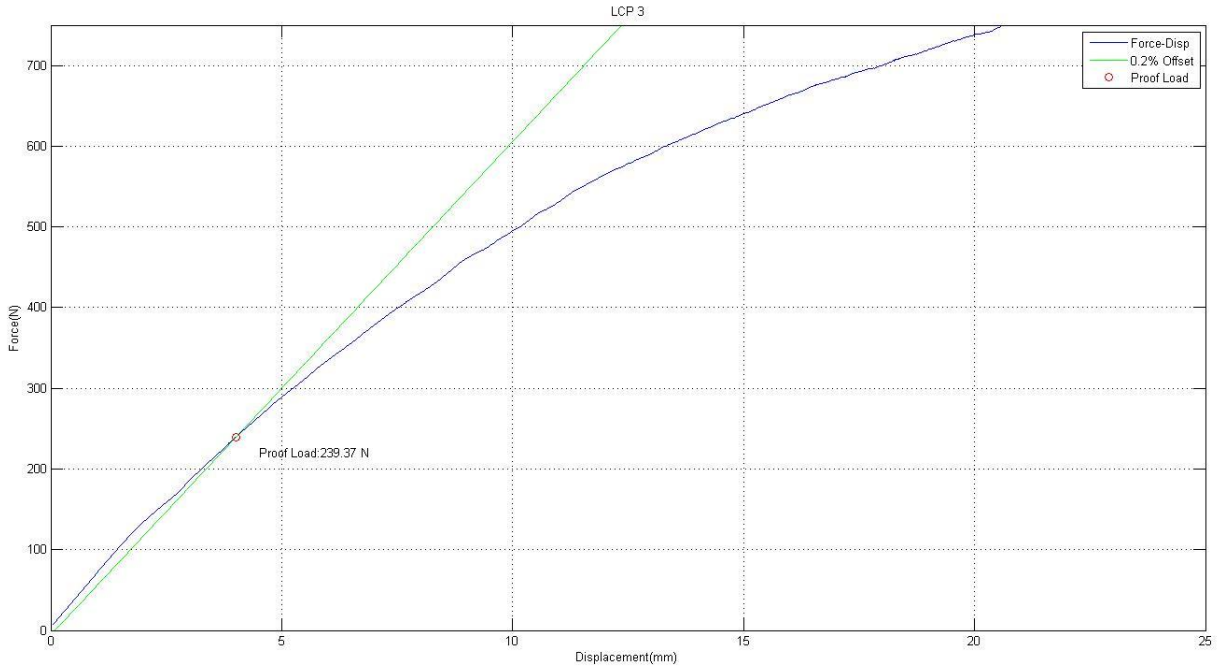

Figure A.27: LCP, Sample 3

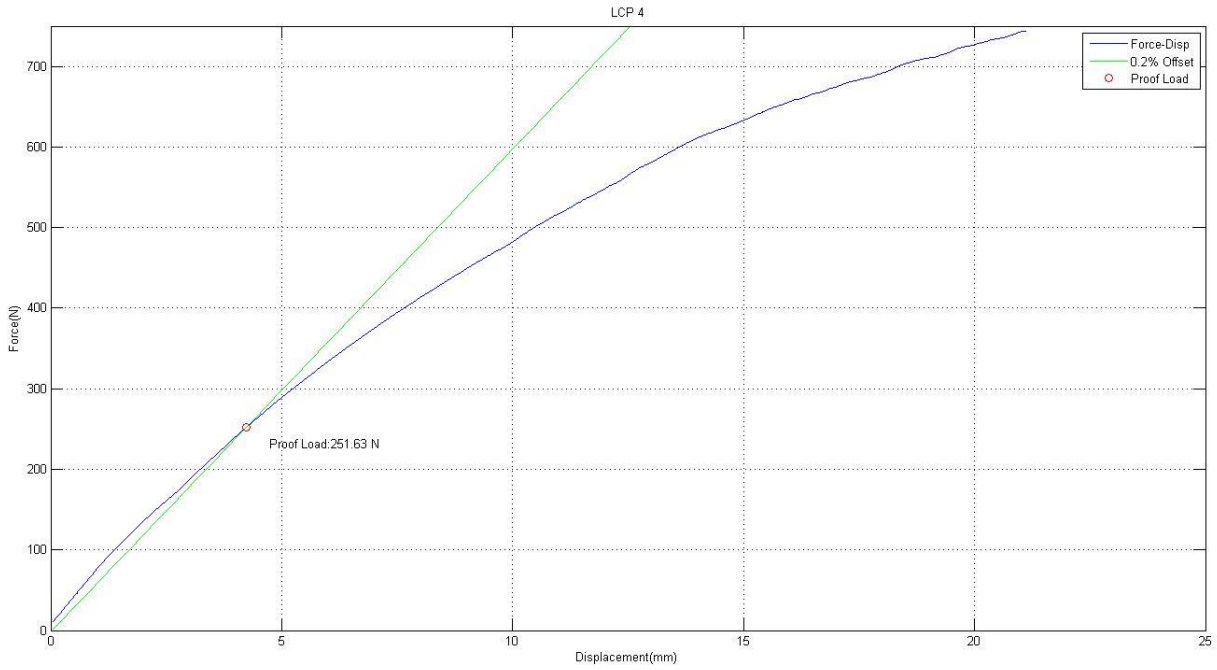

Figure A.28: LCP, Sample 4

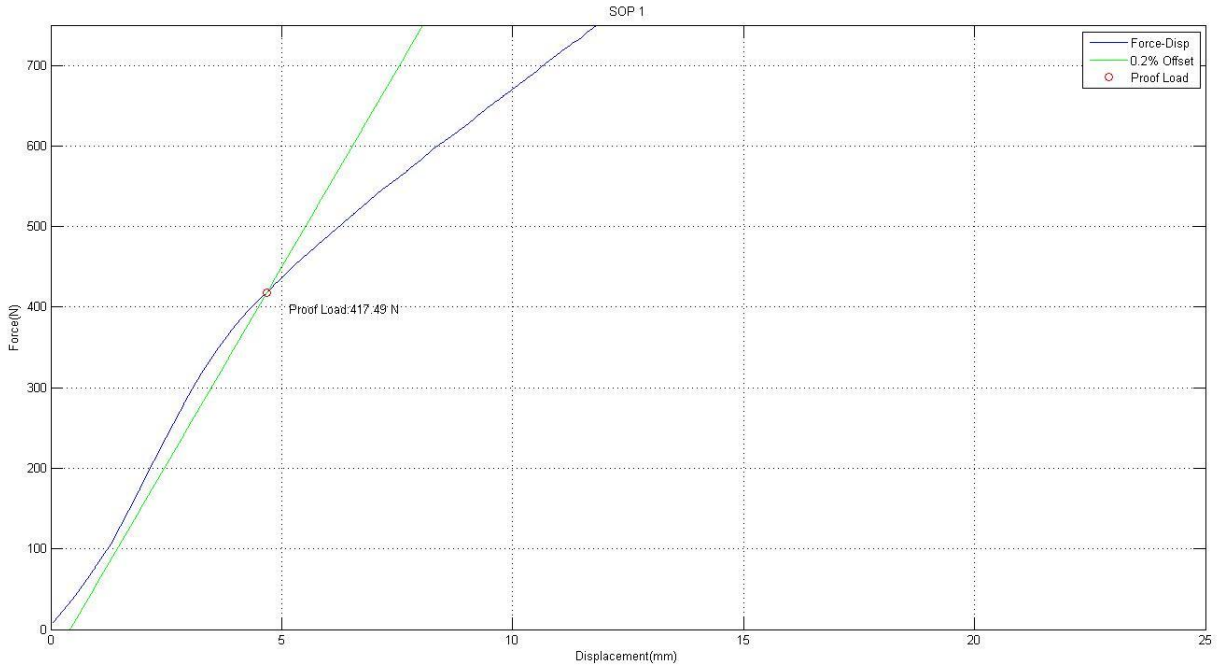

Figure A.29: SOP, Sample 1

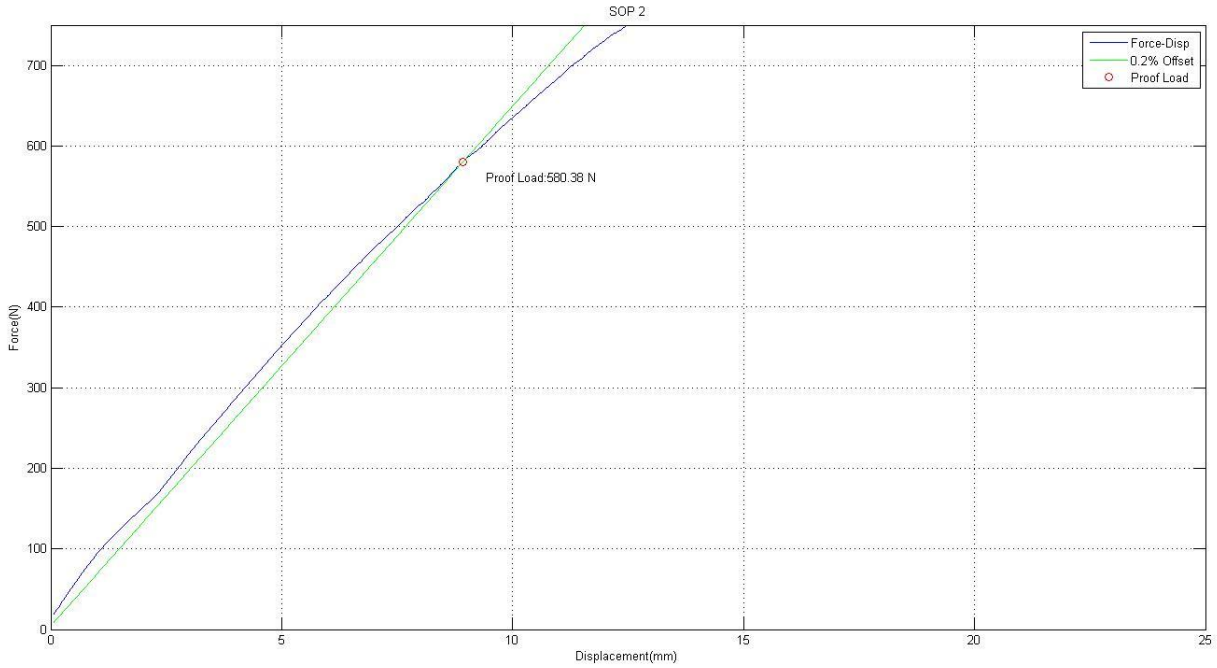

Figure A.30: SOP, Sample 2

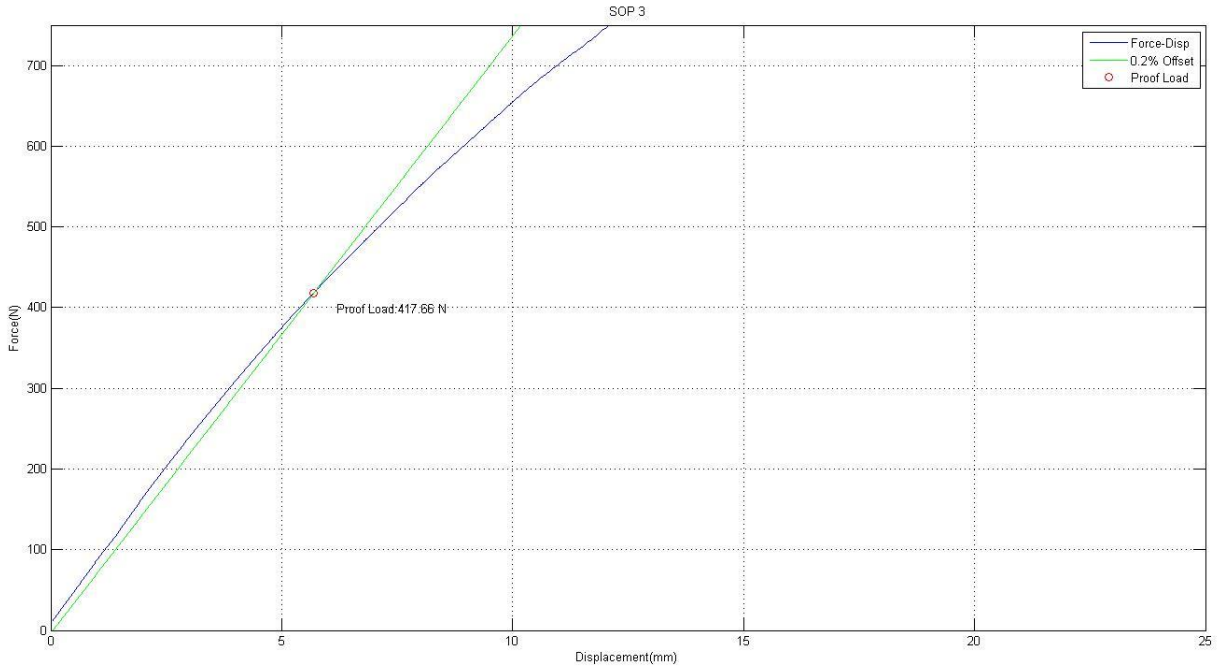

Figure A.31: SOP, Sample 3

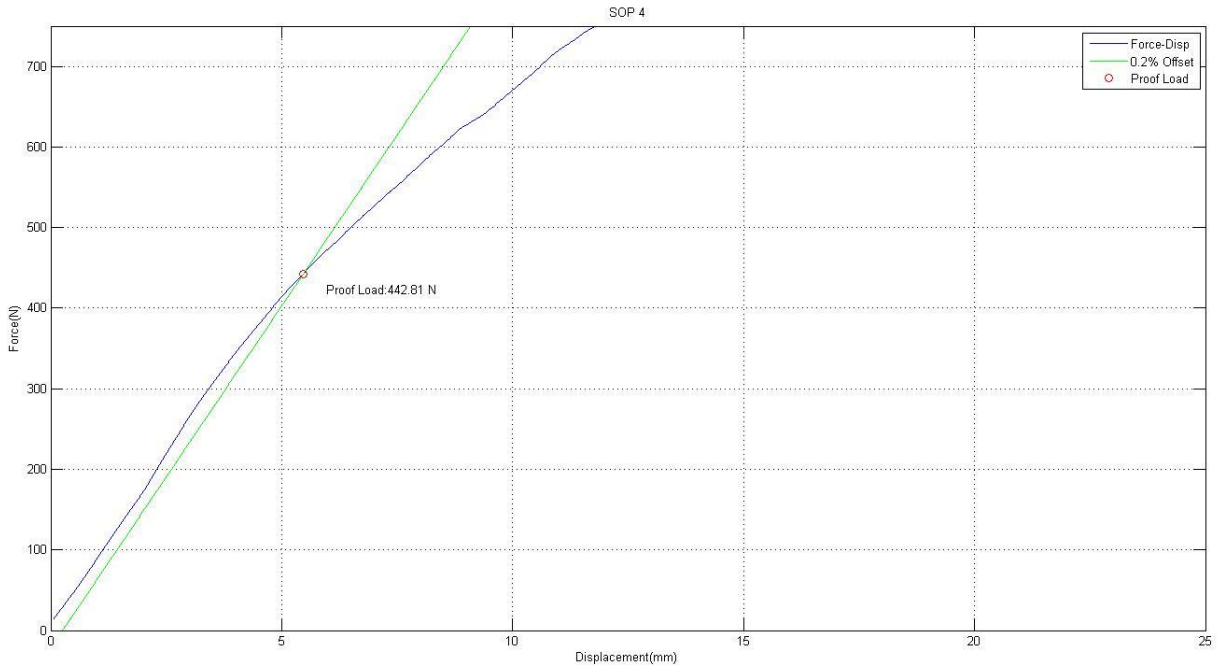

Figure A.32: SOP, Sample 4

Appendix B: Four-Point Bending Calculated Data

Table B.1: Proof Load Calculations.

	Sample:	1	2	3	4	Mean	SD
Proof Load (N)	DCP	358.67	321.00	528.27	327.57	383.88	84.57
	LCDCP	332.11	369.57	328.32	331.89	340.47	16.87
	Ti-LCDCP	219.80	277.38	253.84	226.76	244.45	22.88
	LCP	407.54	240.33	221.95	200.54	267.59	82.02
	ALPS10	189.36	196.57	149.94	281.95	204.46	48.13
	ALPS11	446.30	436.92	467.49	501.78	463.12	24.92
	SOP	417.49	580.38	417.66	442.81	464.59	67.64
	Fixin	329.28	197.00	299.80	342.75	292.21	57.12

Table B.2: Bending Stiffness Calculations.

	Sample:	1	2	3	4	Mean	SD
Bending Stiffness (N/mm)	DCP	51.58	60.79	84.61	87.18	71.04	15.24
	LCDCP	58.77	55.38	57.90	57.28	57.33	1.25
	Ti-LCDCP	44.39	47.91	44.01	40.55	44.21	2.61
	LCP	69.20	76.35	61.13	59.90	66.65	6.65
	ALPS10	41.87	37.19	39.52	41.54	40.03	1.87
	ALPS11	74.43	75.41	76.16	79.13	76.28	1.75
	SOP	98.18	64.52	74.01	84.90	80.40	12.54
	Fixin	46.50	39.90	44.26	46.96	44.40	2.79

Table B.3: Bending Structural Stiffness Calculations.

	Sample:	1	2	3	4	Mean	SD
Bending Structural Stiffness ($N\text{-}m^2$)	DCP	5.59	6.59	9.17	9.44	7.70	1.65
	LCDCP	6.37	6.00	6.27	6.21	6.21	0.14
	Ti-LCDCP	4.81	5.19	4.77	4.39	4.79	0.28
	LCP	7.50	8.27	6.62	6.49	7.22	0.72
	ALPS10	4.54	4.03	4.28	4.50	4.34	0.20
	ALPS11	8.06	8.17	8.25	8.57	8.26	0.19
	SOP	10.64	6.99	8.02	9.20	8.71	1.36
	Fixin	5.04	4.32	4.80	5.09	4.81	0.30

Table B.4: Bending Strength Calculations.

Bending Strength (N-mm)	Sample:	1	2	3	4	Mean	SD
	DCP	8.97	8.03	13.21	8.19	9.60	2.11
	LCDCP	8.30	9.24	8.21	8.30	8.51	0.42
	Ti-LCDCP	5.50	6.93	6.35	5.67	6.11	0.57
	LCP	10.19	6.01	5.55	5.01	6.69	2.05
	ALPS10	4.73	4.91	3.75	7.05	5.11	1.20
	ALPS11	11.16	10.92	11.69	12.54	11.58	0.62
	SOP	10.44	14.51	10.44	11.07	11.61	1.69
	Fixin	8.23	4.93	7.50	8.57	7.31	1.43

Appendix C: Four-Point Bending Minitab Analysis

Bending Stiffness One-Way ANOVA and Tukey Pairwise Comparison

```
Source  DF      SS     MS      F      P
Factor   7  6983.0  997.6  13.11  0.000
Error   24  1825.9   76.1
Total   31  8808.9
S = 8.722   R-Sq = 79.27%   R-Sq(adj) = 73.23%
                             Individual 95% CIs For Mean Based on
                             Pooled StDev
Level     N    Mean   StDev  ---------+---------+---------+---------+
DCP       4  71.038  17.595                      (-----*-----)
LCDCP     4  57.332   1.441             (-----*-----)
Ti-LCDCP  4  44.214   3.009    (-----*-----)
LCP       4  66.645   7.675                   (-----*-----)
ALPS10    4  40.030   2.158  (-----*-----)
ALPS11    4  76.282   2.026                          (-----*-----)
SOP       4  80.403  14.485                             (-----*-----)
Fixin     4  44.403   3.227     (-----*-----)
                             ---------+---------+---------+---------+
                                    45        60        75        90
Pooled StDev = 8.722

Grouping Information Using Tukey Method
          N    Mean  Grouping
SOP       4  80.403  A
ALPS11    4  76.282  A B
DCP       4  71.038  A B
LCP       4  66.645  A B
LCDCP     4  57.332    B C
Fixin     4  44.403      C
Ti-LCDCP  4  44.214      C
ALPS10    4  40.030      C
Means that do not share a letter are significantly different.
```

Bending Structural Stiffness One-way ANOVA and Tukey Pairwise Comparison

```
Source  DF       SS      MS      F      P
Factor   7   81.953  11.708  13.11  0.000
Error   24   21.429   0.893
Total   31  103.382
S = 0.9449   R-Sq = 79.27%   R-Sq(adj) = 73.23%
                             Individual 95% CIs For Mean Based on
                             Pooled StDev
Level     N    Mean   StDev  ---------+---------+---------+---------+
DCP       4  7.6958  1.9061                      (-----*-----)
LCDCP     4  6.2110  0.1561             (-----*-----)
Ti-LCDCP  4  4.7898  0.3260    (-----*-----)
LCP       4  7.2199  0.8315                   (-----*-----)
ALPS10    4  4.3366  0.2338  (-----*-----)
ALPS11    4  8.2639  0.2195                         (-----*-----)
SOP       4  8.7103  1.5692                           (-----*------)
Fixin     4  4.8104  0.3496    (-----*-----)
                             ---------+---------+---------+---------+
                                   4.8       6.4       8.0       9.6
Pooled StDev = 0.9449

Grouping Information Using Tukey Method
          N    Mean  Grouping
SOP       4  8.7103  A
ALPS11    4  8.2639  A B
DCP       4  7.6958  A B
LCP       4  7.2199  A B
LCDCP     4  6.2110    B C
Fixin     4  4.8104      C
Ti-LCDCP  4  4.7898      C
ALPS10    4  4.3366      C
Means that do not share a letter are significantly different.
```

Bending Strength One-way ANOVA with Tukey Pairwise Comparison

```
Source  DF      SS     MS     F      P
Factor   7  167.99  24.00  9.05  0.000
Error   24   63.66   2.65
Total   31  231.65
S = 1.629   R-Sq = 72.52%   R-Sq(adj) = 64.51%
                            Individual 95% CIs For Mean Based on
                            Pooled StDev
Level     N    Mean  StDev  ------+---------+---------+---------+---
DCP       4   9.597  2.441                    (-----*------)
LCDCP     4   8.512  0.487                (------*------)
Ti-LCDCP  4   6.111  0.660      (-----*------)
LCP       4   6.690  2.368        (------*-----)
ALPS10    4   5.111  1.389  (-----*------)
ALPS11    4  11.578  0.719                             (-----*------)
SOP       4  11.615  1.953                             (-----*------)
Fixin     4   7.305  1.649          (------*------)
                            ------+---------+---------+---------+---
                                5.0       7.5      10.0      12.5
Pooled StDev = 1.629

Grouping Information Using Tukey Method
          N    Mean  Grouping
SOP       4  11.615  A
ALPS11    4  11.578  A
DCP       4   9.597  A B
LCDCP     4   8.512  A B C
Fixin     4   7.305    B C
LCP       4   6.690    B C
Ti-LCDCP  4   6.111    B C
ALPS10    4   5.111      C
Means that do not share a letter are significantly different.
```

Appendix D: Cyclic Torsion Staircase Data per Plating System

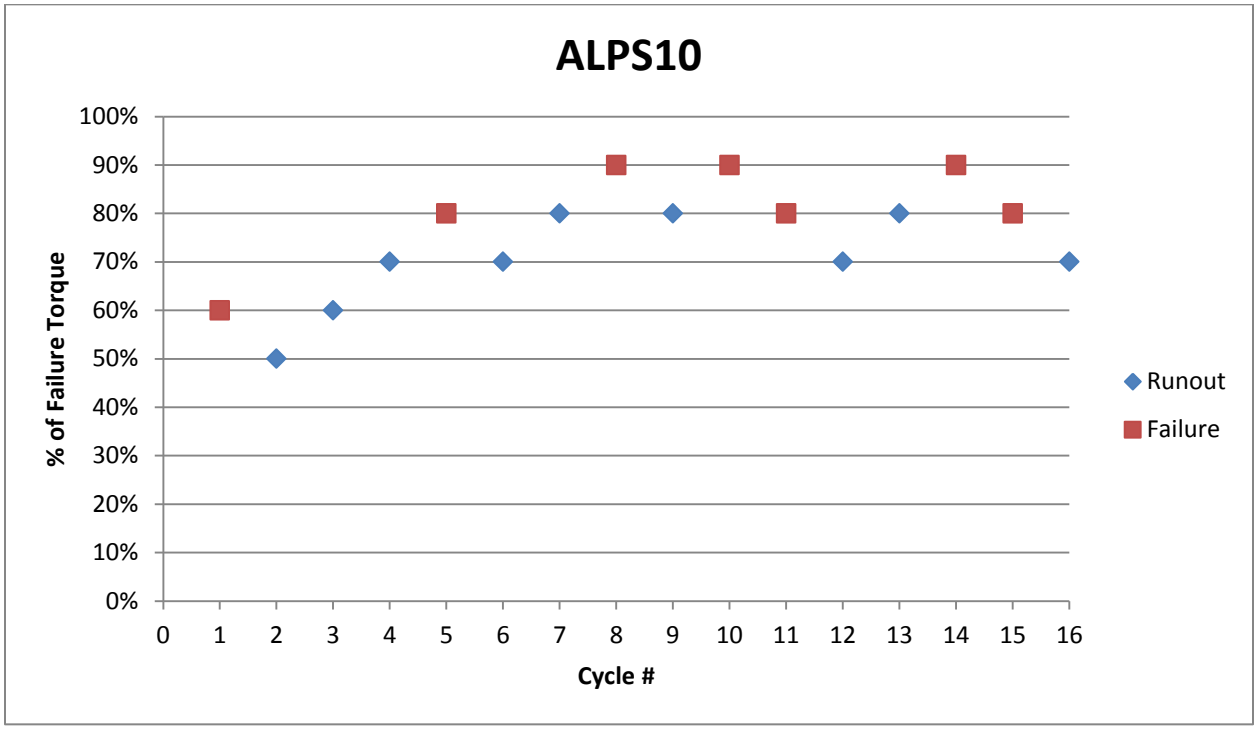

Figure D.1: ALPS10 Staircase Data Summary

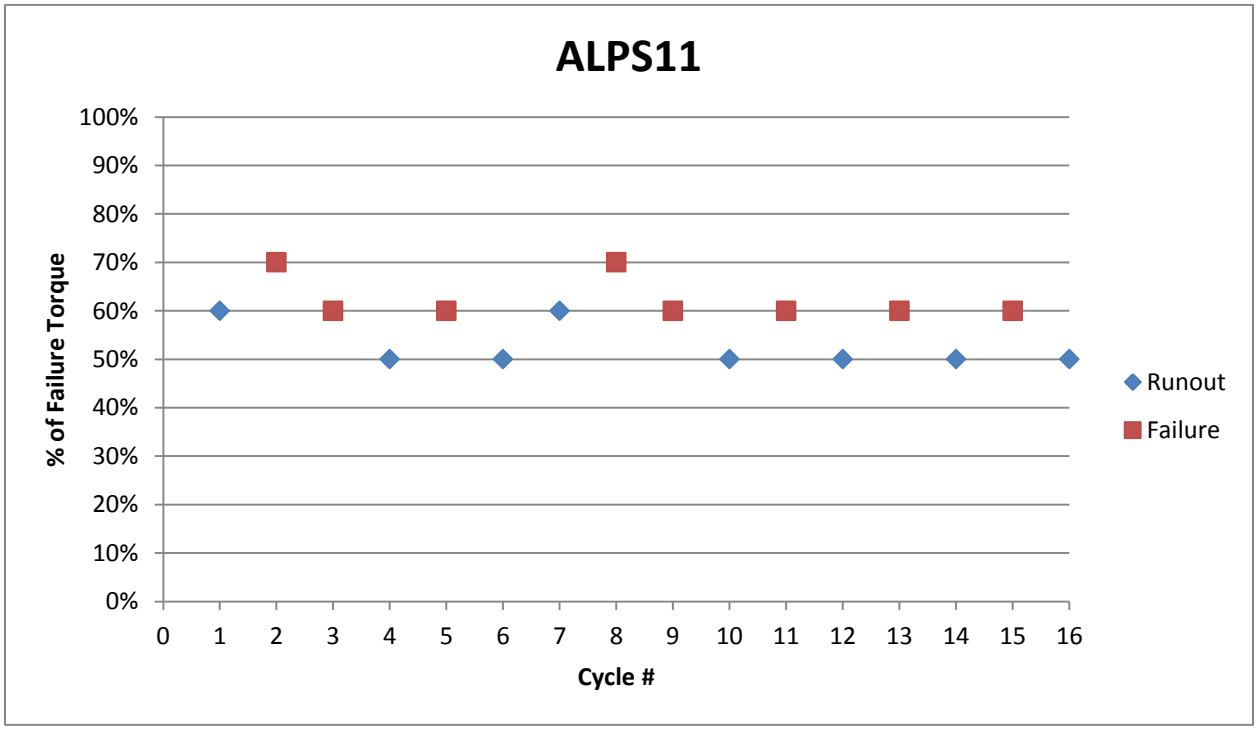

Figure D.2: ALPS11 Staircase Data Summary

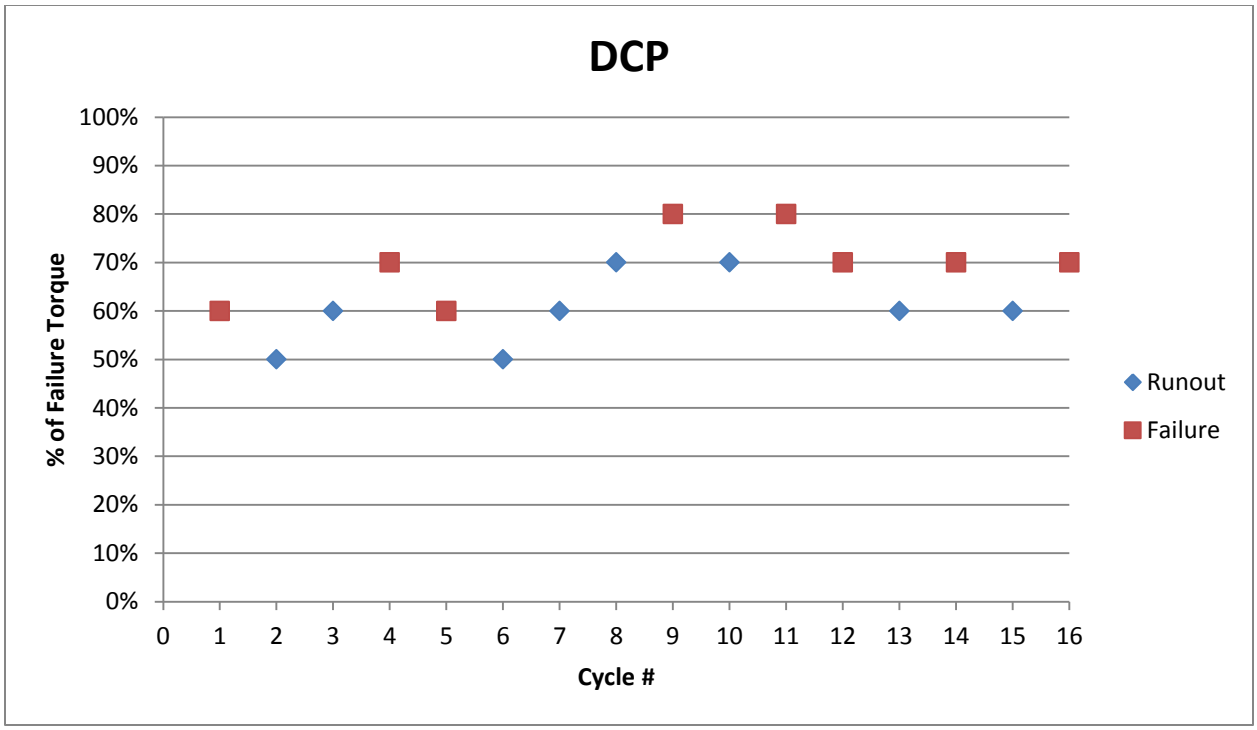

Figure D.3: DCP Staircase Data Summary

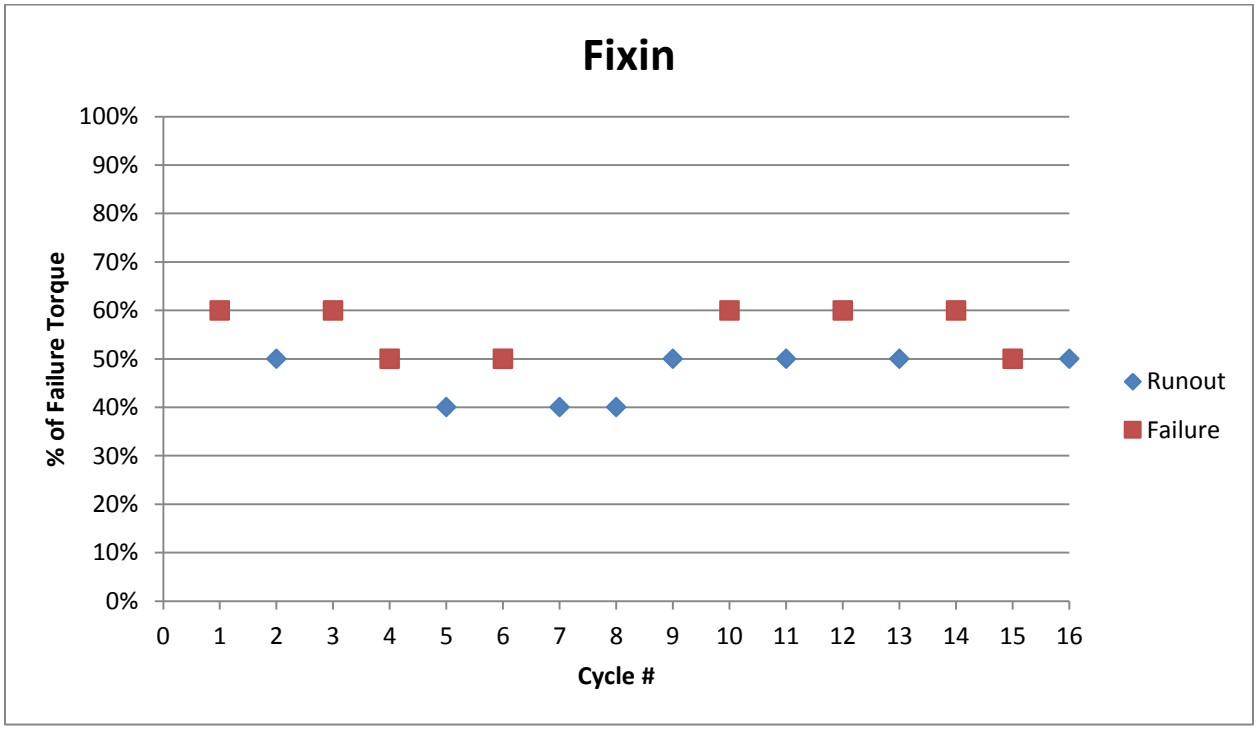

Figure D.4: Fixin Staircase Data Summary

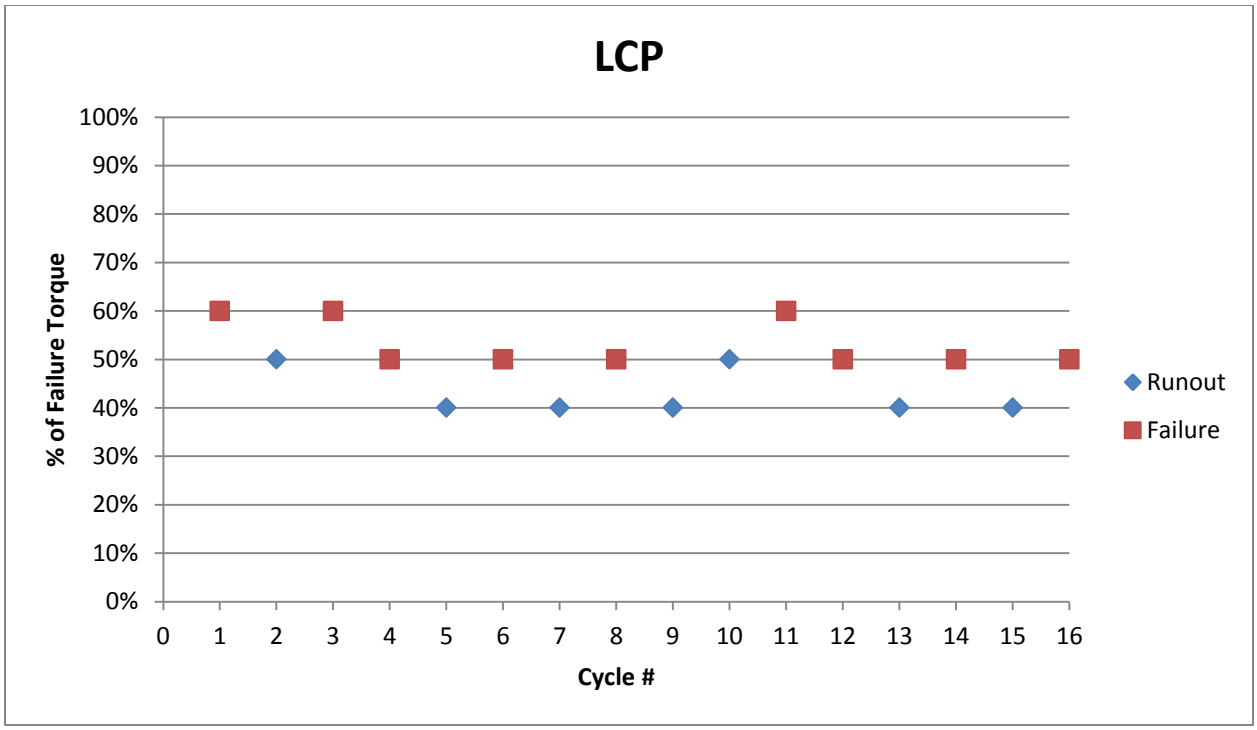

Figure D.5: LCP Staircase Data Summary

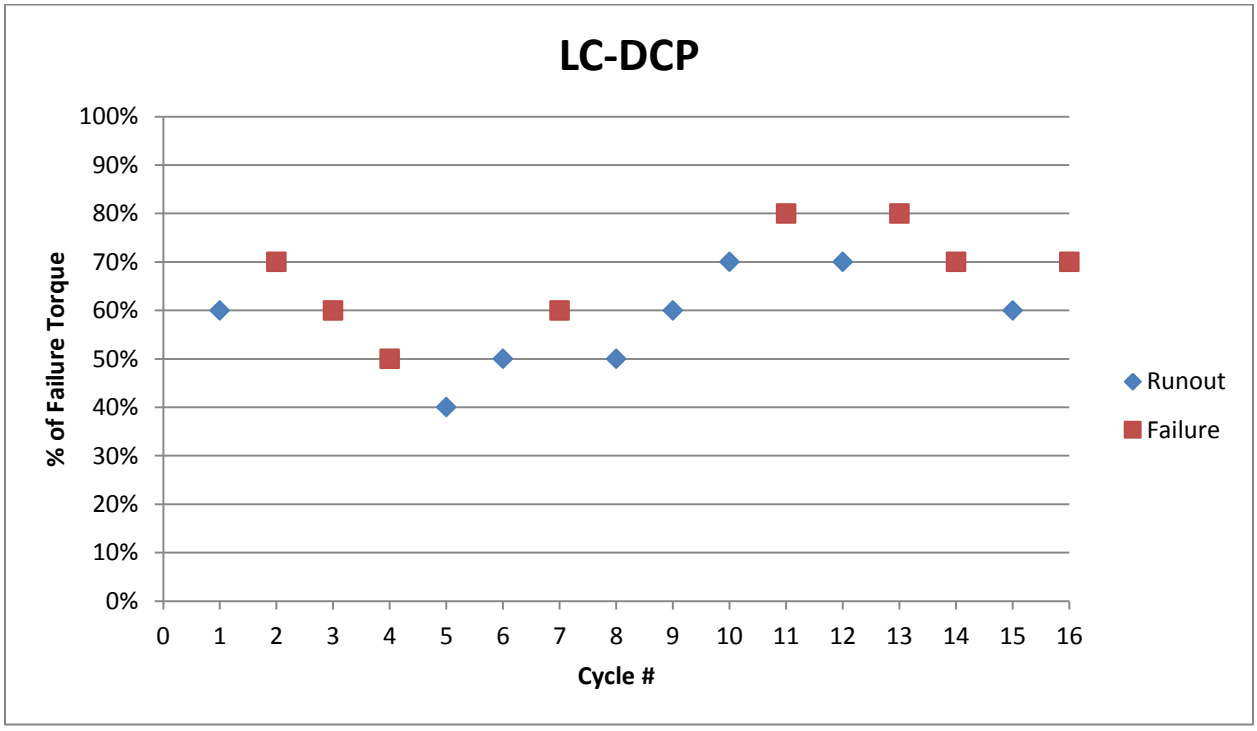

Figure D.6: LC-DCP Staircase Data Summary

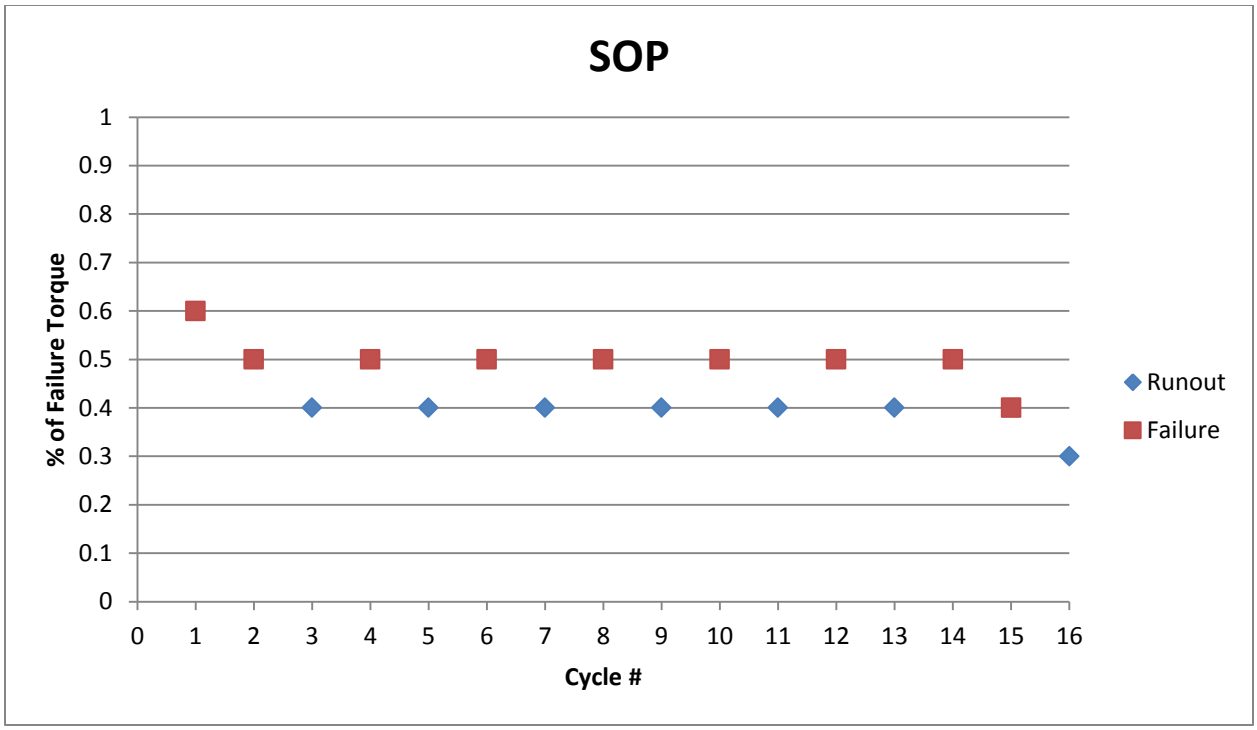

Figure D.7: SOP Staircase Data Summary

Appendix E: Cyclic Torsion Total Angular Rotation and Failure Modes

Angular rotation, per sample, in degrees, at various cycle points.							
Failure Mode Key: Runout = No failure , F Progressive = Progressive, noncatastrophic failure across entire cycle , F Acute = Catastrophic failure prior to end of cycle							
Cycle 1	**ALPS10 (60%)**	**ALPS11 (60%)**	**DCP (60%)**	**Fixin (60%)**	**LCP (60%)**	**LC-DCP (60%)**	**SOP (60%)**
1000	15.99	17.28	12.16	13.83	12.46	9.94	13.94
5000	17.94	18.36	12.83	14.30	14.93	10.03	14.64
10000	19.50	19.50	15.52	14.93	18.23	10.25	19.91
15000	22.29	20.42	N/A	18.32	N/A	10.40	N/A
Mode:	F Progressive	Runout	F Acute	F Acute	F Acute	Runout	F Acute
Rotation:	39%	18%	28%	32%	46%	5%	43%
Cycle 2	**ALPS10 (50%)**	**ALPS11 (70%)**	**DCP (50%)**	**Fixin (54%)**	**LCP (54%)**	**LC-DCP (70%)**	**SOP (50%)**
1000	11.65	20.59	9.39	12.00	11.61	12.79	11.83
5000	12.29	23.34	9.50	12.08	11.93	12.78	12.05
10000	12.52	26.16	10.00	12.08	12.33	13.32	14.77
15000	12.65	N/A	10.02	12.13	13.06	15.27	N/A
Mode:	Runout	F Acute	Runout	Runout	Runout	F Acute	F Acute
Rotation:	9%	27%	7%	1%	12%	19%	25%
Cycle 3	**ALPS10 (60%)**	**ALPS11 (60%)**	**DCP (60%)**	**Fixin (60%)**	**LCP (60%)**	**LC-DCP (60%)**	**SOP (40%)**
1000	15.37	15.89	10.92	13.55	13.85	10.99	9.07
5000	16.38	-88.98	11.25	13.82	15.22	11.41	9.09
10000	16.84	N/A	10.87	-26.8	18.09	13.27	9.15
15000	17.35	N/A	9.94	N/A	N/A	13.44	10.08
Mode:	Runout	F Acute	Runout	F Acute	F Acute	F Acute	Runout
Rotation:	13%	660%	9%	298%	31%	22%	11%
Cycle 4	**ALPS10 (70%)**	**ALPS11 (50%)**	**DCP (70%)**	**Fixin (50%)**	**LCP (50%)**	**LC-DCP (50%)**	**SOP (50%)**
1000	17.75	11.81	13.31	10.59	11.15	7.85	11.94
5000	19.92	12.49	13.58	10.62	11.38	8.03	12.44
10000	21.16	13.22	14.02	12.23	14.21	8.85	14.34
15000	21.53	14.32	16.67	-21.29	17.76	9.20	38.88
Mode:	Runout	Runout	F Progressive	F Acute	F Acute	F Acute	F Acute
Rotation:	21%	21%	25%	301%	59%	17%	226%
Cycle 5	**ALPS10 (80%)**	**ALPS11 (60%)**	**DCP (60%)**	**Fixin (40%)**	**LCP (40%)**	**LC-DCP (40%)**	**SOP (40%)**
1000	24.39	15.81	11.1	8.56	9.11	7.48	8.89
5000	26.66	20.76	11.48	8.65	9.17	7.48	8.89
10000	28.13	N/A	11.74	8.69	9.22	7.47	8.94
15000	29.11	N/A	14.62	8.66	9.24	7.46	9.04
Mode:	F Acute	F Acute	F Progressive	Runout	Runout	Runout	Runout
Rotation:	19%	31%	32%	1%	1%	0%	2%
Cycle 6	**ALPS10 (70%)**	**ALPS11 (50%)**	**DCP (50%)**	**Fixin (50%)**	**LCP (50%)**	**LC-DCP (50%)**	**SOP (50%)**
1000	19.41	13.91	8.29	11.05	10.61	8.56	11.09
5000	20.95	14.07	8.21	11.23	11.13	8.66	12.14
10000	21.53	14.34	8.2	15.8	12.67	8.68	18.23
15000	21.92	14.65	8.26	N/A	N/A	8.73	N/A
Mode:	Runout	Runout	Runout	F Acute	F Acute	Runout	F Acute
Rotation:	13%	5%	0%	43%	19%	2%	64%
Cycle 7	**ALPS10 (80%)**	**ALPS11 (60%)**	**DCP (60%)**	**Fixin (40%)**	**LCP (40%)**	**LC-DCP (60%)**	**SOP (40%)**
1000	20.82	14.58	12.05	8.42	9.1	11.96	8.85
5000	22.5	15.03	12.17	8.12	9.13	12.31	8.88
10000	23.31	15.23	12.36	8.48	9.33	15.35	8.88
15000	24.44	15.41	12.46	8.48	9.6	15.59	8.94
Mode:	Runout	Runout	Runout	Runout	Runout	F Acute	Runout
Rotation:	17%	6%	3%	1%	5%	30%	1%
Cycle 8	**ALPS10 (90%)**	**ALPS11 (70%)**	**DCP (70%)**	**Fixin (50%)**	**LCP (50%)**	**LC-DCP (50%)**	**SOP (50%)**
1000	26.08	24.82	12.91	11.2	9.96	8.2	11.56
5000	30.29	34.05	12.97	11.21	10.87	8.17	11.7
10000	43.77	N/A	13.6	11.23	11.32	8.2	11.99
15000	N/A	N/A	14.04	11.48	12.86	8.2	19.06
Mode:	F Acute	F Acute	Runout	Runout	F Acute	Runout	F Acute
Rotation:	68%	37%	9%	3%	29%	0%	65%

Angular rotation, per sample, in degrees, at various cycle points.							
Failure Mode Key: Runout = No failure , F Progressive = Progressive, noncatastrophic failure across entire cycle , F Acute = Catastrophic failure prior to end of cycle							
Cycle 9	**ALPS10 (80%)**	**ALPS11 (60%)**	**DCP (80%)**	**Fixin (60%)**	**LCP (40%)**	**LC-DCP (60%)**	**SOP (40%)**
1000	20.31	17.43	16.46	13.63	9	10.26	9.08
5000	21.73	18.48	16.66	13.84	8.96	10.23	9.14
10000	22.27	24.18	17.24	16.54	9.85	13.32	9.52
15000	23.52	N/A	20	19.63	11.14	10.32	10.6
Mode:	Runout	F Acute	F Acute	F Acute	Runout	Runout	Runout
Rotation:	16%	39%	22%	44%	24%	1%	17%
Cycle 10	**ALPS10 (90%)**	**ALPS11 (50%)**	**DCP (70%)**	**Fixin (50%)**	**LCP (50%)**	**LC-DCP (70%)**	**SOP (50%)**
1000	26.24	13.79	13.35	11.47	10.15	12.44	10.9
5000	28.83	14.46	13.92	11.59	10.24	12.56	10.99
10000	33.13	14.72	15.53	11.62	10.39	12.55	12.24
15000	N/A	15.1	16.11	11.73	10.75	12.93	34.85
Mode:	F Acute	Runout	Runout	Runout	Runout	Runout	F Acute
Rotation:	26%	9%	21%	2%	6%	4%	220%
Cycle 11	**ALPS10 (80%)**	**ALPS11 (60%)**	**DCP (80%)**	**Fixin (60%)**	**LCP (60%)**	**LC-DCP (80%)**	**SOP (40%)**
1000	20.52	17.63	-27.19	13.09	13.68	15.52	9.27
5000	20.98	18.67	-19.51	14.02	16.54	-9.01	9.2
10000	14.94	-5.63	N/A	-15.31	17.17	N/A	9.24
15000	N/A	N/A	N/A	N/A	N/A	N/A	10.07
Mode:	F Acute	F Acute	F Acute	F Acute	F Acute	F Acute	Runout
Rotation:	27%	132%	-28%	217%	26%	158%	9%
Cycle 12	**ALPS10 (70%)**	**ALPS11 (50%)**	**DCP (70%)**	**Fixin (50%)**	**LCP (50%)**	**LC-DCP (70%)**	**SOP (50%)**
1000	16.68	11.89	13.88	10.99	10.32	12.2	11.71
5000	17.7	12.06	17.81	11	10.78	12.48	11.81
10000	18.08	12.18	28.37	12.81	-12.72	12.64	15.5
15000	18.52	12.34	N/A	13.21	N/A	13.42	N/A
Mode:	Runout	Runout	F Acute	Runout	F Acute	Runout	F Acute
Rotation:	11%	4%	104%	20%	223%	10%	32%
Cycle 13	**ALPS10 (80%)**	**ALPS11 (60%)**	**DCP (60%)**	**Fixin (60%)**	**LCP (40%)**	**LC-DCP (80%)**	**SOP (40%)**
1000	19.63	18.82	10.99	13.52	8.01	13.99	8.75
5000	20.86	-13.61	11.01	15.08	8.04	14.67	8.86
10000	21.36	N/A	11.03	N/A	8.09	16.12	9.65
15000	23.28	N/A	11.59	N/A	8.26	N/A	10.03
Mode:	Runout	F Acute	Runout	F Acute	Runout	F Acute	Runout
Rotation:	19%	172%	5%	12%	1%	15%	15%
Cycle 14	**ALPS10 (90%)**	**ALPS11 (50%)**	**DCP (70%)**	**Fixin (50%)**	**LCP (50%)**	**LC-DCP (70%)**	**SOP (50%)**
1000	23.23	17.4	14.31	11.1	10.86	12.46	11.33
5000	27.37	18.77	15.59	11.24	10.93	13.16	11.39
10000	31.58	19.3	17.68	12.82	12.75	16.91	14.43
15000	N/A	19.88	N/A	N/A	N/A	N/A	N/A
Mode:	F Acute	Runout	F Acute	F Acute	F Acute	F Acute	F Acute
Rotation:	36%	14%	24%	15%	17%	36%	27%
Cycle 15	**ALPS10 (80%)**	**ALPS11 (60%)**	**DCP (60%)**	**Fixin (40%)**	**LCP (40%)**	**LC-DCP (60%)**	**SOP (40%)**
1000	20.23	16.43	10.79	8.53	8.77	10.44	8.92
5000	22.75	17.89	11.17	8.63	8.79	10.58	8.97
10000	24.87	-1.02	11.26	8.69	8.83	10.7	10.16
15000	N/A	N/A	11.32	8.79	9.23	10.74	24.37
Mode:	F Acute	F Acute	Runout	Runout	Runout	Runout	F Acute
Rotation:	23%	106%	5%	3%	5%	3%	173%
Cycle 16	**ALPS10 (70%)**	**ALPS11 (50%)**	**DCP (70%)**	**Fixin (50%)**	**LCP (50%)**	**LC-DCP (70%)**	**SOP (30%)**
1000	15.55	12.81	13.81	10.39	10.74	12.3	6.42
5000	16.97	13.01	13.93	10.41	10.8	13.36	6.5
10000	17.43	13.12	14.77	10.39	12.46	14.2	6.47
15000	17.55	13.34	18.59	10.46	14.64	15.18	6.51
Mode:	Runout	Runout	F Progressive	Runout	F Prog	F Acute	Runout
Rotation:	13%	4%	35%	1%	36%	23%	1%

Appendix F: Cyclic Torsion Probability Plots

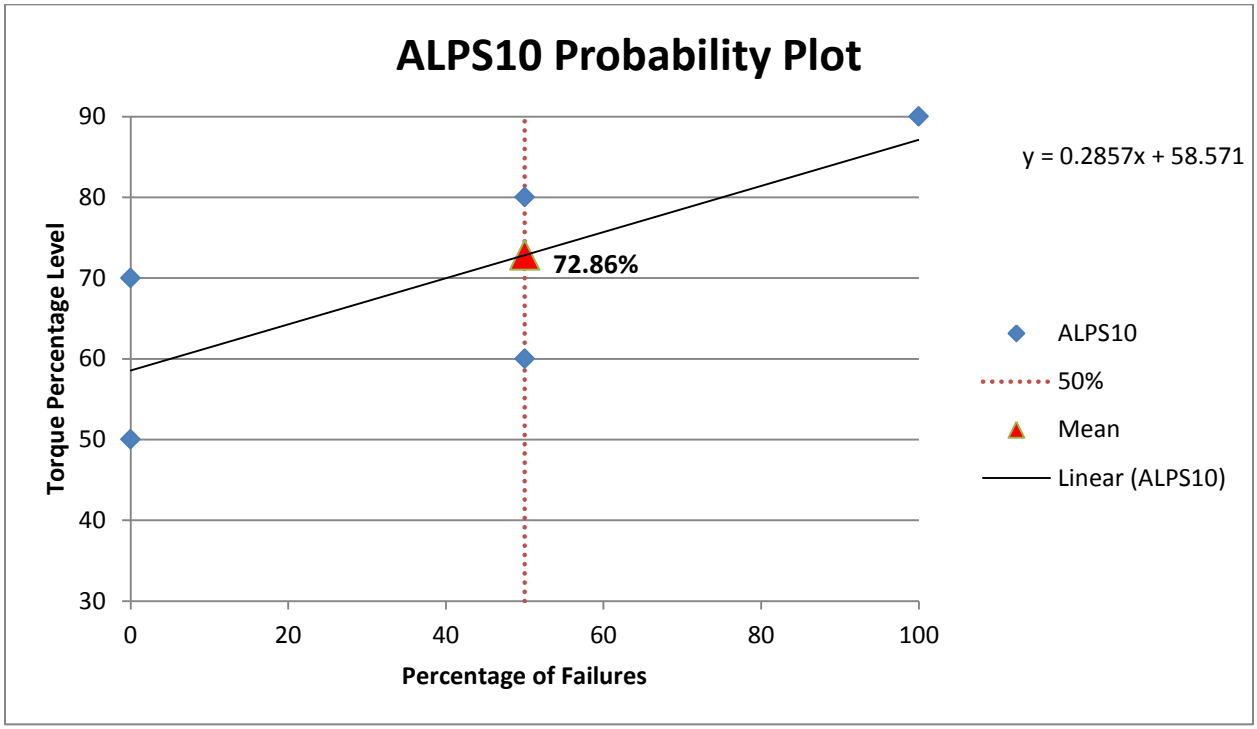

Figure F.1: ALPS10 Probability Plot, Percentage of Failure Torque.

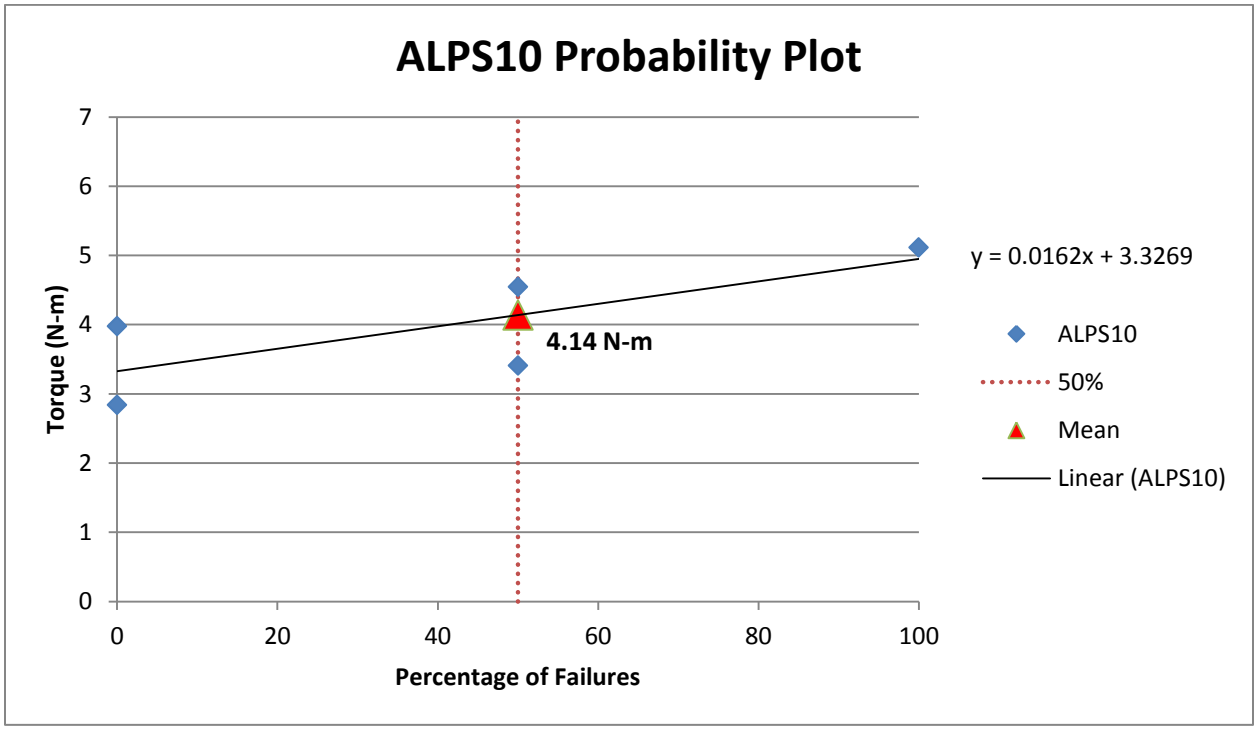

Figure F.2: ALPS10 Probability Plot, Absolute Torque Value.

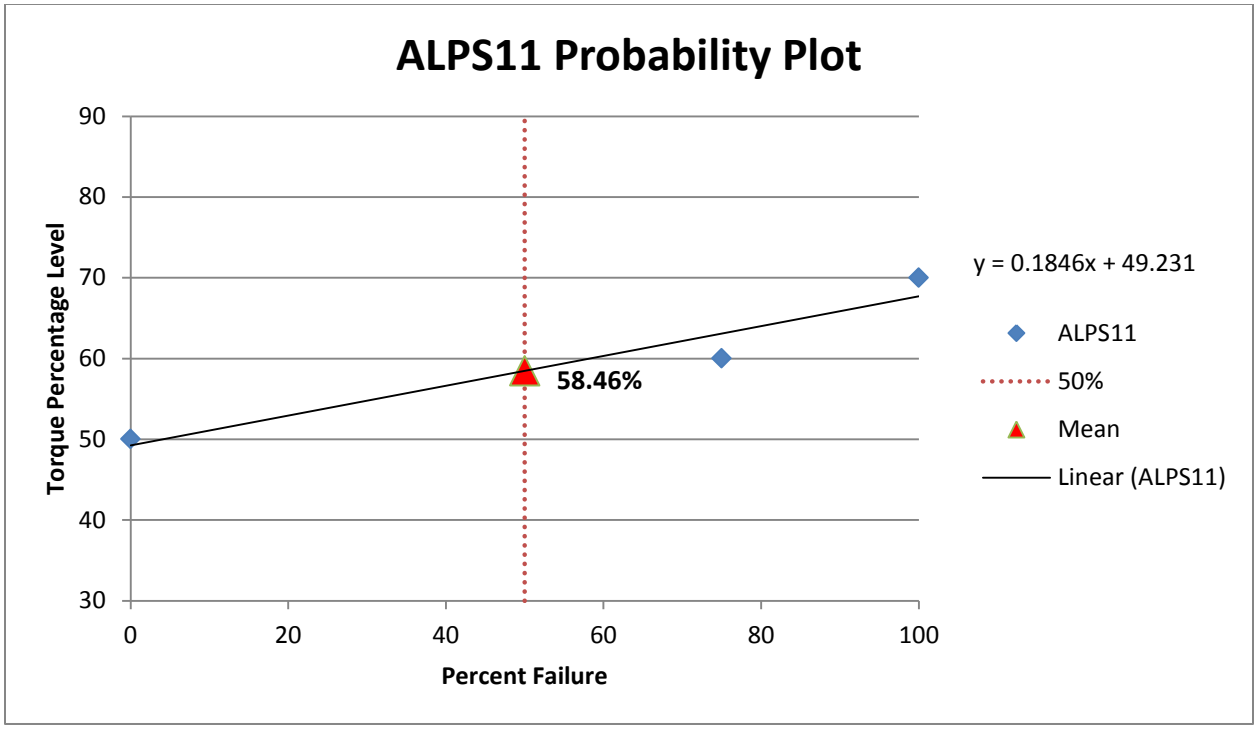

Figure F.3: ALPS11 Probability Plot, Percentage of Failure Torque.

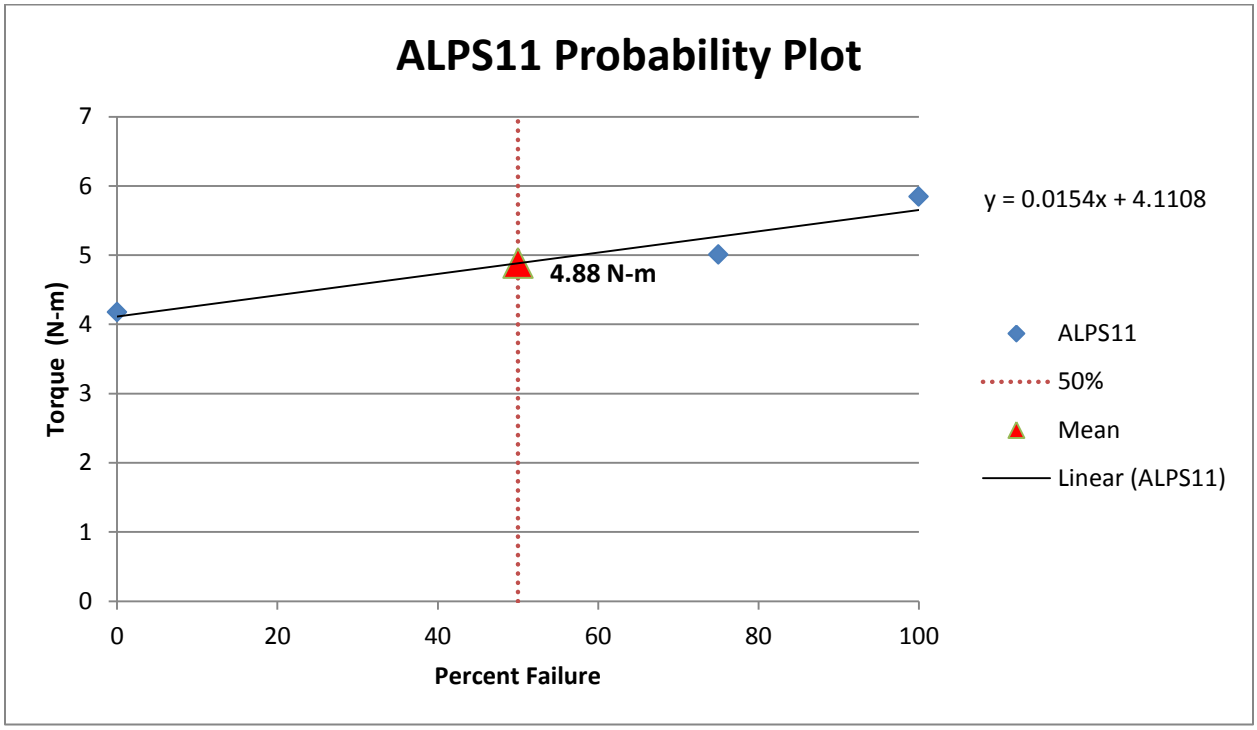

Figure F.4: ALPS11 Probability Plot, Absolute Torque Value.

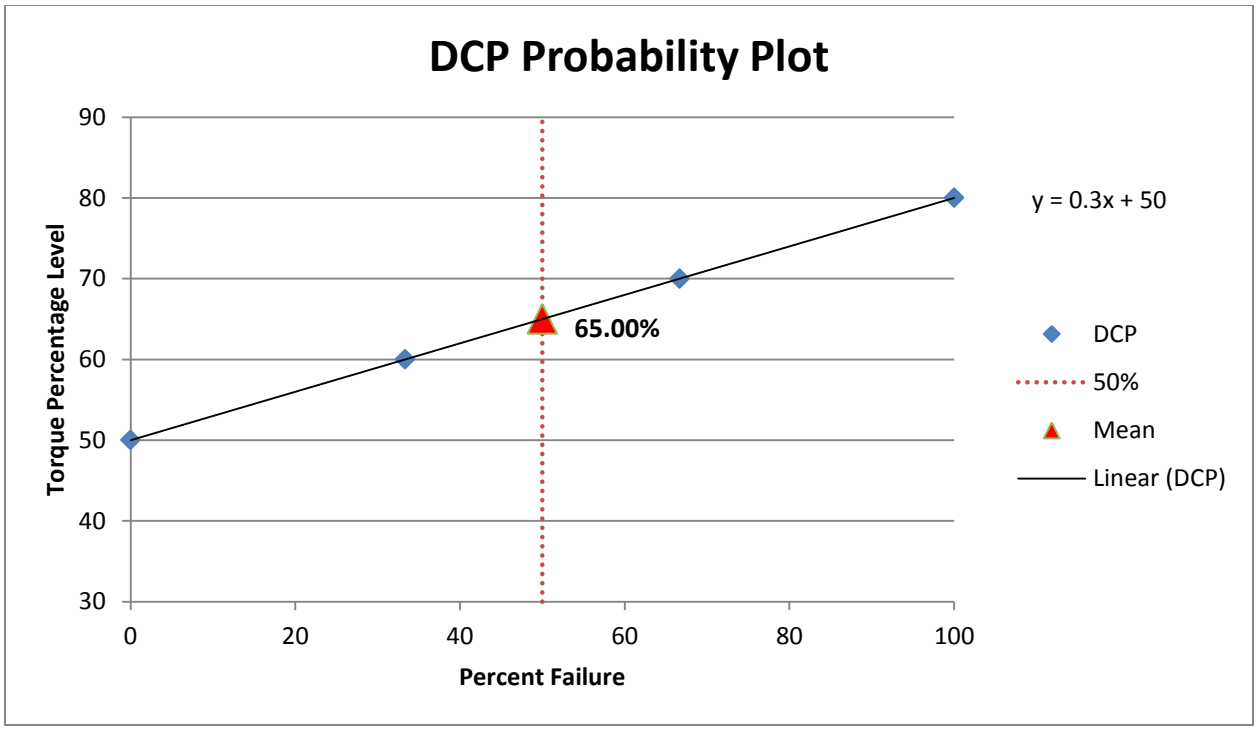

Figure F.5: Probability Plot, Percentage of Failure Torque.

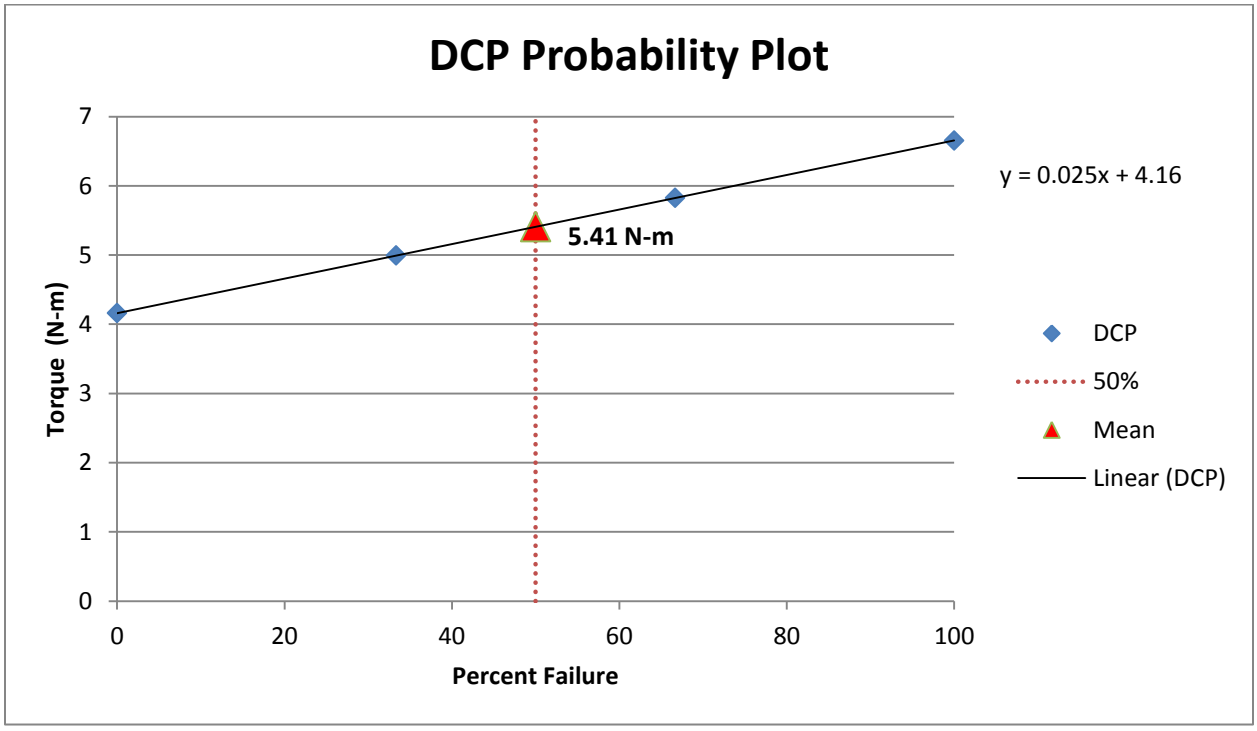

Figure F.6: DCP Probability Plot, Absolute Torque Value.

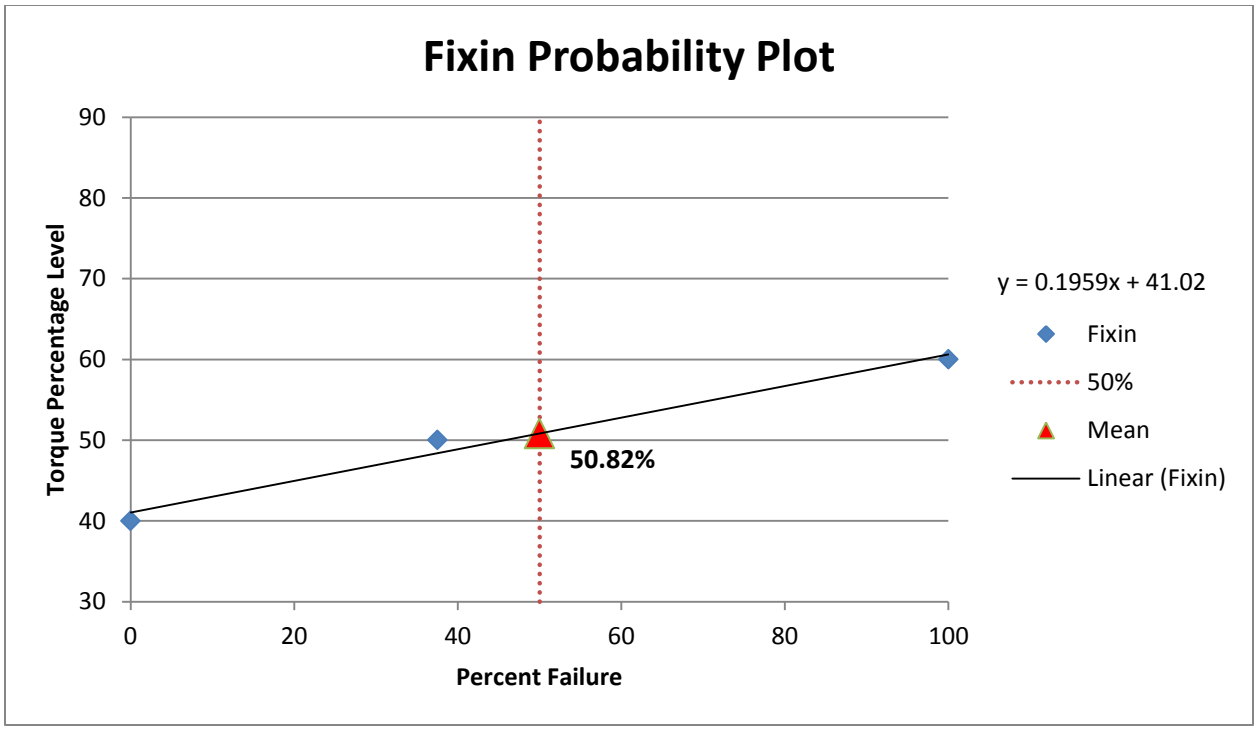

Figure F.7: Fixin Probability Plot, Percentage of Failure Torque.

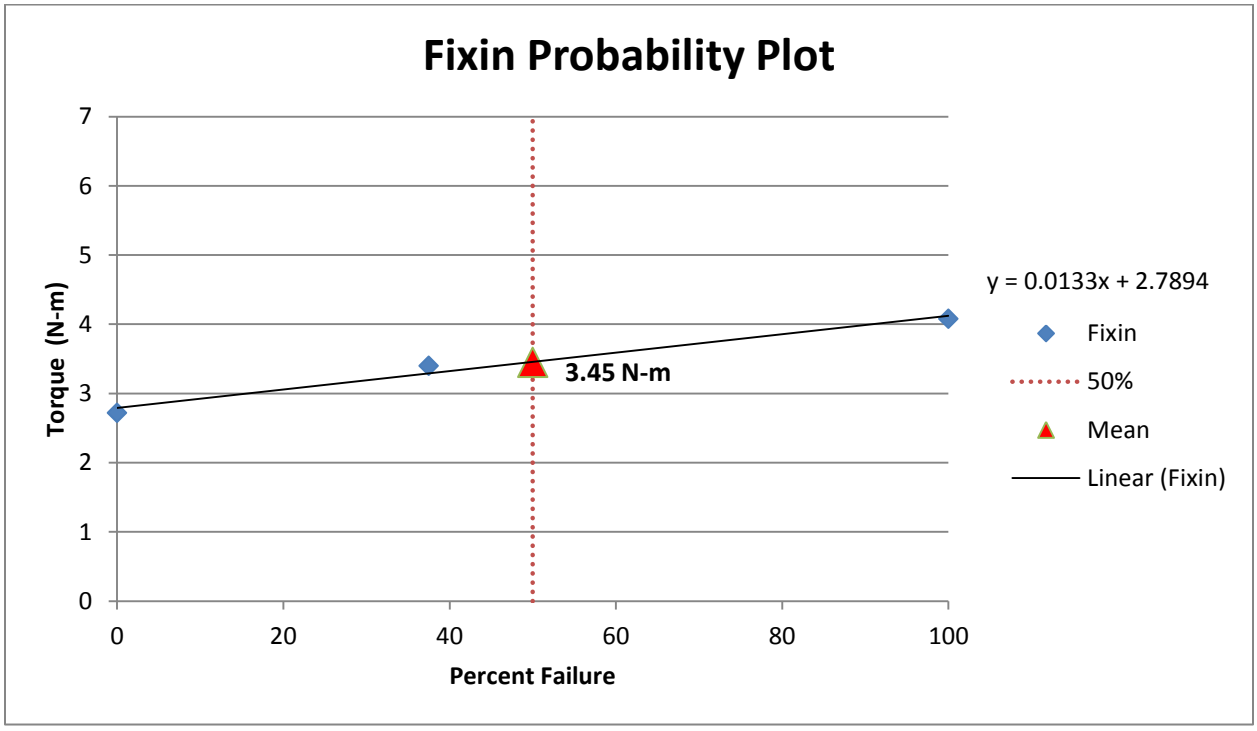

Figure F.8: Fixin Probability Plot, Absolute Torque Value.

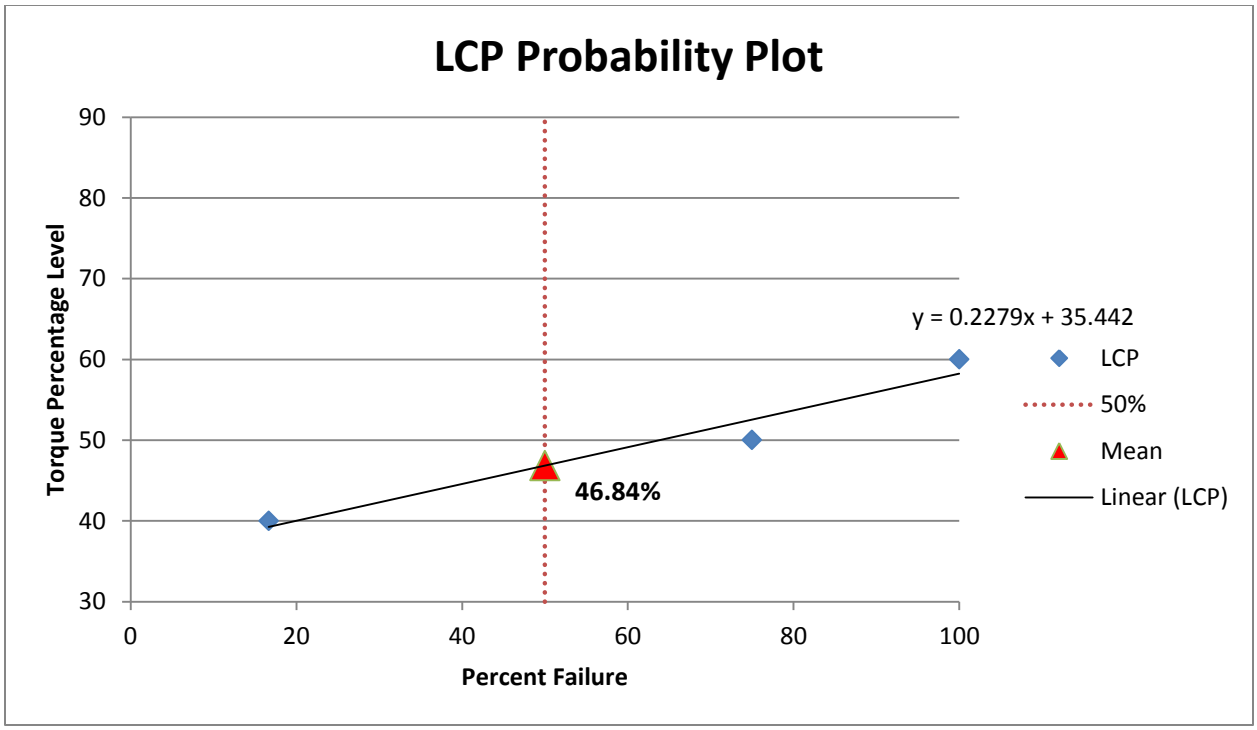

Figure F.9: LCP Probability Plot, Percentage of Failure Torque.

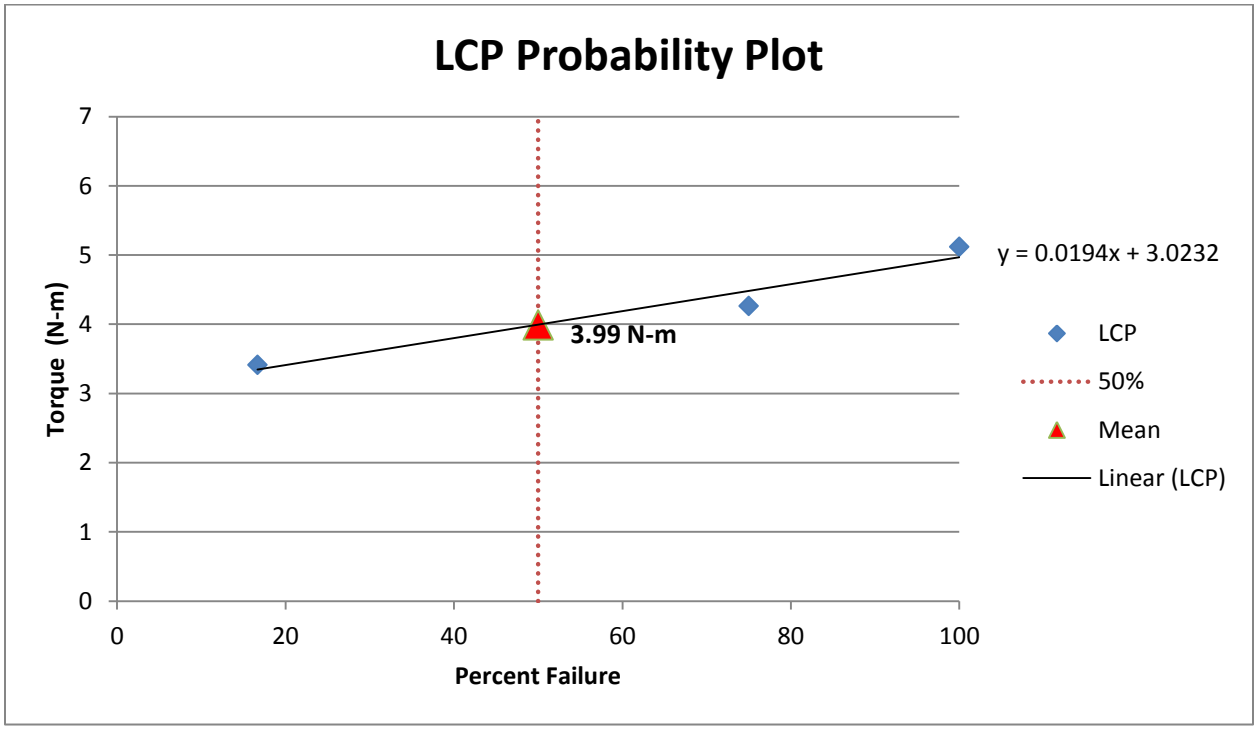

Figure F.10: LCP Probability Plot, Absolute Torque Value.

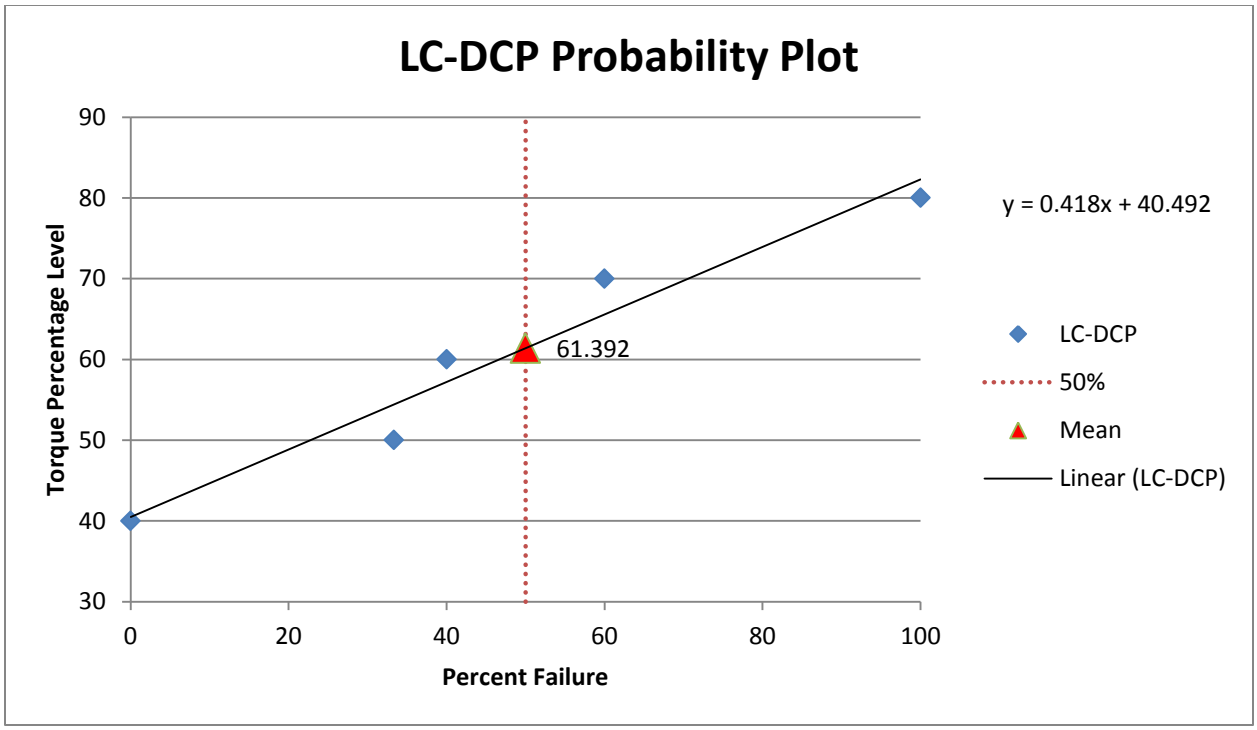

Figure F.11: LC-DCP Probability Plot, Percentage of Failure Torque.

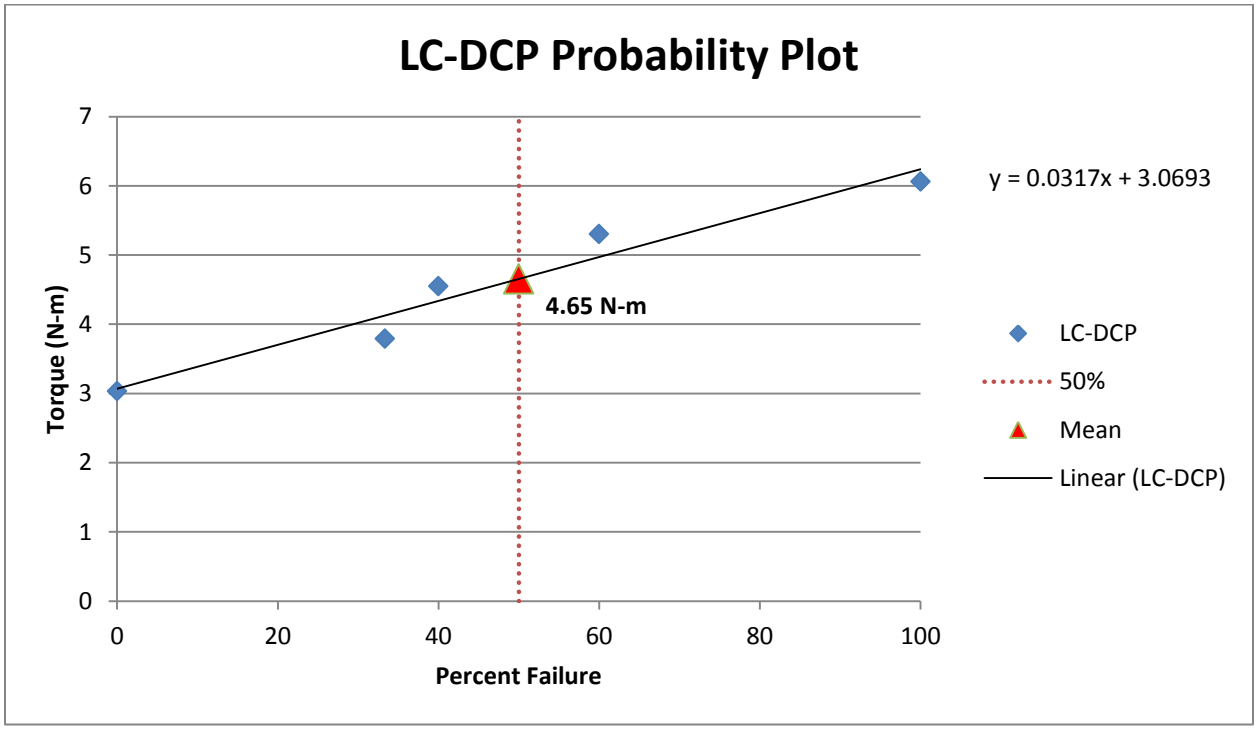

Figure F.12: LC-DCP Probability Plot, Absolute Torque Value.

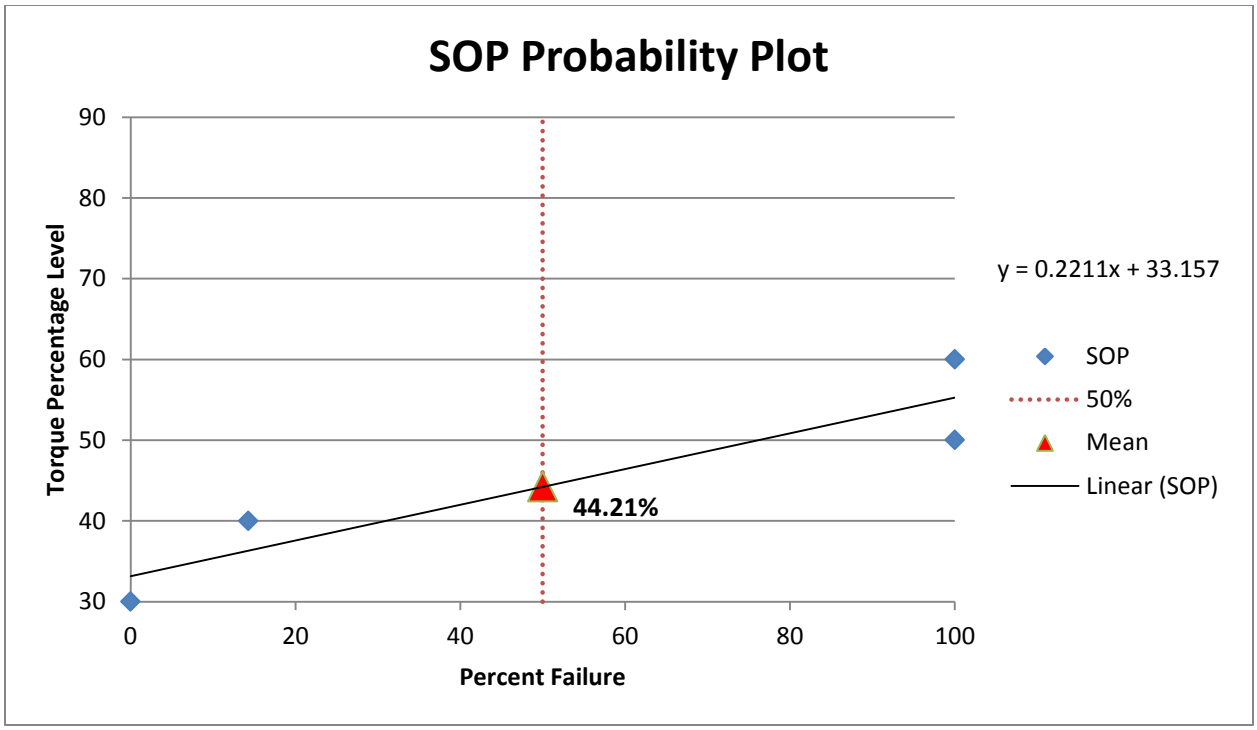

Figure F.13: SOP Probability Plot, Percentage of Failure Torque.

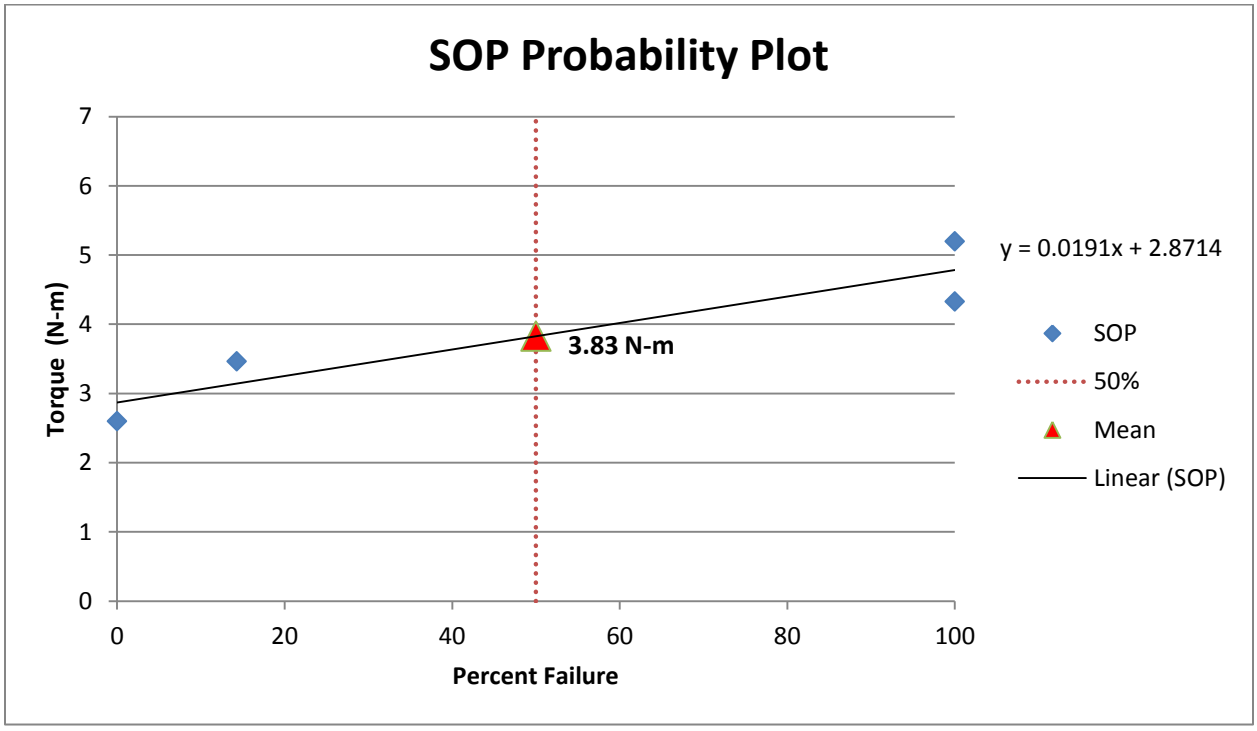

Figure F.14: SOP Probability Plot, Absolute Torque Value.

Appendix G: Dixon-Mood Calculations

Table G.1: ALPS10 Dixon-Mood Calculations.

ALPS10	Range	i	n	i*n	i^2*n		
	90%	3	3	9	27		
	80%	2	3	6	12		
	70%	1	0	0	0	μ	76.43
	60%	0	1	0	0	σDM	16.34
	Total		A = 7	B = 15	C = 39	σSL	20.11

Table G.2: ALPS11 Dixon-Mood Calculations.

ALPS11	Range	i	n	i*n	i^2*n		
	70%	1	2	2	2	μ	57.50
	60%	0	6	0	0	σDM	5.30
	Total		A = 8	B = 2	C = 2	σSL	6.52

Table G.3: DCP Dixon-Mood Calculations.

DCP	Range	i	n	i*n	i^2*n		
	80%	2	2	4	8		
	70%	1	4	4	4	μ	65.00
	60%	0	2	0	0	σDM	8.57
	Total		A = 8	B = 8	C = 12	σSL	10.55

Table G.4: Fixin Dixon-Mood Calculations.

Fixin	Range	i	n	i*n	i^2*n		
	60%	1	5	5	5	μ	51.25
	50%	0	3	0	0	σDM	5.30
	Total		A = 8	B = 5	C = 5	σSL	6.52

Table G.5: LCP Dixon-Mood Calculations.

LCP	Range	i	n	i*n	i^2*n		
	50%	1	2	2	2	μ	47.86
	40%	0	5	0	0	σDM	5.30
	Total		A = 7	B = 2	C = 2	σSL	6.52

Table G.6: LC-DCP Dixon-Mood Calculations.

LC-DCP	Range	i	n	i*n	i^2*n		
	80%	3	2	6	18		
	70%	2	3	6	12		
	60%	1	2	2	2	**μ**	**62.50**
	50%	0	1	0	0	**σDM**	**15.66**
	Total		**A = 8**	**B = 14**	**C = 32**	**σSL**	**19.27**

Table G.7: SOP Dixon-Mood Calculations.

SOP	Range	i	n	i*n	i^2*n		
	60%	3	0	0	0		
	50%	2	0	0	0		
	40%	1	6	6	6	**μ**	**43.57**
	30%	0	1	0	0	**σDM**	**5.30**
	Total		**A = 7**	**B = 6**	**C = 6**	**σSL**	**6.52**

Appendix H: Plot of Runout Torque vs. Rotational Displacement